NANYANG TECHNOLOGICAL UNIVERSITY

Gelatin Methacryloyl Inverted Colloidal Crystal Scaffolds as Artificial Liver Platform

Hitomi Shirahama

Interdisciplinary Graduate School
Nanyang Institute of Technology in Health and Medicine

2017

Gelatin Methacryloyl Inverted Colloidal Crystal Scaffolds as Artificial Liver Platform

Hitomi Shirahama

Interdisciplinary Graduate School

Nanyang Institute of Technology in Health and Medicine

A thesis submitted to the Nanyang Technological University in partial fulfillment of the requirement for the degree of

Doctor of Philosophy

2017

Abstract

Artificial organs are vital for drug development since preclinical animal testing has a limitation in human toxicity prediction, occasionally leading to severe damages. In particular the liver which is an organ that serves the functions in drug metabolism and detoxification, would play a critical role in toxicity screening when reconstructed in vitro. However, primary hepatocytes lose their functions when seeded onto plain substrates, and maintaining the functions ex vivo has been challenging. One of the cues found in liver tissue engineering to keep hepatocyte phenotype is the structural dimensionality; three-dimensional (3D) culture systems which emulate the liver microenvironment, provide enhanced cell-cell interactions and cell-material interactions compared to those in two-dimensions, resulting in prolonged of hepatocyte functions. Therefore, in-vivo-like platforms that mimic the liver microstructure have been in high demand.

The overall goal of this dissertation is to create a liver-mimicking platform that can aid in maintaining hepatic functions. Besides cells, the liver is composed of extracellular matrices (ECM) with highly-ordered, porous structure. On the other hand, fabrication of such ECM-based highly-ordered scaffold has been challenging. Problems lie in high viscosity and in slow crosslinking of the aqueous protein solutions for building complex configuration.

In this thesis, the material chosen for the platform is a photocrosslinkable protein, gelatin methacryloyl (GelMA). Gelatin is a hydrolyzed form of collagen, which is the main component of the liver structure. While preserving biological advantages of collagen/gelatin, the functionalized gelatin can be crosslinked in minutes in the presence of ultraviolet light and a photoinitiator. Furthermore, aqueous solutions of GelMA are much less viscous than the parent materials. However, the synthesis method has not been optimized in a systematic manner, leaving room for improvement. The first work presented in this thesis is to revamp GelMA synthesis through finding appropriate buffer systems and reaction conditions such as pH, molarity, temperature, and time.

The second part of the thesis work entails characterizing the physical properties of GelMA hydrogels with a simplified model. Rheological experiments on mechanical stiffness, swelling measurements in size and mass, and enzymatic degradation experiments were carried out for comprehensive characterization.

Finally, a liver-mimicking hydrogel platform was developed, possessing highly-ordered pores and interconnections. Protein-based inverted colloidal crystal (ICC) scaffolds were fabricated with GelMA and a sacrificial polymer lattice. The use of GelMA enabled easy infiltration into the lattices at a high protein concentration and fast crosslinking. Liver model cells, Huh7.5 cells, in GelMA ICC scaffolds attached well to the surface of GelMA ICC and formed 3D cell constructs with cell multi layers during a culture period of high viability. Relative to GelMA plain surface, cells in GelMA ICC exhibited higher hepatic functions. The results demonstrate the potential of GelMA ICC to be an artificial liver platform – that can maintain hepatic functions and foresee human drug toxicity – and would be contributive to drug discovery and development.

Acknowledgements

This dissertation work would not have been accomplished without any support. I would like to first express my deepest gratitude to my supervisor, Professor Nam-Joon Cho, for his unwavering support, guidance, and encouragement throughout this journey. It is one of my biggest fortunes to have met Professor Cho during an exchange study and be accepted to pursue the doctoral study in his group. I have indeed learned a lot from his passion for translational science, inspiring philosophy, generous care, and a creation of the multidisciplinary team that is collaborative and cheerful. He always advised as well as helped me whenever I was having any difficulties, and it is for that reason that I am truly thankful.

Sincere appreciation extends to Dr. Bae Hoon Lee, a knowledgeable and warm-hearted mentor. He helped me personify each and every idea that I had as a researcher since he has the power of observation, a spirit of cooperation, and persistence as well as patience to cope with difficulties. I am blessed to have worked with him.

I am also grateful to my wonderful collaborators, Dr. Myung Hee Kim, Dr. Jae Ho Lee, Supriya Kumar, Dr. Won-Yong Jeon, Dr. Soon Seng Ng, Dr. Jeongeun Seo, Dr. Seyed Tabaei, Professor Lay Poh Tan, Professor Jeffery S. Glenn, and the large scholar community for their kind support and advice. Technical expertise was received from Biomaterials lab, FACTS lab, Heat Treatment lab, and E-Space from School of Material Science Engineering, as well as NMR facility and Optical Microscopy facility from School of Biological Science. I would also like to thank Professor Seung Ki Moon and Professor Glenn for being in my Thesis Advisory Committee and providing invaluable feedback.

I would also like to appreciate Nanyang Institute of Technology in Health and Medicine, Interdisciplinary Graduate School, and Nanyang Technological University for granting me this opportunity to tackle this interdisciplinary problem in an excellent environment. I am thankful to Agency for Science, Technology and Research (A*STAR) for their financial support in the form of Singapore International Graduate Award throughout the study.

I will cherish my lifetime memory at Engineering in Translational Science group, former Translational Science Group. It is an *amazing*, diverse group, where I have learned different, fantastic things from all the members. I have no doubt that this group continues developing, and everyone will succeed. Special thanks go to Setareh Vafaei, Supriya Kumar, and Şaziye Yorulmaz for the precious moments that we shared.

Reassuring warmth, empowerment, and company, for which I am indebted to my friends: from ETS –the past to current–, at NTU, in Singapore, and overseas.

Lastly, I would like to thank my family for bracing and supporting me in many ways over the whole academic odyssey.

Table of Contents

Table Captions

Figure Captions

Abbreviations

2D	Two-Dimensional
3D	Three-Dimensional
AAT	Alpha 1-Antitrypsin
CB	Carbonate-Bicarbonate
CYP	Cytochrome P450
DMEM	Dulbecco's Modified Eagle Medium
DS	Degree of Substitution
ECM	Extracellular Matrix
ELISA	Enzyme-linked Immunosorbent Assay
G6Pase	Glucose 6-Phosphatase
GelMA	Gelatin Methacryloyl
GO	Graphene Oxide
^{1}H NMR	Proton Nuclear Magnetic Resonance
HCV	Hepatitis C Virus
HNF	Hepatocyte Nuclear Factor
I2959	2-Hydroxy-4'-(2-Hydroxyethoxy)-2-Methylpropiophenone
ICC	Inverted Colloidal Crystal
IEP	Isoelectronic Point
LTE	Liver Tissue Engineering
MAA	Methacrylic Anhydride
NP	Non-parenchymal
PAM	Poly(acrylamide)
PBS	Phosphate Buffered Saline
PEG	Poly(ethylene glycol)
PEGDA	Poly(ethylene glycol) Diacrylate
PEGDMA	Poly(ethylene glycol) Dimethacrylate
PHEMA	Poly(2-hydroxyethyl methacrylate)
PLGA	Poly(lactic-co-glycolic acid)
PS	Polystylene

RGD	Arginine-glycine-aspartic Acid
SEM	Scanning Electron Microscopy
TE	Tissue Engineering
TNBS	2,4,6-Trinitrobenzenesulfonic Acid
UV	Ultraviolet
ZO-1	Zona Occuldens-1

Chapter 1 Introduction

Non-negligible lives were lost at clinical testing and post-marketing during the process of drug development. Animal testing is not always effective, because of species-specific activity of drug metabolism. If a fraction of human liver could be reconstructed ex vivo, which can react with drugs as well as the liver in the body, it would be a potent tool for toxicity prediction. This chapter introduces the current situation of drug development and design philosophy of the proposed artificial liver platform.

1.1. Background

History of drugs stretches back to prehistoric herbal medications, followed by modernization in the nineteenth century starting from alkaloid isolations and synthesis of chloral hydrate [1]. To this date, drugs have been contributing to lives and health of humankind.

There are still a number of diseases, whose drugs are much-anticipated to be developed. These include end-stage liver disease (ESLD), one of the causes of worldwide morbidity and mortality [2], which is mainly progressed from viral infections such as hepatitis C virus (HCV) [3]. The treatment options for ESLD are primarily limited to transplantations, while the number of donors is much less to cover that of patients [4,5].

Currently, the drug discovery/development process is toughening with increasing time and cost. For example, the total time from compound synthesis to New Drug Application approval was reported to be 12.8 years in the 1990s, which increased by more than 60% from 7.9 years in the 1960s [6]. The rise in the cost is more drastic; it was $138 million in 1979 [7], and it marked $1.3 billion in 2005 [8] (cf. **Figure 1.1**).

The biggest risk that pharmaceutical companies face during the development is the failures at the late stage, clinical testing [6]. For instance, an immunomodulatory drug, TGN1412, was applied to six healthy volunteers with five hundredth part of dosage proven to be safe by animal testing. Nevertheless, it brought immediate mortal danger to all the volunteers with multiple organ failures [9]. Another example is fialuridine, a nucleoside analogue for Hepatitis B virus infection. Fifteen patients were treated with the drug after it passed animal testing with different species (mice, rats, dogs, and monkeys). Despite a promising start, the human testing was terminated at weeks 13 due to sudden serious complications. Seven patients experienced abrupt onsets of hepatic failure and lactic acidosis; eventually, five of them lost their lives and two of them underwent the emergent liver transplantation. Drug failures could happen even at post-marketing. Vioxx was developed for inflammatory remedy, found to be causing heart attack after commercialization. It claimed a life of more than 27,000 people and more than $10 billion was needed for settlement [10]. Although animal testing is conducted to avoid such consequences at human testing and post-marketing, the overall success rate of drugs

throughout the human trial is 1 out of 9~10 [11,12], and toxicity accounts for over 20% which is the second behind inefficacy [11].

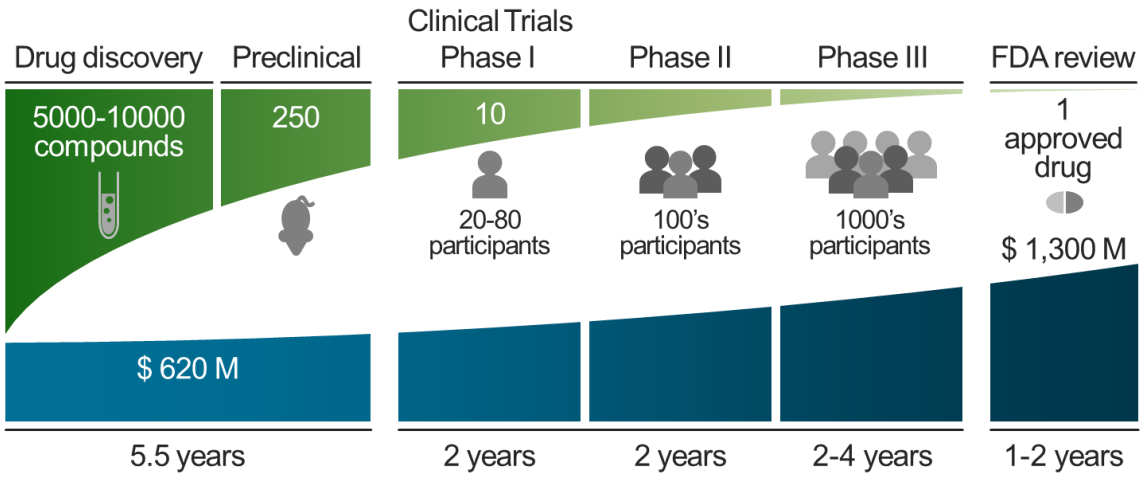

Figure 1.1 Drug development process of Food and Drug Administration (FDA) and its time [13] and cost [8].

One of the reasons why animal testing is not effective enough to predict human toxicity is species-specific metabolism. Once a xenobiotic is taken, it is metabolized first in the liver. The liver has human-specific activities of enzymes [14] and mitochondria [15] that could lead to unique metabolic pathway from the other animals [16]. In a different perspective, these metabolic activities make the liver as a prominent causative site of drug recalls among the organs [17]. Therefore, establishing an artificial liver ex vivo could be a potent tool to predict the human toxicity of the drugs, as well as a reliable platform for developing drugs of ESLD.

The liver has been known, perhaps from an era when myths of Prometheus passed by word of mouth, as the organ which is capable of regenerating itself in the body [18]. If the hepatocytes could regenerate themselves in vitro, it would be a compelling artificial liver platform. However, in practice, primary hepatocytes seeded on plain conventional substrates lose their function significantly [19]. Maintenance of hepatic functions ex vivo is formidable, let alone regeneration ability, and therefore extensive studies have been conducted as liver tissue engineering (LTE).

Many studies have reported that three-dimensional (3D) platforms are superior to those in two-dimensional (2D) platforms, supporting to enhance intercellular interactions

and maintenance of functions [20-22]. Indeed, in general, cells that reside in-vivo-like environment respond closer to in vivo. Still, there is a large gap between LTE platform designs and the liver complex structure. Aside from cells, the liver comprises of extracellular matrices (ECMs) with highly ordered, porous structure. It has been challenging to build such a protein-based architecture that mimic the complex liver configuration because of high viscosity and slowness in crosslinking.

A photocrosslinkable protein, gelatin methacryloyl (GelMA), is a good candidate to overcome these limitations. Gelatin is a hydrolyzed form of collagen, which is the main component of the liver structure [23]. While preserving biological advantages of collagen/gelatin, GelMA can be crosslinked in minutes in the presence of ultraviolet light and a photoinitiator. Also, due to reduced ionic interaction between molecules, an aqueous solution of GelMA is much less viscous compared to the parent materials. Since the synthesis method was developed in 2000 [24], GelMA is utilized in various bio-related applications [25]. However, the functionalization method has room to be modified to be more controllable and effective, which could be beneficial to tailor the mechanical stiffness of GelMA hydrogels.

As aforementioned, liver has highly ordered architecture with a million of regularly arranged hexagonal units called lobule. Inverted colloidal crystal (ICC) scaffolds are one of the promising systems to mimic the lobule structure. It possesses size-controllable, uniform pores that are hexagonally arranged and interconnected. Regarding LTE, early polyacrylamide ICC systems exhibited hepatosphere formation with maintained albumin production [26] and in vivo-like response against nanoparticle toxicity [27]. Recently we developed collagen-coated polyethylene glycol diacrylate (PEGDA) ICC scaffolds for enhancing cell-ECM interaction [28]. The presence of ECM led higher albumin production compared to bare PEGDA ICC, in which cells exhibited an aggregated shape [29]. Also, the albumin level depended on the amount of collagen coating. However, this ICC system requires an additional fabrication step of coating, which could be uneven and different by batch-to-batch. Protein-based ICC system would provide the innate bioactivity, and GelMA has advantages to aid the fabrication process with short crosslinking time and low viscosity. Previous attempts on GelMA macroporous structures showed good viability of the cells in the system. However those platforms lacked uniform

interconnectivity and also their efficacy on cellular function maintenance remained unexplored. The product of GelMA ICC could mimic the liver from materials and structural points of view. And with this emulation of hepatic microenvironment, liver cells in GelMA ICC are expected to retain their functions well.

1.2. Objectives and scopes

The overall goal of this thesis is to create a liver-mimicking platform for drug screening and discovery. We hypothesize that GelMA ICC scaffolds will provide an adequate environment for hepatocytes to maintain liver-specific functions. In order to test this hypothesis, specific aims are established as stated below;

Aim 1. To improve GelMA synthesis to be more efficient and controllable in a systematic manner

Aim 2. To characterize GelMA hydrogel physical properties comprehensively

Aim 3. To establish the fabrication method of GelMA ICC scaffolds

Aim 4. To examine efficacy of GelMA ICC scaffolds on hepatic function maintenance for LTE applications by utilizing a model hepatocyte cell line

1.3. Dissertation overview

This thesis is divided into six chapters. Chapter One gives the background information on LTE and design philosophy of the proposed artificial liver platform. Chapter Two covers the literature reviews including the liver function and structure, and studies conducted on LTE, ICC systems, and GelMA. In Chapter Three, improvements on GelMA synthesis by optimizing reaction conditions such as pH of the reaction solution and other parameters are described. Chapter Four explore comprehensive characterization of GelMA hydrogels from prospectives of mechanical stiffness, swelling, and enzymatic degradation. In Chapter Five, GelMA ICC fabrication and its application to LTE are described. Lastly, Chapter Six provides the conclusion of this dissertation, followed by proposed future research directions.

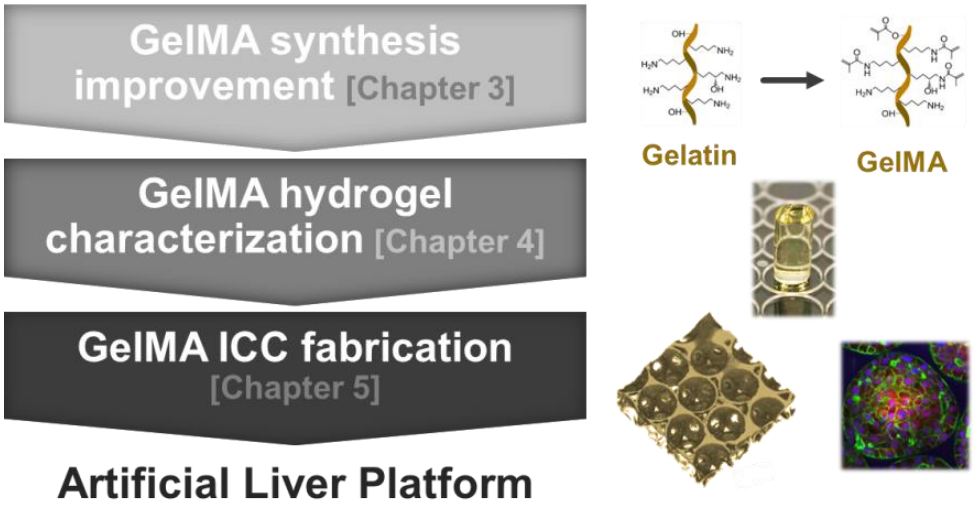

Figure 1.2 Graphical abstract of main contents of this dissertation.

1.4. Findings and Outcomes/Originality

This dissertation led novel outcomes by;

- Improving GelMA synthesis to be efficient and controllable in a facile way by optimizing pH of the reaction solution and other synthesis parameters
- Establishing GelMA ICC scaffold platforms for LTE applications, which can enhance liver functions of the hepatocytes

References

1 Sneader W. in *Drug Discovery: A History* (ed Sneader W) 1-7 (John Wiley & Sons, Ltd, 2006).

2 Lim Y-S, Kim WR. The Global Impact of Hepatic Fibrosis and End-Stage Liver Disease. *Clin Liver Dis* **12**, 733-746 (2008).

3 Shepard CW, Finelli L, Alter MJ. Global epidemiology of hepatitis C virus infection. *The Lancet Infectious Diseases* **5**, 558-567 (2005).

4 Thuluvath PJ *et al.* Liver Transplantation in the United States, 1999-2008. *Am J Transplant* **10**, 1003-1019 (2010).

5 Branger P, Samuel U. (Eurotransplant International Foundation, 2016).

6 DiMasi JA. Trends in Drug Development Costs, Times, and Risks. *Therapeutic Innovation & Regulatory Science* **29**, 375-384 (1995).

7 DiMasi JA, Hansen RW, Grabowski HG. The price of innovation: new estimates of drug development costs. *Journal of Health Economics* **22**, 151-185 (2003).

8 DiMasi JA, Grabowski HG. The cost of biopharmaceutical R&D: is biotech different? *Managerial and Decision Economics* **28**, 469-479 (2007).

9 Suntharalingam G *et al.* Cytokine storm in a phase 1 trial of the anti-CD28 monoclonal antibody TGN1412. *The New England journal of medicine* **355**, 1018-1028 (2006).

10 Horton R. Vioxx, the implosion of Merck, and aftershocks at the FDA. *The Lancet* **364**, 1995-1996 (2004).

11 Kola I, Landis J. Can the pharmaceutical industry reduce attrition rates? *Nature Reviews Drug Discovery* **3**, 711-715 (2004).

12 Hay M, Thomas DW, Craighead JL, Economides C, Rosenthal J. Clinical development success rates for investigational drugs. *Nat Biotechnol* **32**, 40-51 (2014).

13 Ciociola AA *et al.* How Drugs are Developed and Approved by the FDA: Current Process and Future Directions. *The American Journal of Gastroenterology* **109**, 620-623 (2014).

14 Martignoni M, Groothuis GM, de Kanter R. Species differences between mouse, rat, dog, monkey and human CYP-mediated drug metabolism, inhibition and induction. *Expert Opin Drug Metab Toxicol* **2**, 875-894 (2006).

15 Lee E-W, Lai Y, Zhang H, Unadkat JD. Identification of the mitochondrial targeting signal of the human equilibrative nucleoside transporter 1 (hENT1): implications for interspecies differences in mitochondrial toxicity of fialuridine. *J Biol Chem* **281**, 16700-16706 (2006).

16 Lu C, Li AP. Species comparison in P450 induction: effects of dexamethasone, omeprazole, and rifampin on P450 isoforms 1A and 3A in primary cultured hepatocytes from man, Sprague-Dawley rat, minipig, and beagle dog. *Chem Biol Interact* **134**, 271-281 (2001).

17 Piccini JP *et al.* Current challenges in the evaluation of cardiac safety during drug development: translational medicine meets the Critical Path Initiative. *Am Heart J* **158**, 317-326 (2009).

18 Taub R. Liver regeneration: from myth to mechanism. *Nat Rev Mol Cell Biol* **5**, 836-847 (2004).

19 Clayton DF, James E. Darnell J. Changes in liver-specific compared to common gene transcription during primary culture of mouse hepatocytes. *Molecular and Cellular Biology* **3**, 1552-1561 (1983).

20 Cukierman E, Pankov R, Stevens DR, Yamada KM. Taking cell-matrix adhesions to the third dimension. *Science* **294**, 1708-1712 (2001).

21 Dutta RC, Dutta AK. Cell-interactive 3D-scaffold; advances and applications. *Biotechnol Adv* **27**, 334-339 (2009).

22 Schmeichel KL, Bissell MJ. Modeling tissue-specific signaling and organ function in three dimensions. *J Cell Sci* **116**, 2377-2388 (2003).

23 Bedossa P, Paradis V. Liver extracellular matrix in health and disease. *J Pathol* **200**, 504-515 (2003).

24 Bulcke AIVD *et al.* Structural and Rheological Properties of Methacrylamide Modified Gelatin Hydrogels. *Biomacromolecules* **1**, 31-38 (2000).

25 Yue K *et al.* Synthesis, properties, and biomedical applications of gelatin methacryloyl (GelMA) hydrogels. *Biomaterials* **73**, 254-271 (2015).

26 Lee J, Cuddihy MJ, Cater GM, Kotov NA. Engineering liver tissue spheroids with inverted colloidal crystal scaffolds. *Biomaterials* **30**, 4687-4694 (2009).

27 Lee J, Lilly GD, Doty RC, Podsiadlo P, Kotov NA. In vitro toxicity testing of nanoparticles in 3D cell culture. *Small* **5**, 1213-1221 (2009).

28 Shirahama H *et al.* Fabrication of Inverted Colloidal Crystal Poly(ethylene glycol) Scaffold: A Three-dimensional Cell Culture Platform for Liver Tissue Engineering. *J. Vis. Exp.* **114**, e54331 (2016).

29 Kim MH *et al.* Phenotypic regulation of liver cells in a biofunctionalized three-dimensional hydrogel platform. *Integrative Biology* **8**, 156-166 (2015).

Chapter 2 Literature review

The liver has a complex architecture, comprised of a million of hexagonal units. This chapter presents liver biology and introduces strategies taken for engineering a liver-mimicking platform. The studies are viewed from the perspective of structures and materials. Along with the review, particular focuses are placed on studies on inverted colloidal crystal scaffolds and gelatin meathacryloyl, which are core elements of this dissertation.

2.1. Liver biology

2.1.1. Functions of the liver

The liver, the largest internal organ in the body, has a variety of functions to support human life activity. The number of functions is often referred as 500 [1,2]; nevertheless the essential actions can be grouped as 1) plasma protein synthesis, 2) drug metabolism, 3) macronutrient homeostasis, and 4) formation/secretion of bile.

The plasma proteins that the liver synthesizes include albumin, globulin, fibrinogen, and some specific proteins such as alpha 1-antitrypsin (AAT) [3,4]. Albumin is the highest protein component of plasma [5] and its main function is to regulate blood osmotic pressure, taking advantage of its low molecular weight (ca. 67 kDa) [3]. Also, it has various ligands to carry smaller substances (amino acids, drugs, hormones, etc.), aiding them to transport via blood [6]. AAT is a major protease inhibitor in the plasma [7]. Lack of AAT can damage tissues especially the lung, but also can cause liver failures and cirrhosis [8]. The liver is the principal site to synthesize these essential proteins [6,9] and therefore they are often used as functional markers in LTE.

Drug metabolism pathways in the liver are to alter the xenobiotics to be inactivated (Phase One: oxidation, reduction or hydrolysis) and be hydrophilic (Phase Two: complexing or conjugating) for excretion [3]. The Phase One is mainly exerted by groups of the enzyme, cytochrome P450 (CYP). Among its subfamilies, CYP3A is the most important as it engages biotransformation of approximately half of commercialized drugs [10]. However, the isoforms vary across species, which causes ineffective translation of drug toxicity from animal to human. Regarding human, there are four CYP3A members and all of them are human-specific; namely CYP3A4, CYP3A5, CYP3A7 and CYP3A43 [11]. Both CYP3A4 and CYP3A5 play major roles, while catalytic activities are higher with CYP3A4 [12]. Another isoform, CYP3A7, is predominant in the fetal liver and its presence is reduced in the adult liver (averaging 1.6% of CYP3A4 expression) [13]; nevertheless, it has a high catalytic activity for specific hormones and retinoic acids [14]. As for CYP3A43, its function is not well revealed, and its transcription level is limited to around 0.2% of CYP3A4 [15].

Glucose homeostasis is also one of the unique features of the liver. When the blood has high sugar level, glucose is transported into the liver and phosphorylated to encage it

within the cellular membrane. The altered glucose, glucose-6-phosphate, is a key intermediary compound that can undergo different metabolic pathways (e.g. being altered further into glycogen for storage). At a hypoglycemic state, an enzyme, glucose 6-phosphate (G6Pase), dephosphorylates glucose-6-phosphate back to glucose. The glucose is eventually released into the blood by facilitated diffusion, and thus the sugar level in the blood is maintained [16].

Bile is a complex fluid, with bile acids, lipids, cholesterol, etc., and the liver accounts for 60-70% of its production [17]. The bile acids are especially important as they emulsify fats and fat-soluble vitamins to be easily digested in the small intestine. The liver is the only site for bile acids synthesis [18].

These diverse liver functions are regulated by different hepatocyte nucleus factors (HNFs), which transcript genes into proteins. One of the HNFs that play the central roles in differentiated hepatocytes is HNF4α, involving CYP activities [19], glucose secretion [20], lipid homeostasis [21], and bile acid synthesis [22]. Also, HNFs regulate one another; for example, HNF6 controls HNF4α [23] and HNF3α [24], as well as a wide variety of liver-specific genes [25].

2.1.2. Liver structure and composition

As briefly described in Background section, the liver is comprised of a million of hexagonally-arrayed micrometric units (**Figure 2.1**). This unit, lobule, is around 1 mm in diameter and 2 mm in thickness [26]. The main component of the liver is a parenchymal cell, hepatocyte, which spreads cord-like from the central vein. The adjacent cells are connected by tight junctions, and they occupy 78% of the liver volume [27]. Sinusoids spread over the lobule between the cords, supplying blood via large surface area.

The hepatocytes are polygonal-shaped cells with a diameter of 13-30 um [28]. They take the most of the roles of diverse liver functions. As their oxygen uptake is higher than other cells [29], sufficient oxygen provision via blood is crucial.

Other non-parenchymal cells, such as Kupffer cells, sinusoidal endothelial cells, stellate cells, occupy only 6.3% of the volume [27]. However, they play important roles in producing cytokines for regeneration and inflammatory response [30].

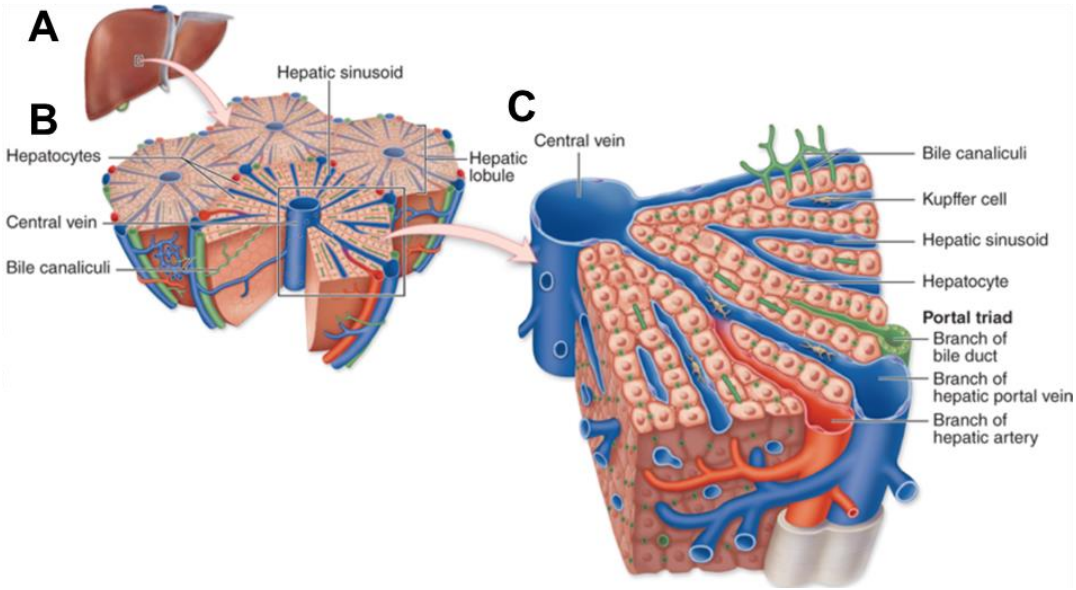

Figure 2.1 The schematic illustrations of **(A)** the liver, **(B)** the hexagonal liver units, lobules, and **(C)** the detail of the lobule microstructure. Redrawn from reference [31].

2.1.3. Extracellular matrices in the liver

Extracellular matrices (ECMs) are non-cellular macromolecules that provide structural integrity and modulate biological processes such as cell attachment, migration, signal transduction, and development [32]. Specifically, as for the liver, they play an important role to maintain differentiation of hepatocytes [33].

Collagens are the most abundant ECM in the liver [34], as well as in the human body [35]. To date, at least 29 different types of collagen were identified [36], yet in common, they have helical structures with three polypeptide chains. Each chain is composed of tripeptide (Glycine-X-Y) repetition, where often X and Y are proline and hydroxyproline, respectively. Also, they have arginine-glycine-aspartic acid (RGD) motifs that can involve cell attachment via integrin.

Fibronectin is another predominant ECM in the liver [37], who has dimer structure with two long peptide chains. It has various domains for cells (e.g. RGD) and ECMs (e.g. collagen and fibrin) to reinforce cell and ECM bindings [38].

In the liver, those ECMs are locally distributed as shown in **Figure 2.2** [37]. Basement membrane proteins such as collagen type IV and laminin are located near the central vein and portal triad (cf. **Figure 2.1C**), compositions of which are analogous to that of other

epithelial organs [26]. In contrast, in the parenchyma, the basement membrane proteins are absent; ECMs in parenchyma dwell in the gap of 0.2-0.5 μm between hepatocytes and sinusoids, called "space of Disse [27]." The site is occupied by mainly fibronectin and collagen type I and as well as a smaller amount of collagen type III and IV [37].

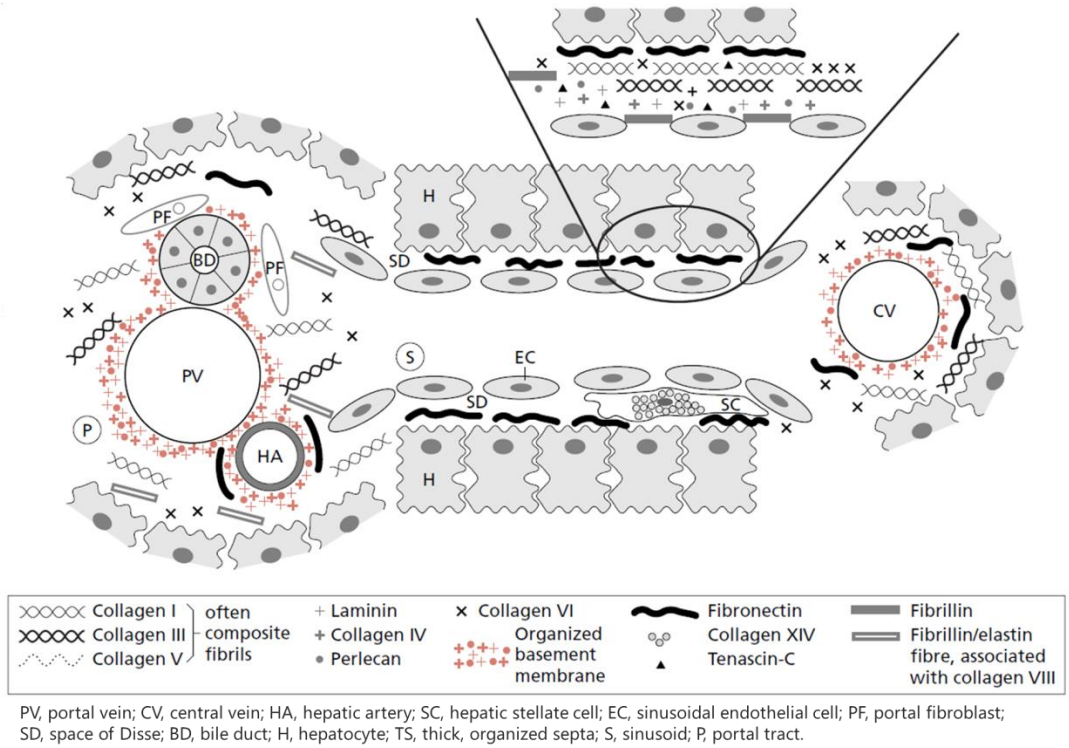

Figure 2.2 Localized ECMs in the liver. Redrawn from reference [37].

2.2. Cell sources of liver tissue engineering

From this subchapter, approaches as LTE are described in different views. As for cells, it is always ideal to use primary liver cells from tissues to engineer an artificial liver. Primary human- and alternatively rat-hepatocyte have been utilized to assess the system on cell function maintenance. However, they have limitations in availability, phenotypic stability over the culture and consistency (donor-dependent), which is constitutive for personalized drug screening but is difficile for high-throughput screening purpose. Therefore hepatocellular carcinoma cell lines, which show liver-specific functions, have also been employed as model cells. The cell lines include HepG2 [39], KYN-1 [40], KYN-2 [41] and Huh7 [42]. The most widely-used cell line is HepG2; meanwhile, a study on gene

expression showed the highest efficacy with Huh7 [42]. A subclone of Huh7, Huh7.5 [43], is permissive to Hepatitis C Virus (HCV) and also used extensively. A platform with such type of cells could be not only a versatile hepatotoxicity tool but also a potent platform for developing drugs for ESLD.

2.3. System designs for liver tissue engineering

2.3.1. 2D systems

In 1983, Clayton et al. reported their experimental result on primary rat hepatocyte seeded on the normal 2D substrate, which showed rapid vanishment of albumin expression within 24 h [44]. Indeed primary hepatocytes cultured in the conventional 2D system lose their hepatic functions within days [45]. Decades of studies have been conducted for maintaining phenotype from different approaches.

Some of the initial studies were directed toward co-culture of feeder cells with hepatocytes. Not only non-parenchymal liver cells [2,46,47] but also various types of cells have been employed; including kidney epithelial cells [48], umbilical vein endothelial cells [49], bone marrow cells [50], pancreatic islets [51] or embryonic fibroblasts [52,53]. Overall heterotypic cellular contact and cytokines from these cells aided hepatocyte with high viability and maintenance of hepatic functions [46,54]. The most widely-used cell is rat embryonic fibroblast, 3T3 cells, and some studies reported the highest albumin production with 3T3 cells among several types of cells co-cultured with rat hepatocytes [55,56].

Another approach was a surface coating of the substrate, on which cells were cultured. The major coating materials are ECMs, which approximate the environment closer to in vivo. The materials include collagen [57], liver ECM extracts [58], laminin-rich tumor-derived matrix (Matrigel® [59]). Cells on those coated-substrates could exhibit longer lifetime and function maintenance in comparison to conventional polystyrene (PS) substrates.

To organize cells in lobule-like structure, some attempts were made from engineering approach. One of the pioneering studies was conducted with a micro-patterned system (**Figure 2.3A**) [60]. They seeded primary rat hepatocyte or lung endothelial cells onto an etched silicon wafer; hepatocyte on the wafer maintained albumin production constantly

until four days. Ho et al. took a similar approach but allowed more precise distribution of HepG2 and endothelial cells with the use of dielectrophoresis of the cells (**Figure 2.3B**) [61]. The result showed enhancement of one of the hepatic functions, CYP1A1 enzyme activity, compared to mono-culture and non-patterned culture. However, these 2D system designs have a limitation in cell-cell and cell-ECM interactions, which were found to be essential.

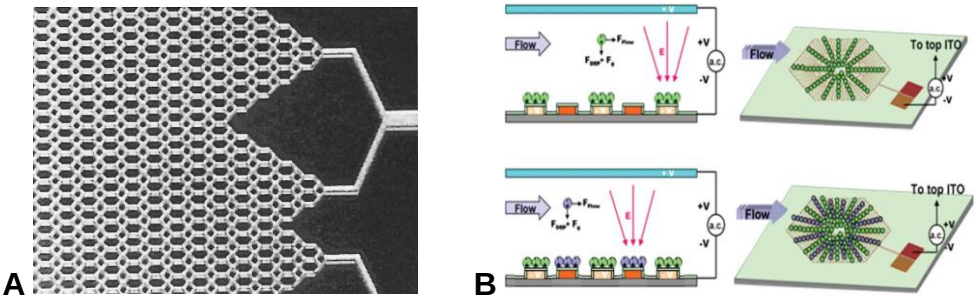

Figure 2.3 Engineering approaches to reconstruct liver-mimicking structure in 2D. **(A)** Micro-patterned wafer, made of silicon and Pyrex. Adopted from reference [60]. **(B)** Lobule-like patterned electrodes to arrange cells by dielectrophoresis. Adopted from reference [61].

2.3.2. 3D systems

The human body is a 3D complex, which has a greater extent of cell-cell and cell-ECM interactions in contrast with 2D culture systems. Studies on tissue engineering are revealing that cells in 3D systems can respond closer to in vivo regarding morphology and functions [62-64].

One of the pioneering 3D approaches in LTE is collagen sandwich configuration by Dunn et al. in 1989 [33] as illustrated in **Figure 2.4A**. In this study, they seeded primary rat hepatocytes onto collagen gel, followed by casting of second collagen layer after one day. Interestingly, this difference of one layer could lead maintenance of polygonal morphology and albumin production for 42 days [33,65]; nonetheless, retention of CYP activity was found to be limited [66]. Cell-matrix interaction can be further enhanced in the form of cell encapsulation, which is to confine the cells in polymer network of low density. This covers non-crosslinked solution (e.g. chitosan [67] and alginate [68,69], as shown in **Figure 2.4B**) as well as crosslinked gels (e.g. collagen [70], synthetic peptide [71,72] and poly(ethylene glycol) diacrylate [PEGDA] [73-75]), inclusive of their composites.

These approaches could alter cellular morphology with longer function maintenance than 2D system [67,73]; however, they lack interplay between cells.

Besides 3D interaction with matrices, studies on hepatospheres revealed that 3D homotypic cellular interaction of hepatocytes are vital as well. In early studies, hepatospheres were formed by culturing cells onto a flat substrate, which was positively-charged [76] and/or coated by proteoglycans [77] (**Figure 2.4C**). Subsequent advanced systems include hanging-drop culture system [78,79], micro-molding techniques [80,81] (**Figure 2.4D**) and rotary cell culture system [82,83], that provided better size control, oxygen supply to the cells, faster spheroid formation, and so on. The hepatospheres exhibited upregulated expressions of adherens junction and tight junction [84,85], emulating vivo situation closely where hepatocytes are securely connected via cell junctions [86]. Indeed a comparative study of 'encapsulated spheroids' and 'encapsulated single cells' revealed the relevance between cell junctions and maintaining hepatic functions [67]. Through a variety of studies, hepatospheres showed prolonged lifetime and hepatic functions as well as efficient hepatotoxicity response [75,87]. However, they have size limitation at around 200 μm, beyond which the hepatocytes in the core of hepatosphere started to suffer from oxygen depletion [88]. Further, the system by its nature lacks cell-ECM interaction.

Some studies explored 3D constructs for hepatocyte seeding; such as sponge-like structure [89-91] and fibrous system [92]. These constructs have larger freedom in system designing (material, porosity, etc.); nevertheless, they lack spatial control over the system.

Advancements in hydrogel-related studies (cf. Subsection 2.4) and microfabrication techniques allowed further strategies to engineer liver-mimicking structures. For example, implementation of the microfluidic system led to the formation of hepatic-cord like structures with the endothelial-like flow as shown in **Figure 2.4E** [93]. Photolithography technique has been applied to obtain cell-laden hydrogels in delicate, liver-like configurations [94-96] (**Figure 2.4F**, **G**). The rise of 3D printing techniques allowed direct designing of 3D scaffolds [97] as well as bioprinting [98,99], whose precursor solution contains cells. In order to overcome the lack of hepatocyte homotypic interaction in cell-laden hydrogel systems, preformed hepatospheres can be incorporated into bioprinting [100] (**Figure 2.4H**). These types of fabrication methods can mimic the lobule structure

better and are ideal for prototype testing; however, they could have a limitation in mass fabrication.

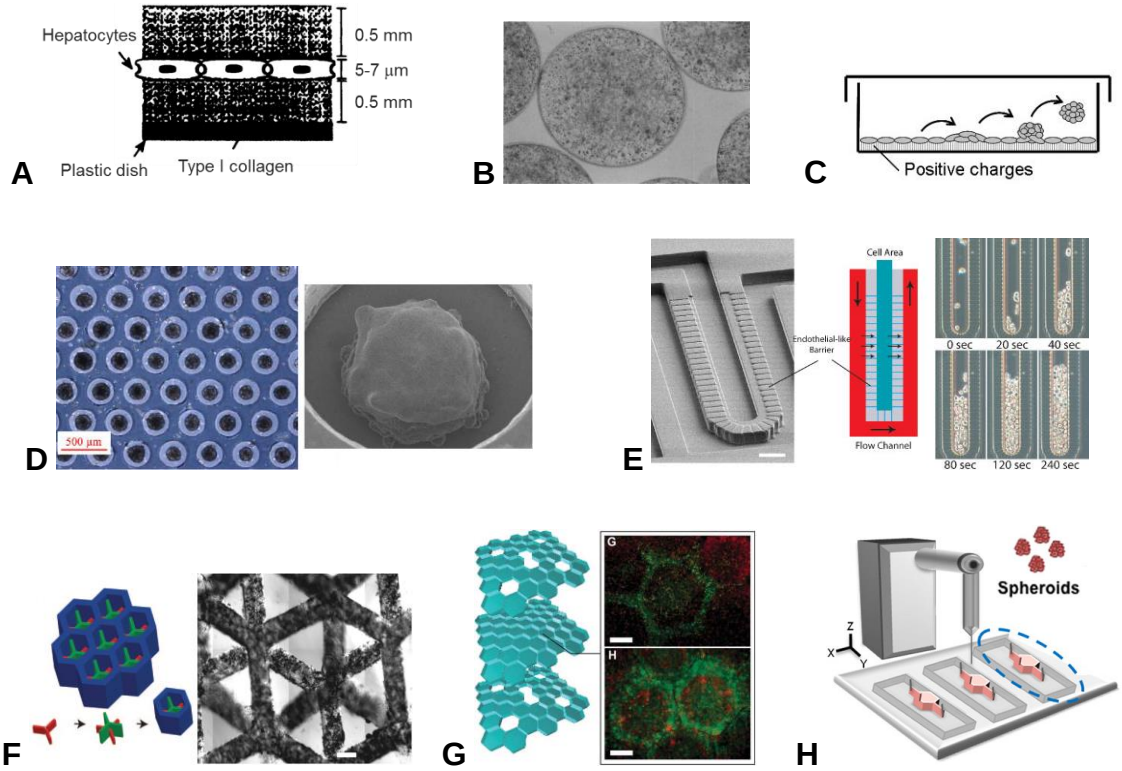

Figure 2.4 Engineering approaches to reconstruct liver-mimicking structure in 3D. **(A)** Collagen sandwich configuration. Redrawn from reference [101]. **(B)** Cell encapsulation in alginate capsules, with a diameter of 0.4-0.5 mm. Adopted from [68]. **(C)** One of the early studies on hepatosphere formation. Adopted from [85]. **(D)** Hepatosphere formation in microwells. Redrawn from reference [80]. **(E)** Hepatic cord-like structure with the endothelial-like flow in the microfluidic system. Redrawn from reference [93]. **(F)** Lobule-like construct by photolithography. Redrawn from [94]. **(G)** The multilayered construct of cell-laden hydrogels. Redrawn from reference [95]. **(H)** Incorporation of bioprinting and microspheres to improve hepatocyte intercellular interaction. Redrawn from reference [100].

Inverted colloidal crystal system

On the other hand, inverted colloidal crystal (ICC) shaped constructs have been developed for versatile applications from photonic devices [102] to energy storage [103]. **Figure 2.5** shows the general fabrication procedure with a base material and sacrificial colloidal crystal lattice [104,105]. It has following advantages: a three-dimensional structure with hexagonal and uniform configuration, size-controllable cavities, and the presence of

interconnection between the cavities. Also, compared to prototype-friendly 3D printing techniques, this process is more compatible with mass production.

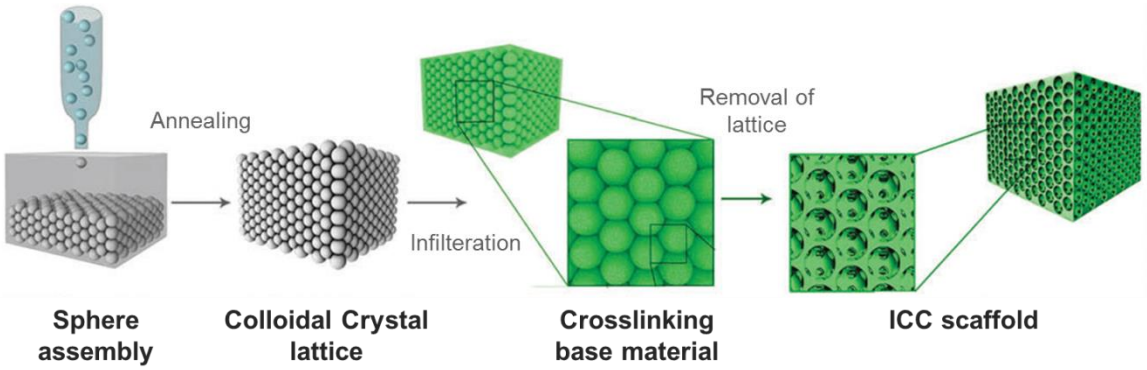

Figure 2.5 Schematic illustration of ICC fabrication process. Redrawn from reference [104].

As for tissue engineering purpose, it was first applied by Peter et al. as the development of PLGA ICC scaffolds on 2001 [106]. Following studies affirmed the efficacy of ICC structure, such as the positive impact of scaffolds' uniformity on cell fate [107], cavity-size dependent influence on cell function maintenance [108,109] and internal diffusion of nutrients/oxygen [110].

To date, various studies were conducted on ICC scaffolds with different cells and materials. The cells include fibroblast [107,111-114], bone marrow stromal cells [115-121], chondrocytes [122,123], stem cells [124-131] and so on. With regards to the liver cell, Kotov et al. first applied with HepG2 cells, demonstrating hepatospheres in the lobule-like cavities (≥ 75 μm) with long-term survival [121]. As for their functions, Lee et al. investigated albumin production of hepatocytes in ICC scaffolds of different pore sizes (50-200 μm) [109]. Initially, cells in smaller cavities (yielding smaller size of hepatospheres) showed a higher secretion level, but those from cells in larger cavities nearly caught up after eight days of culture. Also, the same system with 150 mm-diameter was applied to nanoparticle toxicity check, showing a similar response to in vivo compared to that of the 2D system [132]. However, these scaffolds were made from poly(acrylamide) (PAM), lacking cell-ECM interaction (cf. **Figure 2.6**). Recently our group developed collagen-coated poly(ethylene glycol) diacrylate (PEGDA) ICC scaffolds [133]. Hepatocytes in these scaffolds could have both cell-cell and cell-ECM interaction eminently. The ECM

coating led higher albumin production compared to bare PEGDA ICC, in which cells exhibited aggregated shape. Also, the albumin level depended on collagen amount; cells in contact with a higher amount of collagen led higher albumin production.

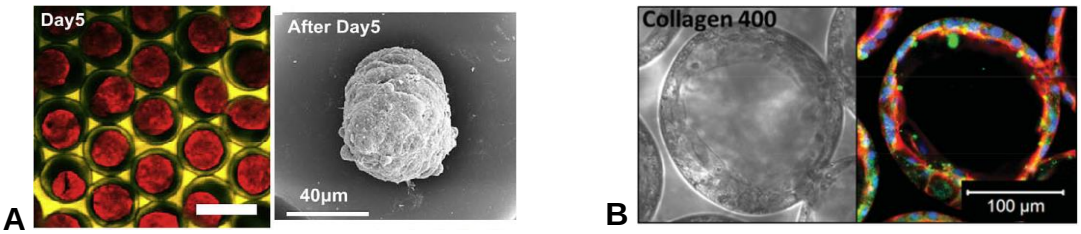

Figure 2.6 Hepatocytes in ICC systems. **(A)** PAM ICC scaffolds. Redrawn from reference [109]. **(B)** PEGDA with collagen layer, conjugated on the surface. Adopted from reference [133].

In terms of materials for ICC scaffolds, most of the approaches were from synthetic polymers (cf. next subsection), such as aforementioned PAM [109,127,128,132,134-139], poly(lactic-co-glycolic acid) (PLGA) [106-108,140-146], poly(ethylene glycol) diacrylate /dimethacrylate (PEGDA or PEGDMA) [104,111,133], Poly(2-hydroxyethyl methacrylate) (PHEMA) [117,129,131,147-150] etc. In order to add bioactivity to the scaffolds, surface coatings were implemented in some studies (collagen [104,133,136,138,147], fibronectin [139] etc.). However, these surface modification method requires one additional step, which could cause uneven coating and batch-to-batch difference. There are fewer but some scaffolds, which are made from native natural polymers such as alginate, chitosan, and gelatin as shown in **Table 2.1**. These systems could provide innate biological cues. However, the base material solutions were prepared at below 10%, due to the high viscosity of aqueous natural-polymer solution [151]. This low concentration can lead to repetitions of the process or low mechanical strength. Also, most systems employed chemical crosslinkers (calcium chloride, genipin, etc.) for crosslinking, which require longer processing time and could result in inhomogeneous crosslinking over the samples.

Recently, Kim et al. developed ICC system based on functionalized protein, gelatin methacryloyl (GelMA) [152]. This photocrosslinkable material allowed crosslinking within 20 min, directly after infiltration. Also, the functionalization reduced intermolecular ionic interaction, reducing the viscosity of the aqueous solution. Hence the concentration was increased to 20%. Mouse mesenchymal stem cells seeded in the scaffolds were highly

viable. However, the system does not have a uniform the structure, as the sacrificial alginate lattices were utilized without annealing. Furthermore, their efficacy on cell function maintenance has not been investigated. Fu et al. demonstrated GelMA macroporous hydrogels to support vascularization in vivo [153]. Yet this system lacks structural uniformity. And importantly, none of the natural polymer-derived ICC scaffolds have been applied to LTE, which keeps their potential veiled.

Table 2.1 Natural polymer-based ICC systems and their applications, crosslinking methods, spheroid size, crosslinking time, base material concentration, and structural characteristics.

Materials	Function/ application	Crosslink-ing method	Spheroid size (μm)	Fabrication procedure and the time*	Concen-tration (w/v %)	Ref
Natural polymer-based ICC systems						
Alginate	Able to disinte-grate in 10 min[b]	$CaCl_2$	250	I: Us.[c], F: 5 h, D: overnight, C: 1 h	4	[130]
Alginate/poly(g-glutamic acid)	Neural tissue engineering	$CaCl_2$ and EDC[d]	158	I: 50min, C: 24 h, D: 24 h (I + D were repeated 8 times)	3	[124,125]
Chitin/chitosan	Cartilage tissue engineering	Genipin	160	I: Us.[c], C: 24 h, D: 24h (I + D were repeated 8 times [122])	3-4	[122,123]
Chitin/chitosan /gelatin	Neural tissue engineering	Genipin	160	I: Us.[c], C: 24 h, D: 24h (I + D were repeated 5-8 times)	2.5	[126]
Chitosan	Hypoallergenic, antibacterial	Physical	148	I: Us.[c], F: 5 h, D: overnight	1	[154]
Chitosan/gelatin	Neural tissue engineering	Genipin	160	I: 50 min, C: 24 h, D: 24h (I + D were repeated 5-8 times)	5	[118,119]
Fibroin	Biophotonics	Physical	0.25-0.35			[155]
Protein-based porous systems						
Bovine serum albumin	Fluidic system	Glutaral-dehyde	0.5	I: 24 h, C: 6 h	4	[156]
GelMA	Regenerative medicine, vascularization	Ultraviolet (UV) light	156, 500-1500	I: Us.[c], C: 5 [153] or 20 [152] min	20	[152,153]
Fibroin	Biophotonics	Physical	0.25-0.5	I&D: 1 [157] or 4 [151] days, C: 1 h	3-8	[151,157, 158]

* I: infilteration, F: freezing, D: drying, C: crosslinking
[a] Concentration of base material, [b] With presence of K_2HPO_4 and ethylenediaminetetraacetic acid (EDTA)
[c] Us.: Unspecified, [d] EDC: 1-ethyl-3-(3-dimethylaminopropyl)carbodiimide hydrochloride

2.4. Materials used for liver tissue engineering

2.4.1. Synthetic polymers

In this subsection, materials used for LTE is described. They are mainly polymers, which can be classified into two groups as synthetic polymers and natural polymers. Synthetic polymers are made from petroleum. Compared with natural polymers, synthetic polymers have following advantages in general; mass production with higher reproducibility, controllable property (e.g. molecular weight), higher mechanical stiffness, and wider options of chemical functionalization as seen in **Table 2.2**.

Table 2.2 Comparison of general characteristics of synthetic and natural polymers used for tissue engineering purpose

Feature/function	Synthetic polymers	Natural polymers
Bioactivity (e.g. RGD)	Limited	**High**
Biocompatibility	Material dependent	**Mostly applicable**
Biodegradability	Material dependent	**Mostly applicable**
Chemical modification	**Relatively wider options**	Relatively limited
Controllability, reproducibility	**High**	Relatively low
Mechanical strength	**Relatively high**	Relatively low

Most widely-used synthetic materials include PAM, PLGA, and poly(ethylene glycol) (PEG) derivatives, which were employed for ICC scaffolds fabrications (cf. previous subsection).

PAM is composed of a repetition of ($-CH_2CHCONH_2-$) unit and utilized in early LTE to immobilize sugar [159-161] (and recently ECMs [162]). The typical crosslinking method is to utilize N,N'-methylenebisacrylamide as a crosslinking monomer with ammonium persulfate and N,N,N',N'-tetramethylethylene-diamine as initiators. Although PAM is biocompatible, there could be some residues of monomer (acrylamide), which is toxic to the cells [163].

PLGA is a co-polymer of lactic acid and glycolic acid. It is a biocompatible material with biodegradability, which can be tailored by the composition ratio. Regarding the formation, simple, direct condensation method is usually adopted. It is utilized in various systems such as a low adherent substrate for spheroid formation [164], fibrous systems

[165,166], 3D solid supports [167], spongy systems [168,169], etc. Since the material is approved for therapeutic use, it is extensively applied for in vivo experiments as well [170-172].

Poly(ethylene glycol) (PEG) is a molecule with repeating ($-OCH_2CH_2-$) units, possessing advantages of biocompatibility, high solubility in water and organic solvents, being easy to be chemically modified, and absence of immunogenic/toxic response. In tissue engineering, particularly PEGDA/DMA has been used, which can be crosslinked in the presence of UV light and photoinitiator [173]. As for LTE, PEGDA/DMA has been utilized for cell encapsulation [73,74,174], micro-patterned system [94], bioink [175], in vivo application [176] and so on.

Despite these advantages, synthetic polymers inevitably lack bioactivities. Especially cell attachment sites (e.g. RGD) are essential not only for adhesion but also to have proper signaling pathway [177]. Therefore in most cases, they are utilized together with natural polymers which are described below.

2.4.2. Natural polymers

Natural polymers are composed of materials that exist in nature such as collagen and fibronectin. They are mostly biocompatible, degradable and possessing innate bioactivities that can affect cell morphology, function, differentiation, fate, etc.

In LTE, the most used natural polymer is collagen. As mentioned in Subsection 2.1.3, it is the most abundant ECM in the liver; therefore the utilization of the collagen can make the system closer to the in vivo environment. It has been utilized for early sandwich culture [33,65] to microfluidic systems [178,179], in vivo study [180] and so on. Also, it has been employed with other materials for adding biological features; the presence of collagen can enhance cell attachment [57], proliferation [133], functions [33,65], etc.

Gelatin is obtained by partial hydrolysis of collagen via acid (pH 1-2) or alkali (pH 12-13) process with a final ultra-heat treatment [181]. These treatments reduce the antigenic aromatic groupings, and therefore gelatin is less immunogenic than collagen [182,183]. Also, it is much less expensive compared to the parent material. Besides, gelatin inherits the advantages of collagen and widely used for 3D cell supports [184,185], bioink [186,187], in vivo study [188] and so on.

Fibronectin is one of the abundant ECMs in the liver, owning different domains for strengthening cell-ECM bindings (c.f. Subsection 2.1.3). However, in LTE, fibronectin is less utilized compared to collagen/gelatin, probably due to its expensiveness. Nevertheless, some studies utilized fibronectin for surface coating [189,190]. Fibronectin itself has the effect to maintain hepatic functions, and they can be further facilitated by mixing with other ECMs [190,191].

Alginate, one of the anionic polysaccharide, can be obtained from brown algae. It possesses advantages of being non-animal source (not immunogenic), able for ionic crosslinking (e.g. with calcium chloride), and relatively low in cost; these allowed the material to be widely employed for LTE including cell encapsulation systems [68,69,192], non-adhesive porous scaffold applications for hepatosphere formation [186], and bio-artificial liver applications [193].

Table 2.3 Natural polymers and their features and advantages on LTE

Natural polymer	Features	Advantages
Collagen	Most abundant ECM in the liver	Cell attachment sites Elongated cell viability Enhanced hepatic functions
Gelatin	Partially hydrolyzed collagen	Inherited advantages from collagen Less immunogenic Economical
Fibronectin	Most abundant in the space of Disse	Cell attachment sites Enlonged cell viability Enhanced hepatic functions
Alginate	Obtained from seaweeds	Non-animal source (not immunogenic) Non-adhesive property for hepatosphere formation Ionic crosslinking Economical

Gelatin methacryloyl

As introduced in the previous subsection, gelatin is one of the attractive biomaterials with good bioactivities and relative inexpensiveness. However, raw gelatin can only form physically crosslinked hydrogels at limited ranges of mass concentration and temperature, yet the hydrogels have weak mechanical integrity. In order to maintain mechanical strength, different covalent crosslinking methods were developed. One of them is to pour

an aqueous solution of chemical crosslinkers (e.g. glutaraldehyde [194] and genipin [195]) into gelatin substrate, which is normally dried or physically crosslinked. An alternative method is to functionalize the gelatin with chemical reagents (e.g. methacrylic anhydride [MAA] and glycidyl methacrylate [196]) to be photocrosslinkable. This method enables quicker, more homogeneous and in situ crosslinking with better control over hydrogel density.

GelMA is a popular type of photocrosslinkable gelatin, which has been utilized for wide bioapplications (e.g., micropatterning [197,198], fluidic systems [199,200], 3D scaffolds [201,202], bioprinting [99,203-205]) with different cells (e.g., fibroblasts [206-208], stem cells [209,210], cartilage [203,211], hepatocytes [99,197]) and composite materials (e.g., carbon nanotubes [212], graphene oxide [213,214], natural polymers [215,216], synthetic polymers [217,218]). The synthesis method is originally developed by Van den Bulcke et al. in 2000, which is to let amino groups of lysine and hydroxyl lysine of gelatin react with MAA in phosphate-buffered saline (PBS) [219]. Their work opened up the new field of research with the material for bioengineering and regenerative applications. Its hydrogels with different mechanical stiffness and crosslinking density are obtainable by changing the ratio of MAA to gelatin and alter the degree of substitution (DS). Also, the aqueous solution of GelMA has low viscosity due to functionalization of the amino groups, reducing intermolecular ionic interactions with carboxyl groups. Moreover, this functionalization does not impair bioactivities of gelatin (cell attachment, biodegradability, etc.), in particular, RGD sites that do not involve in the reaction with MAA. However, GelMA synthesis routes remain suboptimal, leaving room for improving its controllability and efficacy. For example, theoretically, one MAA molecule could react with one amino group. Nonetheless, studies following the original method have reported using an 18-47 molar excess of MAA to obtain GelMA of high DS (> 85%) as summarized in **Figure 2.7**.

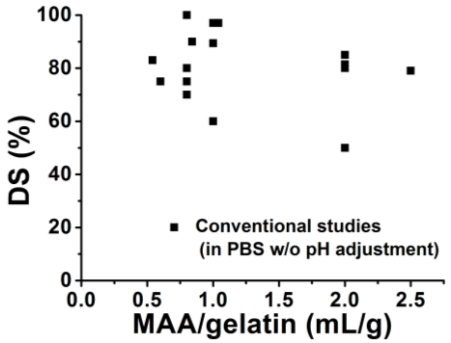

Figure 2.7 Ratio between MAA and gelatin (mL/g) in previous studies that follow the original method. Redrawn from reference [220].

Different attempts have been made in order to improve the reaction efficacy. For instance, Martineau et al. chose a water-miscible organic chemical (dimethyl sulfoxide) as the solvent instead of PBS [221]. This method could hamper hydrolysis of MAA that caused by its contact with water, and improved the DS comparing to the case of using PBS. However, it requires the organic base and an additional precipitation step of with ethanol, which leads to a low yield [152,221]. Another way of improvement is to conduct pH adjustment during the synthesis. This is to maintain the pH of the reaction solution above the isoelectric point (IEP) of gelatin, keeping the free amino groups neutral to let them react with MAA. The use of PBS (pH 7.4) as a buffer is not strong enough for pH maintenance due to a byproduct of the reaction, methacrylic acid, which alters the pH to acidic. Although pH adjustment could improve the efficacy, it still requires a 10–32 molar excess of MAA [222-224]. Further, manual pH adjustment is laborious, and the resulting DS can depend on the operating technique.

Overall, the synthesis methods of an attractive biomaterial, GelMA, have been requiring much MAA consumption and they are not controllable; it is hard to predict what amount of MAA results in a certain DS (cf. **Figure 2.7**). Moreover, the synthesis parameters such as reaction temperature and reaction time are not fully examined. The GelMA synthesis has some room to be improved.

2.5. Summary: Rationales of system design

In order to build an artificial liver platform for drug screening and development, it is important that the platform is not only effective but also amenable for mass production.

Toward that end, as for cells, hepatocellular carcinoma cell lines were selected in lieu of primary human hepatocytes. Among the cell lines, Huh7.5 was chosen for their characteristic of HCV permissivity. With this model cell, a designed platform could be a potent platform to develop drugs for the acute liver diseases, in addition to being a versatile tool for hepatotoxicity testing.

The configuration chosen for the platform was ICC, which is similar to the structure of liver lobule. It has the uniform, interconnected cavities that realize good diffusivity of oxygen and nutrients into the structure. This accessibility is especially important for hepatocytes as their oxygen uptake is high. Also, the 3D cell culture in ICC system can enhance intercellular interaction, which is found to be essential for the hepatocytes to maintain their functions.

It is imperative for the cells to have sufficient physical and biochemical supports. Regarding material, GelMA was chosen as it is biocompatible, less immunogenic, possessing cell attachment sites, and relatively inexpensive. It is compatible with ICC fabrication process since GelMA is low in viscosity, allowing easy infiltering of its aqueous solution into sacrificial lattices. Also, it can be crosslinked in fast and uniform fashion via photopolymerization.

In summary, on the basis of literature review, GelMA ICC scaffold with Huh7.5 cells was designed as the artificial liver platform.

References

1 Bhatia SN, Underhill GH, Zaret KS, Fox IJ. Cell and tissue engineering for liver disease. *Sci Transl Med* **6**, 245sr242 (2014).

2 Shulman M, Nahmias Y. in *Epithelial Cell Culture Protocols: Second Edition* (eds Randell HS, Fulcher LM) 287-302 (Humana Press, 2013).

3 Campbell I. Liver: metabolic functions. *Anaesthesia & Intensive Care Medicine* **7**, 51-54 (2006).

4 Bhan AK, Grand RJ, Colten HR, Alper CA. Liver in α_1-antitrypsin deficiency: morphologic observations and in vitro synthesis of α_1-antitrypsin. *Pediatr Res* **10**, 35-40 (1976).

5 Schaller J, Gerber S, Kämpfer U, Lejon S, Trachsel C. in *Human Blood Plasma Proteins: Structure and Function* Ch. 3, 17-20 (John Wiley & Sons, Ltd, 2008).

6 Weisiger RA. in *Textbook of Hepatology: From Basic Science to Clinical Practice, Third Edition* (eds Rodés J *et al.*) Ch. Synthetic function, (Blackwell Publishing Ltd, 2008).

7 Laurell C-B. in *Protides of Biological Fluids: Proceedings of the Twenty-second Colloquium* (ed Peelers H) 3-12 (Pergamon Press, 1974).

8 Graziadei IW *et al.* Increased risk of chronic liver failure in adults with heterozygous α_1-antitrypsin deficiency. *Hepatology* **28**, 1058-1063 (1998).

9 Janciauskiene SM *et al.* The discovery of α1-antitrypsin and its role in health and disease. *Respir Med* **105**, 1129-1139 (2011).

10 Zuber R, Anzenbacherová E, Anzenbacher P. Cytochromes P450 and experimental models of drug metabolism. *Journal of Cellular and Molecular Medicine* **6**, 189-198 (2002).

11 Martignoni M, Groothuis GM, de Kanter R. Species differences between mouse, rat, dog, monkey and human CYP-mediated drug metabolism, inhibition and induction. *Expert Opin Drug Metab Toxicol* **2**, 875-894 (2006).

12 Wrighton SA *et al.* Studies on the expression and metabolic capabilities of human liver cytochrome P450IIIA5 (HLp3). *Mol Pharmacol* **38**, 207-213 (1990).

13 Burk O *et al.* Molecular mechanisms of polymorphic CYP3A7 expression in adult human liver and intestine. *J Biol Chem* **277**, 24280-24288 (2002).

14 Rodriguez-Antona C, Jande M, Rane A, Ingelman-Sundberg M. Identification and phenotype characterization of two CYP3A haplotypes causing different enzymatic capacity in fetal livers. *Clin Pharmacol Ther* **77**, 259-270 (2005).

15 Gellner K *et al.* Genomic organization of the human CYP3A locus: identification of a new, inducible CYP3A gene. *Pharmacogenetics* **11**, 111-121 (2001).

16 Dancygier H, Merle U, Stremmel W, Niederau C. in *Clinical Hepatology: Principles and Practice of Hepatobiliary Diseases* 75-102 (Springer Berlin Heidelber, 2010).

17 Leuschner U. in *Clinical Hepatology: Principles and Practice of Hepatobiliary Diseases* 103-125 (Springer Berlin Heidelberg, 2010).

18 Chiang JY. Bile acids: regulation of synthesis. *J Lipid Res* **50**, 1955-1966 (2009).

19 Tirona RG *et al.* The orphan nuclear receptor HNF4α determines PXR- and CAR-mediated xenobiotic induction of CYP3A4. *Nat Med* **9**, 220-224 (2003).

20 Yoon JC *et al.* Control of hepatic gluconeogenesis through the transcriptional coactivator PGC-1. *Nature* **413**, 131-138 (2001).

21 Hayhurst GP, Lee YH, Lambert G, Ward JM, Gonzalez FJ. Hepatocyte nuclear factor 4α (nuclear receptor 2A1) is essential for maintenance of hepatic gene expression and lipid homeostasis. *Molecular and Cellular Biology* **21**, 1393-1403 (2001).

22 Inoue Y *et al.* Regulation of bile acid biosynthesis by hepatocyte nuclear factor 4alpha. *J Lipid Res* **47**, 215-227 (2006).

23 Hatzis P, Talianidis I. Regulatory mechanisms controlling human hepatocyte nuclear factor 4α gene expression. *Molecular and cellular biology* **21**, 7320-7330 (2001).

24 Samadani U, Costa RH. The transcriptional activator hepatocyte nuclear factor 6 regulates liver gene expression. *Molecular and cellular biology* **16**, 6273-6284 (1996).

25 Costa RH, Holterman A-XL, Rausa FM, Adami GR. in *The liver : biology and pathobiology* (eds Arias IM, Boyer JL) Ch. 5, 59-75 (Lippincott Williams & Wilkins, 2001).

26 Godoy P *et al.* Recent advances in 2D and 3D in vitro systems using primary hepatocytes, alternative hepatocyte sources and non-parenchymal liver cells and their use in investigating mechanisms of hepatotoxicity, cell signaling and ADME. *Arch Toxicol* **87**, 1315-1530 (2013).

27 Dancygier H. *Clinical Hepatology: Principles and Practice of Hepatobiliary Diseases*. Vol. 1 (Springer, 2010).

28 Lele RD, Lele VR. in *Molecular Nuclear Medicine: The Challenge of Genomics and Proteomics to Clinical Practice* (eds Feinendegen LE *et al.*) 527-562 (Springer Berlin Heidelberg, 2003).

29 Wagner BA, Venkataraman S, Buettner GR. The rate of oxygen utilization by cells. *Free Radic Biol Med* **51**, 700-712 (2011).

30 Taub R. Liver regeneration: from myth to mechanism. *Nat Rev Mol Cell Biol* **5**, 836-847 (2004).

31 Mescher AL. *Junqueira's Basic Histology: Text and Atlas*. 14 edn, (McGraw-Hill Education, 2015).

32 Hynes RO. The Extracellular Matrix: Not Just Pretty Fibrils. *Science* **326**, 1216-1219 (2009).

33 Dunn JC, Yarmush ML, Koebe HG, Tompkins RG. Hepatocyte function and extracellular matrix geometry: long-term culture in a sandwich configuration. *Faseb J* **3**, 174-177 (1989).

34 Bedossa P, Paradis V. Liver extracellular matrix in health and disease. *J Pathol* **200**, 504-515 (2003).

35 Di Lullo GA, Sweeney SM, Korkko J, Ala-Kokko L, San Antonio JD. Mapping the ligand-binding sites and disease-associated mutations on the most abundant protein in the human, type I collagen. *J Biol Chem* **277**, 4223-4231 (2002).

36 Soderhall C *et al.* Variants in a novel epidermal collagen gene (COL29A1) are associated with atopic dermatitis. *PLoS Biol* **5**, e242 (2007).

37 Wells RG. in *Textbook of Hepatology: From Basic Science to Clinical Practice, Third Edition* (eds Rodés J *et al.*) Ch. Synthetic function, (Blackwell Publishing Ltd, 2008).

38 Martinez-Hernandez A, Amenta PS. The hepatic extracellular matrix: I. Components and distribution in normal liver. *Virchows Archiv A Pathological Anatomy and Histopathology* (1993).

39 Aden DP, Fogel A, Plotkin S, Damjanov I, Knowles BB. Controlled synthesis of HBsAg in a differentiated human liver carcinoma-derived cell line. *Nature* **282**, 615-616 (1979).

40 Yano H, Kojiro M, Nakashima T. A new human hepatocellular carcinoma cell line (KYN-1) with a transformation to adenocarcinoma. *In Vitro Cellular & Developmental Biology* **22**, 637-646 (1986).

41 Haramaki M *et al.* Expression of CD44 in Human Hepatocellular Carcinoma Cell Lines. *Hepatology* **21**, 1276-1284 (1995).

42 Nakabayashi H, Taketa K, Miyano K, Yamane T, Sato J. Growth of human hepatoma cells lines with differentiated functions in chemically defined medium. *Cancer Res* **42**, 3853-3863 (1982).

43 Blight KJ, McKeating JA, Rice CM. Highly Permissive Cell Lines for Subgenomic and Genomic Hepatitis C Virus RNA Replication. *J Virol* **76**, 13001-13014 (2002).

44 Clayton DF, James E. Darnell J. Changes in liver-specific compared to common gene transcription during primary culture of mouse hepatocytes. *Molecular and Cellular Biology* **3**, 1552-1561 (1983).

45 Gómez-Lechón MJ *et al.* Long-term expression of differentiated functions in hepatocytes cultured in three-dimensional collagen matrix. *J Cell Physiol* **177**, 553-562 (1998).

46 Yamamoto N, Imazato K, Masumoto A. Stimulation of Growth of Primary Cultured Adult Rat Hepatocytes without Growth Factors by Coculture with Nonparenchymal Liver Cells. *Exp Cell Res* **172**, 228-242 (1987).

47 Mitaka T, Sato F, Mizuguchi T, Yokono T, Mochizuki Y. Reconstruction of hepatic organoid by rat small hepatocytes and hepatic nonparenchymal cells. *Hepatology* **29**, 111-125 (1999).

48 Donato MT, Castell JV, Gómez-Lechón MJ. Cytochrome P450 activities in pure and co-cultured rat hepatocytes. Effects of model inducers. *In Vitro Cellular & Developmental Biology* **30A**, 825-832 (1994).

49 Liu Y, Li H, Yan S, Wei J, Li X. Hepatocyte cocultures with endothelial cells and fibroblasts on micropatterned fibrous mats to promote liver-specific functions and capillary formation capabilities. *Biomacromolecules* **15**, 1044-1054 (2014).

50 Naughton BA, Román JS, Sibanda B, Weintraub JP, Kamali V. Stereotypic culture systems for liver and bone marrow; evidence for the Development of Functional Tissue In Vitro and Following Inplantation In Vivo. *Biotechnol Bioeng* **43**, 810-825 (1993).

51 Kneser U *et al.* Interaction of hepatocytes and pancreatic islets cotransplanted in polymeric matrices. *Virchows Archiv* **435**, 125–132 (1999).

52 Bhatia SN, Balis UJ, Yarmush ML, Toner M. Microfabrication of Hepatocyte Fibroblast Co-cultures; Role of Homotypic Cell Interactions. *Biotechnology Progress* **14**, 378-387 (1998).

53 Kuri-Harcuch W, Mendoza-Figueroa T. Cultivation of adult rat hepatocytes on 3T3 cells: expression of various liver differentiated functions. *Differentiation* **41**, 148-157 (1989).

54 Bhandari RNB *et al.* Liver tissue engineering: A role for co-culture systems in modifying hepatocyte function and viability. *Tissue Eng* **7**, 345-357 (2001).

55 Bhatia SN, Balis UJ, Yarmush ML, Toner M. Effect of cell–cell interactions in preservation of cellular phenotype: cocultivation of hepatocytes and nonparenchymal cells. *Faseb J* **13**, 1883-1900 (1999).

56 Cho CH, Berthiaume F, Tilles AW, Yarmush ML. A new technique for primary hepatocyte expansion in vitro. *Biotechnol Bioeng* **101**, 345-356 (2008).

57 Nakajima H, Shimbara N. Functional Maintenance of Hepatocytes on Collagen Gel Cultured with Simple Serum-Free Medium Containing Sodium Selenite. *Biochem Biophys Res Commun* **222**, 664-668 (1996).

58 Koide N *et al.* Continued high albumin production by multicellular spheroids of adult rat hepatocytes formed in the presence of liver-derived proteoglycans. *Biochem Biophys Res Commun* **161**, 385-391 (1989).

59 Bissell DM, Arenson DM, Maher JJ, Roll FJ. Support of cultured hepatocytes by a laminin-rich gel. Evidence for a functionally significant subendothelial matrix in normal rat liver. *J Clin Invest* **79**, 801-812 (1987).

60 Kaihara S *et al.* Silicon Micromachining to Tissue Engineer Branched Vascular Channels for Liver Fabrication. *Tissue Eng* **6**, 105-117 (2000).

61 Ho C-T *et al.* Liver-cell patterning lab chip: mimicking the morphology of liver lobule tissue. *Lab Chip* **13**, 3578-3587 (2013).

62 Cukierman E, Pankov R, Stevens DR, Yamada KM. Taking cell-matrix adhesions to the third dimension. *Science* **294**, 1708-1712 (2001).

63 Dutta RC, Dutta AK. Cell-interactive 3D-scaffold; advances and applications. *Biotechnol Adv* **27**, 334-339 (2009).

64 Schmeichel KL, Bissell MJ. Modeling tissue-specific signaling and organ function in three dimensions. *J Cell Sci* **116**, 2377-2388 (2003).

65 Dunn JCY, Tompkins RG, Yarmush ML. Long-term in vitro function of adult hepatocytes in a collagen sandwich configuration. *Biotechnology Progress* **7**, 237-245 (1991).

66 Richert L *et al.* Evaluation of the effect of culture configuration on morphology, survival time, antioxidant status and metabolic capacities of cultured rat hepatocytes. *Toxicology in Vitro* **16**, 89-99 (2001).

67 Yu SH, Buchholz R, Kim SK. Encapsulation of rat hepatocyte spheroids for the development of artificial liver. *Biotechnol Tech* **13**, 609-614 (1999).

68 Liu ZC, Chang TMS. Effects of bone marrow cells on hepatocytes: When co-cultured or co-encapsulated together. *Artif Cell Blood Sub* **28**, 365-374 (2000).

69 Kinasiewicz A *et al.* Culture of C3A cells in alginate beads for fluidized bed Bioartificial liver. *Transpl P* **39**, 2911-2913 (2007).

70 Nishikawa Y, Tokusashi Y, Kadohama T, Nishimori H, Ogawa K. Hepatocytic cells form bile duct-like structures within a three-dimensional collagen gel matrix. *Exp Cell Res* **223**, 357-371 (1996).

71 Genove E *et al.* Functionalized self-assembling peptide hydrogel enhance maintenance of hepatocyte activity in vitro. *Journal of Cellular and Molecular Medicine* **13**, 3387-3397 (2009).

72 Wang S, Nagrath D, Chen PC, Berthiaume F, Yarmush ML. Three-dimensional primary hepatocyte culture in synthetic self-assembling peptide hydrogel. *Tissue Eng Part A* **14**, 227-236 (2008).

73 Lee W, Cho N-J, Xiong A, Glenn JS, Frank CW. Hydrophobic nanoparticles improve permeability of cell-encapsulating poly(ethylene glycol) hydrogels while maintaining patternability. *Proc Natl Acad Sci U S A* **107**, 20709-20714 (2010).

74 Lee BH *et al.* Modulation of Huh7.5 spheroid formation and functionality using modified PEG-based hydrogels of different stiffness. *PLoS One* **10**, e0118123 (2015).

75 Kim M, Lee JY, Jones CN, Revzin A, Tae G. Heparin-based hydrogel as a matrix for encapsulation and cultivation of primary hepatocytes. *Biomaterials* **31**, 3596-3603 (2010).

76 Okubo H *et al.* Formation of multicellular spheroids composed of adult rat hepatocytes in dishes with positively charged surfaces and under other nonadherent environments. *Exp Cell Res* **186**, 227-235 (1990).

77 Shinji T, Koide N, Tsuji T. Glycosaminoglycans Partially Substitute for Proteoglycans in Spheroid Formation of Adult-Rat Hepatocytes in Primary Culture. *Cell Struct Funct* **13**, 179-188 (1988).

78 Kelm JM, Timmins NE, Brown CJ, Fussenegger M, Nielsen LK. Method for generation of homogeneous multicellular tumor spheroids applicable to a wide variety of cell types. *Biotechnol Bioeng* **83**, 173-180 (2003).

79 Lin RZ, Chou LF, Chien CC, Chang HY. Dynamic analysis of hepatoma spheroid formation: roles of E-cadherin and β1-integrin. *Cell Tissue Res* **324**, 411-422 (2006).

80 Fukuda J, Sakai Y, Nakazawa K. Novel hepatocyte culture system developed using microfabrication and collagen/polyethylene glycol microcontact printing. *Biomaterials* **27**, 1061-1070 (2006).

81 Napolitano AP, Chai P, Dean DM, Morgan JR. Dynamics of the self-assembly of complex cellular aggregates on micromolded nonadhesive hydrogels. *Tissue Eng* **13**, 2087-2094 (2007).

82 Nyberg SL *et al.* Rapid, large-scale formation of porcine hepatocyte spheroids in a novel spheroid reservoir bioartificial liver. *Liver Transpl* **11**, 901-910 (2005).

83 Khaoustov VI *et al.* Induction of three-dimensional assembly of human liver cells by simulated microgravity. *In Vitro Cell Dev Biol Anim* **35**, 501-509 (1999).

84 Gevaert E *et al.* High throughput micro-well generation of hepatocyte micro-aggregates for tissue engineering. *PLoS One* **9**, e105171 (2014).

85 Lin RZ, Chang HY. Recent advances in three-dimensional multicellular spheroid culture for biomedical research. *Biotechnol J* **3**, 1172-1184 (2008).

86 Vinken M *et al.* Involvement of cell junctions in hepatocyte culture functionality. *Crit Rev Toxicol* **36**, 299-318 (2006).

87 van Zijl F, Mikulits W. Hepatospheres: Three dimensional cell cultures resemble physiological conditions of the liver. *World J Hepatol* **2**, 1-7 (2010).

88 Curcio E *et al.* Mass transfer and metabolic reactions in hepatocyte spheroids cultured in rotating wall gas-permeable membrane system. *Biomaterials* **28**, 5487-5497 (2007).

89 Li JL, Pan JL, Zhang LG, Guo XJ, Yu YT. Culture of primary rat hepatocytes within porous chitosan scaffolds. *Journal of Biomedical Materials Research Part A* **67A**, 938-943 (2003).

90 Saavedra YG, Mateescu MA, Averill-Bates DA, Denizeau F. Polyvinylalcohol three-dimensional matrices for improved long-term dynamic culture of hepatocytes. *J Biomed Mater Res A* **66**, 562-570 (2003).

91 Dvir-Ginzberg M, Gamlieli-Bonshtein I, Agbaria R, Cohen S. Liver tissue engineering within alginate scaffolds: Effects of cell-seeding density on hepatocyte viability, morphology, and function. *Tissue Eng* **9**, 757-766 (2003).

92 Wang T, Feng ZQ, Leach MK, Wu JH, Jiang Q. Nanoporous fibers of type-I collagen coated poly(L-lactic acid) for enhancing primary hepatocyte growth and function. *Journal of Materials Chemistry B* **1**, 339-346 (2013).

93 Lee PJ, Hung PJ, Lee LP. An artificial liver sinusoid with a microfluidic endothelial-like barrier for primary hepatocyte culture. *Biotechnol Bioeng* **97**, 1340-1346 (2007).

94 Liu Tsang V *et al.* Fabrication of 3D hepatic tissues by additive photopatterning of cellular hydrogels. *Faseb J* **21**, 790-801 (2007).

95 Yanagawa F *et al.* Directed assembly of cell-laden microgels for building porous three-dimensional tissue constructs. *J Biomed Mater Res A* **97**, 93-102 (2011).

96 Ma C *et al.* On-Chip Construction of Liver Lobule-like Microtissue and Its Application for Adverse Drug Reaction Assay. *Analytical chemistry* **88**, 1719-1727 (2016).

97 Ovsianikov A *et al.* Laser fabrication of three-dimensional CAD scaffolds from photosensitive gelatin for applications in tissue engineering. *Biomacromolecules* **12**, 851-858 (2011).

98 Bertassoni LE *et al.* Direct-write bioprinting of cell-laden methacrylated gelatin hydrogels. *Biofabrication* **6**, 024105 (2014).

99 Billiet T, Gevaert E, De Schryver T, Cornelissen M, Dubruel P. The 3D printing of gelatin methacrylamide cell-laden tissue-engineered constructs with high cell viability. *Biomaterials* **35**, 49-62 (2014).

100 Bhise NS *et al.* A liver-on-a-chip platform with bioprinted hepatic spheroids. *Biofabrication* **8**, 014101 (2016).

101 Berthiaume F, Moghe PV, Toner M, Yarmush ML. Effect of extracellular matrix topology on cell structure, function, and physiological responsiveness: hepatocytes cultured in a sandwich configuration. *Faseb J* **10**, 1471-1484 (1996).

102 Nucara L, Greco F, Mattoli V. Electrically responsive photonic crystals: a review. *Journal of Materials Chemistry C* **3**, 8449-8467 (2015).

103 Armstrong E, O'Dwyer C. Artificial opal photonic crystals and inverse opal structures - fundamentals and applications from optics to energy storage. *Journal of Materials Chemistry C* **3**, 6109-6143 (2015).

104 Kim MH *et al.* Phenotypic regulation of liver cells in a biofunctionalized three-dimensional hydrogel platform. *Integrative Biology* **8**, 156-166 (2015).

105 Shirahama H *et al.* Fabrication of Inverted Colloidal Crystal Poly(ethylene glycol) Scaffold: A Three-dimensional Cell Culture Platform for Liver Tissue Engineering. *J. Vis. Exp.* **114**, e54331 (2016).

106 Ma PX, Choi J-W. Biodegradable Polymer Scaffolds with Wel-Defined Interconnected Spherical Pore Network. *Tissue Eng* **7**, 23-33 (2001).

107 Choi S-W, Zhang Y, Xia Y. Three-Dimensional Scaffolds for Tissue Engineering: The Importance of Uniformity in Pore Size and Structure. *Langmuir* **26**, 19001-19006 (2010).

108 Cuddihy MJ, Kotov NA. Poly(lactic-co-glycolic acid) bone scaffolds with inverted colloidal crystal geometry. *Tissue Eng Part A* **14**, 1639-1649 (2008).

109 Lee J, Cuddihy MJ, Cater GM, Kotov NA. Engineering liver tissue spheroids with inverted colloidal crystal scaffolds. *Biomaterials* **30**, 4687-4694 (2009).

110 Shanbhag S, Lee J, Kotov N. Diffusion in three-dimensionally ordered scaffolds with inverted colloidal crystal geometry. *Biomaterials* **26**, 5581-5585 (2005).

111 Stachowiak AN, Bershteyn A, Tzatzalos E, Irvine DJ. Bioactive Hydrogels with an Ordered Cellular Structure Combine Interconnected Macroporosity and Robust Mechanical Properties. *Advanced Materials* **17**, 399-403 (2004).

112 Galperin A, Long TJ, Ratner BD. Degradable, Thermo-Sensitive Poly(N-isopropyl acrylamide)-Based Scaffolds with Controlled Porosity for Tissue Engineering Applications. *Biomacromolecules* **11**, 2583–2592 (2010).

113 Lu J *et al.* Hybrid inverse opals for regulating cell adhesion and orientation. *Nanoscale* **6**, 10650-10656 (2014).

114 Wang YC, Tang ZM, Feng ZQ, Xie ZY, Gu ZZ. Stretched inverse opal colloid crystal substrates-induced orientation of fibroblast. *Biomed Mater* **5**, 35011 (2010).

115 Zhang Y, Wang S, Eghtedari M, Motamedi M, Kotov NA. Inverted-Colloidal-Crystal Hydrogel Matrices as Three-Dimensional Cell Scaffolds. *Adv Funct Mater* **15**, 725–731 (2005).

116 Liu Y, Wang S, Lee JW, Kotov NA. A floating self-assembly route to colloidal crystal templates for 3D cell scaffolds. *Chemistry of materials* **17**, 4918-4924 (2005).

117 Liu Y, Wang S. 3D inverted opal hydrogel scaffolds with oxygen sensing capability. *Colloids Surf B Biointerfaces* **58**, 8-13 (2007).

118 Yang J-T, Kuo Y-C, Chiu K-H. Peptide-modified inverted colloidal crystal scaffolds with bone marrow stromal cells in the treatment for spinal cord injury. *Colloids Surf B Biointerfaces* **84**, 198-205 (2011).

119 Kuo Y-C, Chiu K-H. Inverted colloidal crystal scaffolds with laminin-derived peptides for neuronal differentiation of bone marrow stromal cells. *Biomaterials* **32**, 819-831 (2011).

120 Liu Y *et al.* Rapid aqueous photo-polymerization route to polymer and polymer-composite hydrogel 3D inverted colloidal crystal scaffolds. *J Biomed Mater Res A* **83**, 1-9 (2007).

121 Kotov NA *et al.* Inverted Colloidal Crystals as Three-Dimensional Cell Scaffolds. *Langmuir* **20**, 7887-7892 (2004).

122 Kuo Y-C, Tsai Y-T. Inverted colloidal crystal scaffolds for uniform cartilage regeneration. *Biomacromolecules* **11**, 731–739 (2010).

123 Kuo Y-C, Tsai Y-T. Heparin-conjugated scaffolds with pore structure of inverted colloidal crystals for cartilage regeneration. *Colloids Surf B Biointerfaces* **82**, 616-623 (2011).

124 Kuo Y-C, Chung C-Y. TATVHL peptide-grafted alginate/poly(γ-glutamic acid) scaffolds with inverted colloidal crystal topology for neuronal differentiation of iPS cells. *Biomaterials* **33**, 8955-8966 (2012).

125 Kuo Y-C, Chen C-W. Inverted colloidal crystal scaffolds with induced pluripotent stem cells for nerve tissue engineering. *Colloids and Surfaces B: Biointerfaces* **102**, 789-794 (2013).

126 Kuo Y-C, Lin C-C. Accelerated nerve regeneration using induced pluripotent stem cells in chitin–chitosan–gelatin scaffolds with inverted colloidal crystal geometry. *Colloids and Surfaces B: Biointerfaces* **103**, 595-600 (2013).

127 Lee J, Kotov NA. Notch ligand presenting acellular 3D microenvironments for ex vivo human hematopoietic stem-cell culture made by layer-by-layer assembly. *Small* **5**, 1008-1013 (2009).

128 Nichols JE *et al.* In vitro analog of human bone marrow from 3D scaffolds with biomimetic inverted colloidal crystal geometry. *Biomaterials* **30**, 1071-1079 (2009).

129 Madden LR *et al.* Proangiogenic scaffolds as functional templates for cardiac tissue engineering. *Proc Natl Acad Sci U S A* **107**, 15211-15216 (2010).

130 Zhang Y, Xia Y. Formation of Embryoid Bodies with Controlled Sizes and Maintained Pluripotency in Three-Dimensional Inverse Opal Scaffolds. *Adv Funct Mater* **22**, 121-129 (2012).

131 Galperin A *et al.* Integrated bi-layered scaffold for osteochondral tissue engineering. *Adv Healthc Mater* **2**, 872-883 (2013).

132 Lee J, Lilly GD, Doty RC, Podsiadlo P, Kotov NA. In vitro toxicity testing of nanoparticles in 3D cell culture. *Small* **5**, 1213-1221 (2009).

133 Kim MH *et al.* Biofunctionalized Hydrogel Microscaffolds Promote 3D Hepatic Sheet Morphology. *Macromol Biosci* **16**, 314-321 (2016).

134 Silva Jd, Lautenschlager F, Sivaniah E, Guck JR. The cavity-to-cavity migration of leukaemic cells through 3D honey-combed hydrogels with adjustable internal dimension and stiffness. *Biomaterials* **31**, 2201-2208 (2010).

135 da Silva J, Lautenschlager F, Kuo CH, Guck J, Sivaniah E. 3D inverted colloidal crystals in realistic cell migration assays for drug screening applications. *Integr Biol (Camb)* **3**, 1202-1206 (2011).

136 Lee J *et al.* Implantable microenvironments to attract hematopoietic stem/cancer cells. *Proc Natl Acad Sci U S A* **109**, 19638-19643 (2012).

137 Wang Y, Bahng JH, Che Q, Han J, Kotov NA. Anomalously Fast Diffusion of Targeted Carbon Nanotubes in Cellular Spheroids. *ACS Nano* **9**, 8231-8238 (2015).

138 Lee J, Kohl N, Shanbhang S, Parekkadan B. Scaffold-integrated microchips for end-to-end in vitro tumor cell attachment and xenograft formation. *Technology (Singap World Sci)* **3**, 179-188 (2015).

139 Lee Y-h, Huang J-r, Wang Y-k, Lin K-h. Three-dimensional fibroblast morphology on compliant substrates of controlled negative curvature. *Integr Biol (Camb)* **5**, 1447-1455 (2013).

140 Shanbhag S, Wang S, Kotov NA. Cell distribution profiles in three-dimensional scaffolds with inverted-colloidal-crystal geometry: modeling and experimental investigations. *Small* **1**, 1208-1214 (2005).

141 Choi S-W, Zhang Y, Thomopoulos S, Xia Y. In Vitro Mineralization by Preosteoblasts in Poly(dl-lactide-co-glycolide) Inverse Opal Scaffolds Reinforced with Hydroxyapatite Nanoparticles. *Langmuir* **26**, 12126-12131 (2010).

142 Zhang Y, Choi S-W, Xia Y. Modifying the Pores of an Inverse Opal Scaffold With Chitosan Microstructures for Truly Three-Dimensional Cell Culture. *Macromol Rapid Commun* **33**, 296-301 (2012).

143 Choi SW, Zhang Y, Macewan MR, Xia Y. Neovascularization in biodegradable inverse opal scaffolds with uniform and precisely controlled pore sizes. *Adv Healthc Mater* **2**, 145-154 (2013).

144 Cai X *et al.* Investigation of Neovascularization in Three-Dimensional Porous ScaffoldsIn Vivoby a Combination of Multiscale Photoacoustic Microscopy and Optical Coherence Tomography. *Tissue Engineering Part C: Methods* **19**, 196-204 (2013).

145 Zhang YS, Yao J, Wang LV, Xia Y. Fabrication of Cell Patches Using Biodegradable Scaffolds with a Hexagonal Array of Interconnected Pores (SHAIPs). *Polymer* **55**, 445-452 (2014).

146 Zhang YS, Regan KP, Xia Y. Controlling the pore sizes and related properties of inverse opal scaffolds for tissue engineering applications. *Macromol Rapid Commun* **34**, 485-491 (2013).

147 Bryant SJ, Cuy JL, Hauch KD, Ratner BD. Photo-patterning of porous hydrogels for tissue engineering. *Biomaterials* **28**, 2978-2986 (2007).

148 Underwood RA *et al.* Quantifying the effect of pore size and surface treatment on epidermal incorporation into percutaneously implanted sphere-templated porous biomaterials in mice. *J Biomed Mater Res A* **98**, 499-508 (2011).

149 Long TJ, Takeno M, Sprenger CC, Plymate SR, Ratner BD. Capillary force seeding of sphere-templated hydrogels for tissue-engineered prostate cancer xenografts. *Tissue Eng Part C Methods* **19**, 738-744 (2013).

150 Bhrany AD, Irvin CA, Fujitani K, Liu Z, Ratner BD. Evaluation of a sphere-templated polymeric scaffold as a subcutaneous implant. *JAMA Facial Plast Surg* **15**, 29-33 (2013).

151 Swinerd VM, Collins AM, Skaer NJV, Gheysens T, Mann S. Silk inverse opals from template-directed beta-sheet transformation of regenerated silk fibroin. *Soft Matter* **3**, 1377-1380 (2007).

152 Kim J, Bencherif SA, Li WA, Mooney DJ. Cell-friendly inverse opal-like hydrogels for a spatially separated co-culture system. *Macromol Rapid Commun* **35**, 1578-1586 (2014).

153 Fu J, Fan C, Lai WS, Wang D. Enhancing vascularization of a gelatin-based micro-cavitary hydrogel by increasing the density of the micro-cavities. *Biomed Mater* **11**, 055012 (2016).

154 Choi S-W, Xie J, Xia Y. Chitosan-Based Inverse Opals: Three-Dimensional Scaffolds with Uniform Pore Structures for Cell Culture. *Advanced Materials* **21**, 2997-3001 (2009).

155 Kim S *et al.* Silk inverse opals. *Nat Photonics* **6**, 817-822 (2012).

156 Jiang Y *et al.* Protein-based inverse opal: a novel support for enzyme immobilization *Enzyme and Microbial Technology* **In press** (2016).

157 Caixeiro S, Gaio M, Marelli B, Omenetto FG, Sapienza R. Silk-Based Biocompatible Random Lasing. *Advanced Optical Materials* **4**, 998-1003 (2016).

158 Burke KA, Brenckle MA, Kaplan DL, Omenetto FG. Evaluation of the Spectral Response of Functionalized Silk Inverse Opals as Colorimetric Immunosensors. *ACS Appl Mater Interfaces* **8**, 16218-16226 (2016).

159 Weigel PH *et al.* Adhesion of hepatocytes to immobilized sugars. A threshold phenomenon. *J Biol Chem* **254**, 10830-10838 (1979).

160 Weigel PH, Schmell E, Lee YC, Roseman S. Specific adhesion of rat hepatocytes to beta-galactosides linked to polyacrylamide gels. *J Biol Chem* **253**, 330-333 (1978).

161 Weigel PH. Rat hepatocytes bind to synthetic galactoside surfaces via a patch of asialoglycoprotein receptors. *The Journal of cell biology* **87**, 855-861 (1980).

162 Olsen AL *et al.* Hepatic stellate cells require a stiff environment for myofibroblastic differentiation. *AJP: Gastrointestinal and Liver Physiology* **301**, G110-G118 (2011).

163 Awad ME, Abdel-Rahman MS, Hassan SA. Acrylamide toxicity in isolated rat hepatocytes. *Toxicol In Vitro* **12**, 699-704 (1998).

164 Thomas RJ *et al.* The effect of three-dimensional co-culture of hepatocytes and hepatic stellate cells on key hepatocyte functions in vitro. *Cells Tissues Organs* **181**, 67-79 (2005).

165 Kaihara S *et al.* Survival and function of rat hepatocytes cocultured with nonparenchymal cells or sinusoidal endothelial cells on biodegradable polymers under flow conditions. *J Pediatr Surg* **35**, 1287-1290 (2000).

166 Kim SS *et al.* Dynamic seeding and in vitro culture of hepatocytes in a flow perfusion system. *Tissue Eng* **6**, 39-44 (2000).

167 Kim SS *et al.* Survival and function of hepatocytes on a novel three-dimensional synthetic biodegradable polymer scaffold with an intrinsic network of channels. *Ann Surg* **228**, 8-13 (1998).

168 Hasirci V *et al.* Expression of liver-specific functions by rat hepatocytes seeded in treated poly(lactic-co-glycolic) acid biodegradable foams. *Tissue Eng* **7**, 385-394 (2001).

169 Zhu XH, Lee LY, Jackson JSH, Tong YW, Wang CH. Characterization of porous poly(D,L-Lactic-co-glycolic acid) sponges fabricated by supercritical CO2 gas-foaming method as a scaffold for three-dimensional growth of hep3B cells. *Biotechnol Bioeng* **100**, 998-1009 (2008).

170 Li J *et al.* Growth and metabolism of human hepatocytes on biomodified collagen poly(lactic-co-glycolic acid) three-dimensional scaffold. *Asaio J* **52**, 321-327 (2006).

171 Mooney DJ *et al.* Long-term engraftment of hepatocytes transplanted on biodegradable polymer sponges. *J Biomed Mater Res* **37**, 413-420 (1997).

172 Kim SS *et al.* Small intestinal submucosa as a small-caliber venous graft: A novel model for hepatocyte transplantation on synthetic biodegradable polymer scaffolds with direct access to the portal venous system. *J Pediatr Surg* **34**, 124-128 (1999).

173 Papavasiliou G, Turturro MV, Christenson M. Synthetic PEG hydrogel extracellular matrix mimics for the vascularization of engineered tissues. *Cardiovascular Pathology* **22**, e31-e32 (2013).

174 Cho N-J *et al.* Viral infection of human progenitor and liver-derived cells encapsulated in three-dimensional PEG-based hydrogel. *Biomed Mater* **4**, 011001 (2009).

175 Skardal A *et al.* A hydrogel bioink toolkit for mimicking native tissue biochemical and mechanical properties in bioprinted tissue constructs. *Acta Biomater* **25**, 24-34 (2015).

176 Chen AA *et al.* Humanized mice with ectopic artificial liver tissues. *Proc Natl Acad Sci U S A* **108**, 11842–11847 (2011).

177 Giancotti FG. Integrin Signaling. *Science* **285**, 1028-1033 (1999).

178 Sudo R *et al.* Transport-mediated angiogenesis in 3D epithelial coculture. *Faseb J* **23**, 2155-2164 (2009).

179 Kane BJ, Zinner MJ, Yarmush ML, Toner M. Liver-specific functional studies in a microfluidic array of primary mammalian hepatocytes. *Analytical Chemistry* **78**, 4291-4298 (2006).

180 Zhao Y *et al.* In vivo generation of thick, vascularized hepatic tissue from collagen hydrogel-based hepatic units. *Tissue Eng Part C Methods* **16**, 653-659 (2010).

181Gorgieva S, Kokol V. *Collagen- vs. Gelatine-Based Biomaterials and Their Biocompatibility: Review and Perspectives*. (InTech, 2011).

182 Lynn AK, Yannas IV, Bonfield W. Antigenicity and immunogenicity of collagen. *J Biomed Mater Res B Appl Biomater* **71**, 343-354 (2004).

183 Starin WA. The Antigenic Properties of Gelatin. *J Infect Dis* **23**, 139-158 (1918).

184 He JK *et al.* Fabrication and characterization of chitosan/gelatin porous scaffolds with predefined internal microstructures. *Polymer* **48**, 4578-4588 (2007).

185 Gong H, Agustin J, Wootton D, Zhou JG. Biomimetic design and fabrication of porous chitosan-gelatin liver scaffolds with hierarchical channel network. *J Mater Sci Mater Med* **25**, 113-120 (2014).

186 Wang XH *et al.* Generation of three-dimensional hepatocyte/gelatin structures with rapid prototyping system. *Tissue Eng* **12**, 83-90 (2006).

187 Jeon H *et al.* Generation of Multilayered 3D Structures of HepG2 Cells Using a Bio-printing Technique. *Gut and Liver* (2016).

188 Yang Z *et al.* In vitro and in vivo characterization of silk fibroin/gelatin composite scaffolds for liver tissue engineering. *J Digest Dis* **13**, 168-178 (2012).

189 Donato MT, Castell JV, Gómez-Lechón MJ. Co-cultures of hepatocytes with epithelial-like cell lines: Expression of drug-biotransformation activities by hepatocytes. *Cell Biology and Toxicology* **7**, 1-14 (1991).

190 Zhu XH, Gan SK, Wang CH, Tong YW. Proteins combination on PHBV microsphere scaffold to regulate Hep3B cells activity and functionality: A model of liver tissue engineering system. *Journal of Biomedical Materials Research Part A* **83A**, 606-616 (2007).

191 Ouchi H, Otsu E, Kuzumaki T, Iuchi Y, Ishikawa K. Synergistic induction by collagen and fibronectin of liver-specific genes in rat primary cultured hepatocytes. *Arch Biochem Biophys* **358**, 58-62 (1998).

192 Coward SM, Selden C, Mantalaris A, Hodgson HJF. Proliferation rates of HepG2 cells encapsulated in alginate are increased in a microgravity environment compared with static cultures. *Artif Organs* **29**, 152-158 (2005).

193 Rahman TM, Selden C, Khalil M, Diakanov I, Hodgson HJF. Alginate-encapsulated human hepatoblastoma cells in an extracorporeal perfusion system improve some systemic parameters of liver failure in a xenogeneic model. *Artif Organs* **28**, 476-482 (2004).

194 Farris S, Song J, Huang Q. Alternative reaction mechanism for the cross-linking of gelatin with glutaraldehyde. *J Agric Food Chem* **58**, 998-1003 (2010).

195 Sisson K, Zhang C, Farach-Carson MC, Chase DB, Rabolt JF. Evaluation of Cross-Linking Methods for Electrospun Gelatin on Cell Growth and Viability. *Biomacromolecules* **10**, 1675-1680 (2009).

196 Sivakumar M, Radhakrishnan PRG, Kothandaraman H. Grafting of Glycidyl Methacrylate onto Gelatin. *Journal of Applied Polymer Science* **43**, 1789-1794 (1991).

197 Bae H *et al.* Cell-laden microengineered pullulan methacrylate hydrogels promote cell proliferation and 3D cluster formation. *Soft Matter* **7**, 1903-1911 (2011).

198 Eng G *et al.* Assembly of complex cell microenvironments using geometrically docked hydrogel shapes. *Proc Natl Acad Sci U S A* **110**, 4551-4556 (2013).

199 Hsieh HY *et al.* Gradient static-strain stimulation in a microfluidic chip for 3D cellular alignment. *Lab Chip* **14**, 482-493 (2014).

200 Hasan A, Paul A, Memic A, Khademhosseini A. A multilayered microfluidic blood vessel-like structure. *Biomed Microdevices* **17**, 88 (2015).

201 Gauvin R *et al.* Microfabrication of complex porous tissue engineering scaffolds using 3D projection stereolithography. *Biomaterials* **33**, 3824-3834 (2012).

202 Boere KW *et al.* Covalent attachment of a three-dimensionally printed thermoplast to a gelatin hydrogel for mechanically enhanced cartilage constructs. *Acta Biomater* **10**, 2602-2611 (2014).

203 Schuurman W *et al.* Gelatin-Methacrylamide Hydrogels as Potential Biomaterials for Fabrication of Tissue-Engineered Cartilage Constructs. *Macromol Biosci* **13**, 551-561 (2013).

204 Hoch E, Hirth T, Tovar GEM, Borchers K. Chemical tailoring of gelatin to adjust its chemical and physical properties for functional bioprinting. *Journal of Materials Chemistry B* **1**, 5675 (2013).

205 Levato R *et al.* Biofabrication of tissue constructs by 3D bioprinting of cell-laden microcarriers. *Biofabrication* **6**, 035020 (2014).

206 Aubin H *et al.* Directed 3D cell alignment and elongation in microengineered hydrogels. *Biomaterials* **31**, 6941-6951 (2010).

207 Nichol JW *et al.* Cell-laden microengineered gelatin methacrylate hydrogels. *Biomaterials* **31**, 5536-5544 (2010).

208 Xiao W *et al.* Synthesis and characterization of photocrosslinkable gelatin and silk fibroin interpenetrating polymer network hydrogels. *Acta Biomater* **7**, 2384-2393 (2011).

209 Lin H, Lozito TP, Alexander PG, Gottardi R, Tuan RS. Stem cell-based microphysiological osteochondral system to model tissue response to interleukin-1beta. *Mol Pharm* **11**, 2203-2212 (2014).

210 Nemeth CL *et al.* Enhanced chondrogenic differentiation of dental pulp stem cells using nanopatterned PEG-GelMA-HA hydrogels. *Tissue Eng Part A* **20**, 2817-2829 (2014).

211 Lin H, Cheng AW, Alexander PG, Beck AM, Tuan RS. Cartilage tissue engineering application of injectable gelatin hydrogel with in situ visible-light-activated gelation capability in both air and aqueous solution. *Tissue Eng Part A* **20**, 2402-2411 (2014).

212 Shin SR *et al.* Carbon Nanotube Reinforced Hybrid Microgels as Scaffold Materials for Cell Encapsulation. *ACS Nano* **6**, 362-372 (2012).

213 Paul A *et al.* Injectable Graphene Oxide Hydrogel-Based Angiogenic Gene Delivery System for Vasculogenesis and Cardiac Repair. *ACS Nano* **8**, 8050-8062 (2014).

214 Cha C *et al.* Controlling mechanical properties of cell-laden hydrogels by covalent incorporation of graphene oxide. *Small* **10**, 514-523 (2014).

215 Levett PA *et al.* A biomimetic extracellular matrix for cartilage tissue engineering centered on photocurable gelatin, hyaluronic acid and chondroitin sulfate. *Acta Biomater* **10**, 214-223 (2014).

216 Wang H *et al.* Cell-laden photocrosslinked GelMA-DexMA copolymer hydrogels with tunable mechanical properties for tissue engineering. *J Mater Sci Mater Med* **25**, 2173-2183 (2014).

217 Hutson CB *et al.* Synthesis and characterization of tunable poly(ethylene glycol): gelatin methacrylate composite hydrogels. *Tissue Eng Part A* **17**, 1713-1723 (2011).

218 Daniele MA, Adams AA, Naciri J, North SH, Ligler FS. Interpenetrating networks based on gelatin methacrylamide and PEG formed using concurrent thiol click chemistries for hydrogel tissue engineering scaffolds. *Biomaterials* **35**, 1845-1856 (2014).

219 Bulcke AIVD *et al.* Structural and Rheological Properties of Methacrylamide Modified Gelatin Hydrogels. *Biomacromolecules* **1**, 31-38 (2000).

220 Shirahama H, Lee BH, Tan LP, Cho NJ. Precise Tuning of Facile One-Pot Gelatin Methacryloyl (GelMA) Synthesis. *Sci Rep* **6**, 31036 (2016).

221 Martineau L, Peng HT, Shek PN. Development of a novel biomaterial: Part II. Evaluation of a photo cross-linking method. (Defence Research and Development Canada, Toronto, 2005).

222 Hoch E, Schuh C, Hirth T, Tovar GEM, Borchers K. Stiff gelatin hydrogels can be photo-chemically synthesized from low viscous gelatin solutions using molecularly functionalized gelatin with a high degree of methacrylation. *Journal of Materials Science: Materials in Medicine* **23**, 2607-2617 (2012).

223 Sutter M, Siepmann J, Hennink WE, Jiskoot W. Recombinant gelatin hydrogels for the sustained release of proteins. *J Control Release* **119**, 301-312 (2007).

224 Engelhardt S *et al.* Fabrication of 2D protein microstructures and 3D polymer-protein hybrid microstructures by two-photon polymerization. *Biofabrication* **3**, 025003 (2011).

Chapter 3 Improvement of Gelatin methacryloyl synthesis*

Gelatin methacryloyl (GelMA) is one of the most widely-used photocrosslinkable, natural protein-based material, which is applicable for wide range of bioapplications. However, its synthesis method has limited control over the degree of substitution (DS) and low efficacy. In this chapter, improvement of GelMA synthesis is described. By considering pH of the reaction solution and other experimental parameters, high DS was achieved with much low reactant consumption.

* This chapter was published substantially as: (1) Lee BH[†], Shirahama H[†], Tan LP[‡], Cho NJ[‡]. "Efficient and Controllable Synthesis of Highly Substituted Gelatin Methacrylamide for Mechanically Stiff Hydrogels." *RSC Advances* **5**, 106094-106097 (2015). (2) Shirahama H[†], Lee BH[†], Tan LP[‡], Cho NJ[‡]. "Precise Tuning of Facile One-pot Gelatin Methacryloyl (GelMA) Synthesis." *Scientific Reports* **6**, 31036 (2016). ([†] denotes equal first authors; [‡] denotes equal corresponding authors).

3.1. Introduction

Gelatin is an attractive biomaterial that is obtained from the partial hydrolysis of collagen, the most abundant protein in the human body [1]. It is biocompatible, biodegradable, and suitable for a wide range of cell types. Gelatin can provide adequate cell attachment via RGD (Arg-Gly-Asp) motifs [2], and it plays an important role in cell proliferation [3], function [4], and differentiation [5]. Furthermore, gelatin is less immunogenic than collagen [6,7] due to the reduced presence of aromatic groups [8]. In addition, gelatin is relatively easy to obtain and low in cost compared with other natural materials.

Raw gelatin can only form a physical hydrogel at specific concentrations and temperatures, albeit with low mechanical strength. To improve hydrogel stiffness, a number of crosslinking strategies have been adopted, including the use of crosslinking chemicals (e.g., glutaraldehyde [9] and genipin [10]) and chemical modification to support photo-crosslinking (e.g., glycidyl methacrylate [11] and methacrylic anhydride [MAA]). Compared with the use of crosslinking chemicals, photo-crosslinking methods provide fast, uniform in situ curing. Among the chemicals used for gelatin modification, MAA is the most widely used. The product, gelatin methacryloyl (GelMA), has been used in various bio-applications.

The method of synthesizing GelMA was originally developed by Van Den Bulcke et al. in 2000 [12]. Briefly, MAA monomers react with lysine and hydroxyl lysine groups of gelatin by dissolving the gelatin in phosphate buffer solution (PBS) at 50 °C (cf. **Figure 3.1**). Their report opened up a new arena for GelMA in biomaterial research and tissue engineering applications. However, GelMA synthesis remains suboptimal, leaving considerable room for improvement especially in its controllability and efficacy [13]. For example, in theory, one MAA molecule could react with one lysine group. Nevertheless, studies following the original method have reported using MAA of 18-47 times higher than that for high degree of substitution (DS) (> 85%) [14-19].

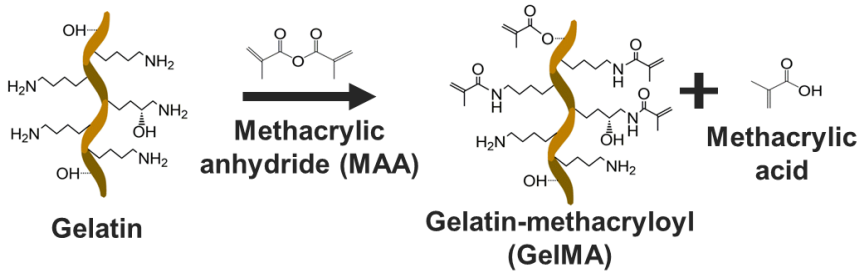

Figure 3.1 Schematic illustration of gelatin methacryloyl (GelMA) synthesis. Redrawn from reference [20].

Various attempts have been made to enhance the synthesis scheme to improve reaction efficacy. For example, Martineau et al. used a water-miscible organic solvent (dimethyl sulfoxide, DMSO) as the buffer choice rather than PBS [21]. This method effectively hindered MAA's contact with water, which can result in hydrolysis, and certainly improved the DS in comparison with the use of PBS. However, it requires an organic base and an additional step of precipitation with ethanol, which leads to a low yield [21,22].

Another means of synthesis is to employ pH adjustment during synthesis to keep the free amino groups neutral to react with MAA. The essence of this method is to maintain the pH of the reaction solution above the isoelectric point (IEP) of the gelatin, keeping the free amino groups of lysine neutral to allow them to react with MAA. The IEP differs for different types of gelatin: 8-9 for type A and 5-6 for type B [23]. The use of PBS (pH 7.4) as a buffer is not sufficient for pH maintenance because a byproduct of the reaction, methacrylic acid (**Figure 3.1**), alters the pH, rendering it acidic. In turn, the free amino groups of gelatin become ionized, which inhibits the reaction with MAA (cf. **Figure 3.2**). Although pH adjustment leads to improved efficacy, it still requires a 10-32 molar excess of MAA [24-26]. In addition, manual pH adjustment is laborious, and the eventual DS is highly dependent on the operating technique.

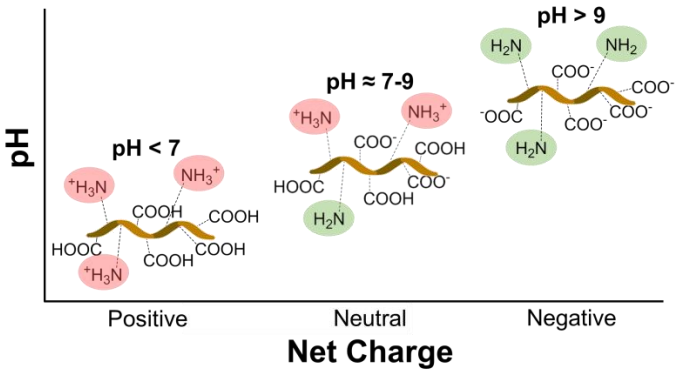

Figure 3.2 Schematic illustration of how solution pH affects the charging of functional groups of type A gelatin. Redrawn from reference [27].

We hypothesize that maintaining a pH above the corresponding IEP of the gelatin type would provide highly efficient conversion of gelatin into GelMA. In addition, to the best of our knowledge, there is no comprehensive understanding of how reaction parameters (e.g. gelatin concentration, reaction temperature and molar ratio) affect the DS. The goal of this study is to develop a suitable reaction scheme to convert type A gelatin into GelMA by considering pH of the reaction solution and to systematically examine reaction parameters. To this end, a sodium carbonate–bicarbonate (CB) buffer system was introduced to provides a suitable buffer range around pH 9.0, which is above the corresponding IEP of the gelatin molecules (pH 7–9). First, we examined the efficacy of CB buffer on DS with/without manual pH maintenance. Next, CB buffer molarity and other experimental parameters are thoroughly optimized to achieve high DS without manual pH adjustment.

3.2. Experimental details

3.2.1. Synthesis of gelatin methacryloyl

Effect of CB buffer and pH maintenance

First we have investigated effect of CB buffer employment with and without pH maintenance as following protocol: Type A gelatin of 175 bloom, derived from acid-cured porcine skin tissue, was dissolved at 10 w/v% at 60 °C in two buffer systems (PBS and 0.1 M CB buffer [3.18 g sodium carbonate and 5.86 g sodium bicarbonate in 1 L distilled water]). GelMA was prepared by reaction of free amino groups of lysine/hydroxylysine amino acids in the gelatin with MAA (94%) at 0.1 mL per gram of

gelatin at 50 °C for 3 h. One-sixth of 1 mL MAA (167 μL) was added every 30 minutes for 3 h in a drop-wise format to the gelatin solutions with or without pH adjustment at 600 rpm stirring speed. After 3 h of reaction, the solutions were readjusted to a pH of 7.4, filtered with standard filter paper and membrane filter with 0.2 μm pore diameter, dialyzed using a PALL Minimate TFF Capsule (with 10 kDa molecular weight cut-off) at 40 °C for 1 day, lyophilized, and stored at -20 °C until further use. MAA concentration-dependent experiments were also conducted with different feed ratios of MAA (mL) to gelatin (g) ranging from 0.0125:1 to 0.2:1 were added into 10 w/v% gelatin in CB buffer. The synthesis condition was the same as in CB with pH maintenance at 9.0. In order to investigate the effect of pH on the degree of substitution in CB buffer solutions, pH dependent experiments were carried out at the fixed feed ratio of MAA (0.1 mL) to gelatin (1 g) in different pHs (7, 8, 9, 10, and 11) of CB buffer solutions. All chemicals were purchased from Sigma-Aldrich.

Comprehensive optimization toward facile one-pot synthesis

Similarly, comprehensive optimization of experimental parameters was conducted as following protocol: The gelatin was dissolved in CB buffer, and the pH was adjusted with 5 M sodium hydroxide or 6 M hydrochloric acid. Subsequently, MAA was added to the gelatin solution under magnetic stirring. The reaction proceeded for 3 h, and then the pH was readjusted to 7.4 to stop the reaction. After being filtered, dialyzed, and lyophilized, the samples were stored at -20 °C until further use. The standard conditions of the synthesis were: CB buffer at 0.25 M, initial pH adjustment at pH 9, MAA amount at 0.1 mL per gram of gelatin concentration at 10 w/v%, reaction temperature at 50 °C and reaction time for 3 h. In performing detailed characterization of the synthesized GelMA scheme, the following experimental parameters were investigated: CB molarities (0.1, 0.25, 0.5, 0.75, and 1 M), initial pHs (pH 8, 9, 10, and 11), MAA/gelatin feed ratios (MAA/gelatin: 0.0125, 0.25, 0.5, 0.1, and 0.2 mL/g), gelatin concentrations (1, 2.5, 5, 10, and 20 w/v%) and reaction temperatures (35, 40, 45, and 50 °C).

Reaction kinetic experiments

To investigate reaction efficacy, reaction kinetic experiments were performed by sampling the reaction solution at different reaction time points, namely, 0, 1, 5, 10, 15, 30, 60, 120, and 180 min after MAA addition. Each sample of 10 mL was immediately quenched with a 5- to 10-fold amount of water, dialyzed and lyophilized for the determination of DS. For supplemental inspection, 300 μ L of the reaction solution was taken at each time point, immediately frozen (without dialysis) at -80 °C, and lyophilized for ^{1}H NMR measurement.

3.2.2. ^{1}H NMR analysis

^{1}H-NMR (400 MHz Varian) experiments were conducted in order to directly verify the DS of GelMA. Around 50 mg of each lyophilized GelMA sample was dissolved in 1 mL of deuterium oxide (D_2O) at 40 °C. The peak area of aromatic acids in the GelMA samples was employed as a reference in each spectrum. The peak area of lysine methylene protons appearing at around 2.8 ppm was used for calculation of the DS as follows [28];

$$\text{DS (\%)} = \left(1 - \frac{\text{the area of lysine methylene of GelMA}}{\text{the area of lysine methylene of gelatin}}\right) \times 100$$

3.2.3. TNBS measurement

For quantification of the DS, 2,4,6-trinitrobenzene-sulfonic acid (TNBS), which can change its color by reaction with primary amino groups, was used as follows: Gelatin and GelMA samples were separately dissolved in 0.1 M sodium bicarbonate buffer (pH 8.5) at a concentration of 1.6 mg/mL. Then, 0.5 mL of 0.01% TNBS solution was added to 0.5 mL of each sample solution. The sample solutions were mixed well and incubated at 37 °C for 2 h. Subsequently, 0.5 mL of 10 w/v% sodium dodecyl sulfate (SDS) and 0.25 mL of 1N HCl were added to each sample in order to stop the reaction and the absorbance of each solution was measured at 335 nm. The molar concentration of primary amino groups in each GelMA solution was determined by comparison with glycine standard solutions [29], which were prepared at 0, 8 16, 32, and 64 μg/mL.

3.3. Results and discussions

3.3.1. Multiple process

Effect of buffer and sequential pH adjustment

First, we investigated the effect of buffer system on the solution pH during the course of the reaction between gelatin and MAA as presented in **Figure 3.3** and **Table 3.1.** Two buffer systems were selected: PBS (a neutral buffer) and CB (an alkaline buffer). In each case, 1 mL of MAA was initially added to 10 g of gelatin, which is a relatively low feed ratio compared to the conventional feed ratio of MAA (6–20 mL) to type A gelatin (10 g) in order to obtain GelMA with a degree of substitution above 85%. Type A gelatin has approximately 2.86 mmol of lysine per 10 g according to the literature; [30] hence, the reaction molar ratio of MAA (6.31 mmol per 1 mL) to lysine (2.86 mmol per 10 g gelatin) is around 2.2 to 1 in our reaction scheme. As depicted in **Figure 3.3**, the sequential loading of MAA (0.167 mL at each step) every 30 min at 50 C for 3 h was applied, and the solution pHs were monitored as the reactions progressed. All buffer solutions decreased in pH as the reaction proceeded due to an increase in the amount of methacrylic acid generated as a by-product. After gelatin was dissolved in PBS at pH 7.4 and CB buffer at pH 9.7, the pHs of PBS and CB buffers dropped to 5.3 and 7.8, respectively. The final pHs of PBS and CB were 3.7 and 5.3, respectively, after 3 h reaction.

Table 3.1 Comparison of GelMA preparation methods in feed ratio, buffer system, pH and DS

Group	Conventional method	PBS w/o pH adjustment	PBS at pH 7.8	CB w/o pH adjustment	CB at pH 9.0
Gelatin (w/v%)	10	10	10	10	10
MAA (% v/v)	6-20	1	1	1	1
MAA (mL) /gelatin (g)	0.6-2/1	0.1/1	0.1/1	0.1/1	0.1/1
Molar ratio (MAA/amine)	13-44	2.2	2.2	2.2	2.2
Buffer	PBS	PBS	PBS	CB	CB
pH adjustment	No	No	Six times at pH 7.8	No	Six times at pH 9.0
DS from NMR (%)		47	87	78	100
DS from TNBS (%)	> 85	51.81 ± 0.16	80.35 ± 0.49	76.24 ± 0.54	97.20 ± 0.28

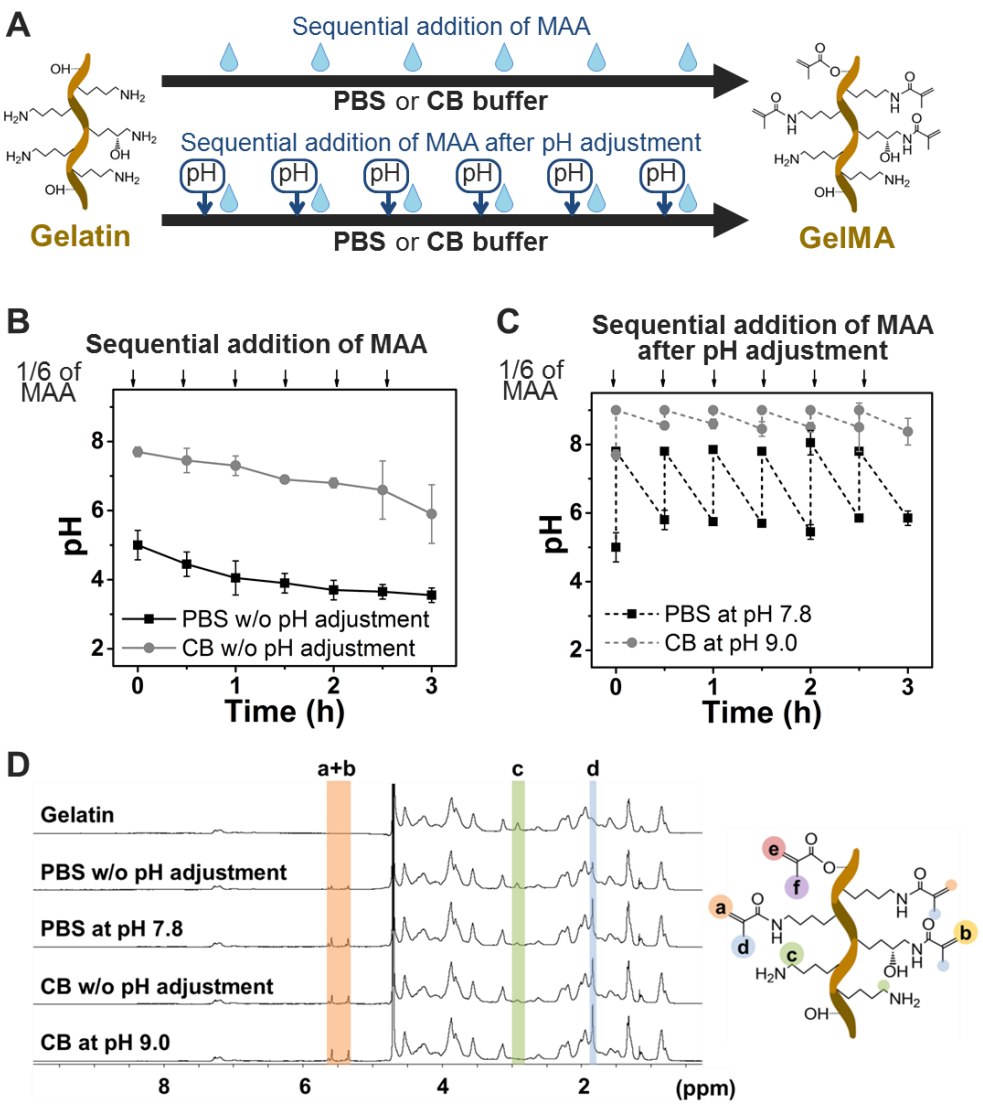

Figure 3.3 (A) Schematic illustration of for different experimental conditions. **(B)** Change in solution pH of PBS and CB buffer systems during reaction progress (without pH adjustment). **(C)** Change in solution pH of PBS and CB buffer systems during reaction progress (with pH adjustment before each MAA addition step). Error bars indicate the relative standard deviations of two different samples (n = 2). **(D)** ^{1}H-NMR verification of GelMA conversion based on DS values. Peaks correspond to acrylic protons (2H) of methacrylamide grafts of lysine groups (a) and those of hydroxyl lysine groups (b), methylene protons (2H) of unreacted lysine groups (c), methyl protons (3H) of methacrylamide grafts (d), acrylic protons (2H) of methacrylated grafts of hydroxyl groups (e), and methyl protons (3H) of methacrylated grafts of hydroxyl groups (f). Redrawn from reference [27].

The pHs of the two buffer systems dropped more rapidly compared to the same reactions without pH adjustment, indicating that MAA could be consumed more quickly

due to the reaction with regenerated free amino groups and continual hydrolysis of MAA at pH maintenance. The yield was 67-73% for all the groups.

Next, in order to calculate the DS in the GelMA products, we conducted the 2,4,6-trinitrobenzene sulfonic acid (TNBS) assay for determination of unreacted free amino groups in gelatin. Reactions in PBS without pH adjustment resulted in a DS of 51.81 ± 0.16% while similar reactions in CB buffer resulted in a DS of 76.24 ± 0.54%, as presented in **Table 3.1.** With pH adjustments, significant improvements were observed for both buffer systems, with a DS of 80.35 ± 0.49% for PBS (at pH 7.8) and a DS of 97.20 ± 0.28% for CB buffer (at pH 9.0). ^{1}H-NMR analysis was also used to verify the extent of the DS. The results are in agreement with the aforementioned values as depicted in **Figure 3.3D**. There were minimal side reactions with hydroxyl groups of gelatin other than amino groups in all experimental groups, while the spectra of the gelatin derivatives at $5.6 \leq \delta \leq 6.1$ ppm appeared when a 10–20 : 1 molar ratio of MAA to type B gelatin was employed in PBS .

Effect of methacrylic anhydride/gelatin feed ratio

The dependence on MAA concentration was also investigated in CB buffer with pH 9 adjustment, as presented in **Figure 3.4**. The concentrations of MAA added to gelatin (10 g per 100 mL, 10 w/v%) ranged from 0.125 to 2% v/v, which correspond to a range of molar ratios of amino groups to MAA from 1 : 0.275 to 1 : 4.4. All the gelatin solutions reacted with different amounts of MAA at pH 9 adjustment in CB buffer. The pH of each reaction solution dropped in proportion to the amount of MAA added which is directly associated with the production of the methacrylic acid by-product. The DS results achieved with our improved scheme are presented in **Figure 3.4B** alongside results obtained by the conventional scheme in past studies. In the conventional method using PBS, it was difficult to control the DS beyond 80–90% because a higher feed ratio of MAA to gelatin might produce more by-product (methacrylic acid) and cause protonation of the remaining free amino groups. Even a feed ratio of 0.6-2.0 mL (MAA)/g (gelatin) (13–44 molar excess of MAA over free amino groups) was limited to producing type A GelMA with a DS of 90% or less with the conventional method. By contrast, using our method, the DS of GelMA increased up to around 97% or more in a nearly linear and

controllable manner based on the feed ratio—a more than three-fold improvement in DS over the conventional method in a similar range of feed ratios.

Indeed, the feed ratio from 0.0125 to 0.1 mL (MAA)/1 g (gelatin) led to type A GelMA with DS ranging from 22.32 ± 1.27 to 97.20 ± 0.27%. The feed ratio of 0.1 mL (MAA) to 1 g (gelatin) corresponding to a 2.2-fold molar excess of MAA over free amino groups yielded a near-100% DS. The feed ratio of 0.2 mL (MAA) to 1 g (gelatin) caused free amino groups to be completely consumed and additionally some hydroxyl groups on amino acids reacted with MAA, as interpreted from the ^{1}H-NMR data showing peaks at between 6.1 and 5.7 ppm (**Figure 3.4C**). Therefore, type A GelMA with a DS ranging from 20 to 100% could be tailored within a low concentration of MAA (1% v/v) with a negligible degree of side reactions of hydroxyl groups of gelatin with MAA.

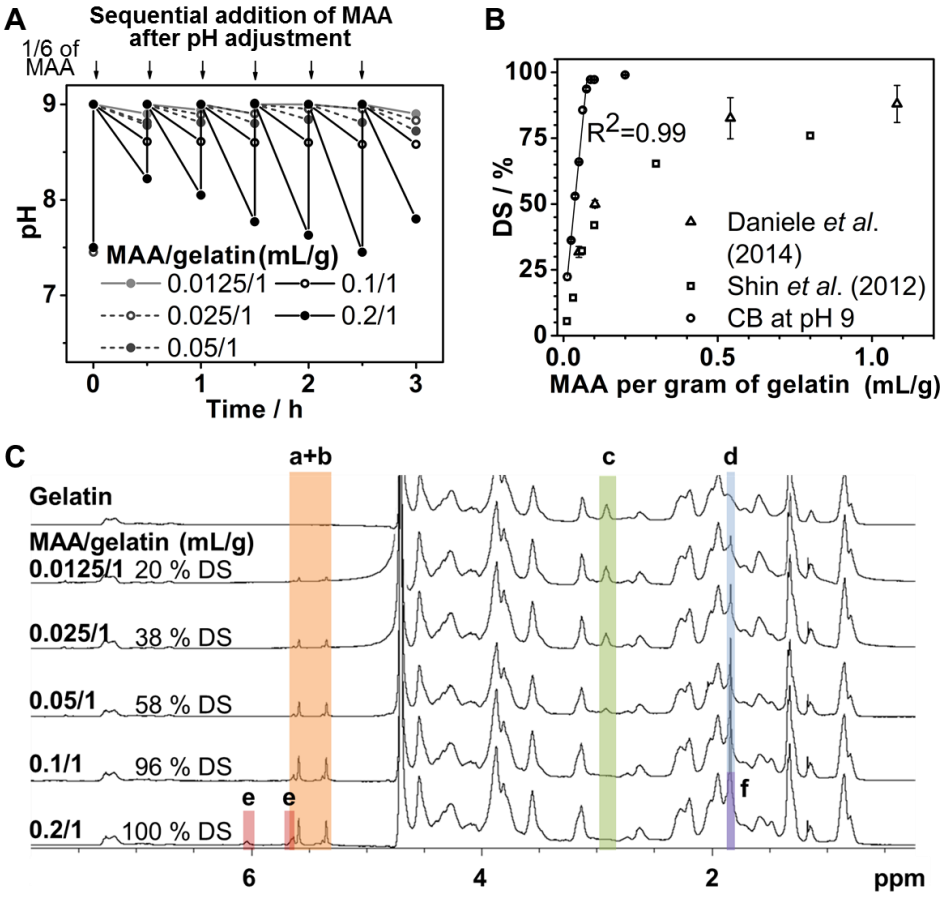

Figure 3.4 (A) Change in solution pH of CB buffer system as a function of MAA/gelatin feed ratio. **(B)** DS versus MAA/gelatin feed ratio in comparison with previous studies. **(C)** ^{1}H-NMR verification and its DS values. Redrawn from reference [27].

3.3.2. Facile one-pot process

Effect of molarity of alkali buffer

As the effect of CB buffer is confirmed, we further optimized molarity of CB buffer, hypothesizing that a higher CB molarity can simplify the synthesis scheme by omitting manual, sequential process (**Figure 3.5**).

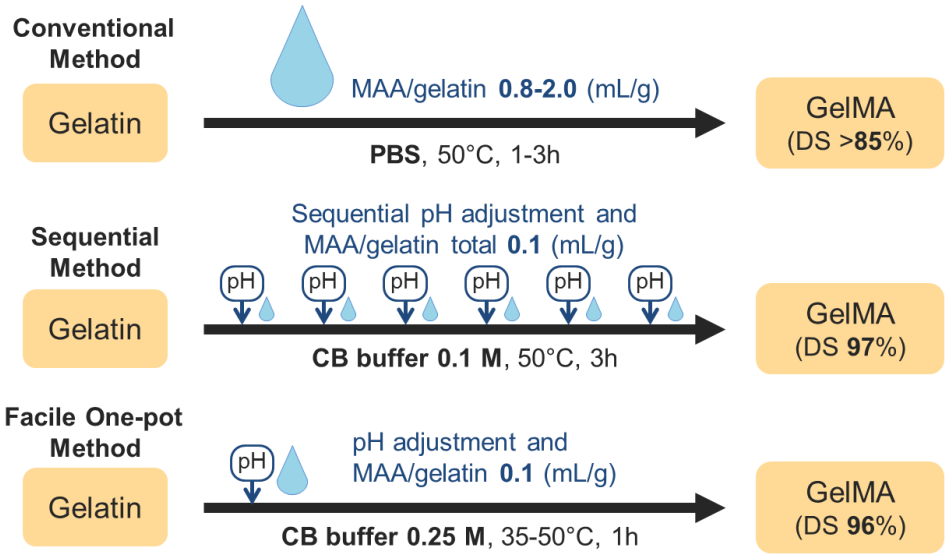

Figure 3.5 Schematic illustration of different synthesis processes of GelMA and their respective degrees of substitution.

Therefore we first altered the molar concentration of CB buffer, which is comprised of sodium carbonate and sodium bicarbonate as shown in **Figure 3.6**. The control range of the CB molar concentration was set from 0.1 to 1 M, with the aim of maintaining the pH at a level higher than that of the IEP of type A gelatin during the reaction. Further, we initially adjusted the pH to 9 prior to the reaction with MAA. The gelatin solution was prepared at a concentration of 10 w/v%, and 0.1 mL of MAA per gram of gelatin was used, the same conditions as those used in our previous study (cf. **Table 3.1).** This MAA amount was calculated to be a 2.2-fold molar excess over the free amino group of gelatin, with reference to the literature (0.286 mmol of amino groups per gram of gelatin). The pH changes in each reaction solution were monitored every 30 min for 3 h during the reaction at 50 °C, as shown in **Figure 3.6**A. During synthesis, reaction solutions with a higher CB buffer concentration had a greater buffering capacity and hence were able to

maintain more closely the original pH up to completion of the reaction scheme. However, in both the 0.1 M and 0.25 M CB buffer cases, we observed a sharp drop in pH to 6.6 during the initial reaction, signifying that the reaction took place within a short period of time. Furthermore, after 30 min of reaction, we observed a slight increase in pH, which suggests that the reaction might be completed, and that the pH of the solution was being restored by the CB buffer capacity. To measure DS as a function of CB buffer concentration, TNBS assay was conducted after completion of the reaction. The results showed that the DS decreased significantly with an increase in the CB buffer concentration, particularly above 0.5 M CB buffer solution. This supports that the hydrolysis of MAA is further accelerated in CB buffer solutions with a higher molarity (**Figure 3.6**B). This trend was also observed in experimental results obtained by proton nuclear magnetic resonance (^{1}H NMR) analysis, as shown in **Figure 3.6**C.

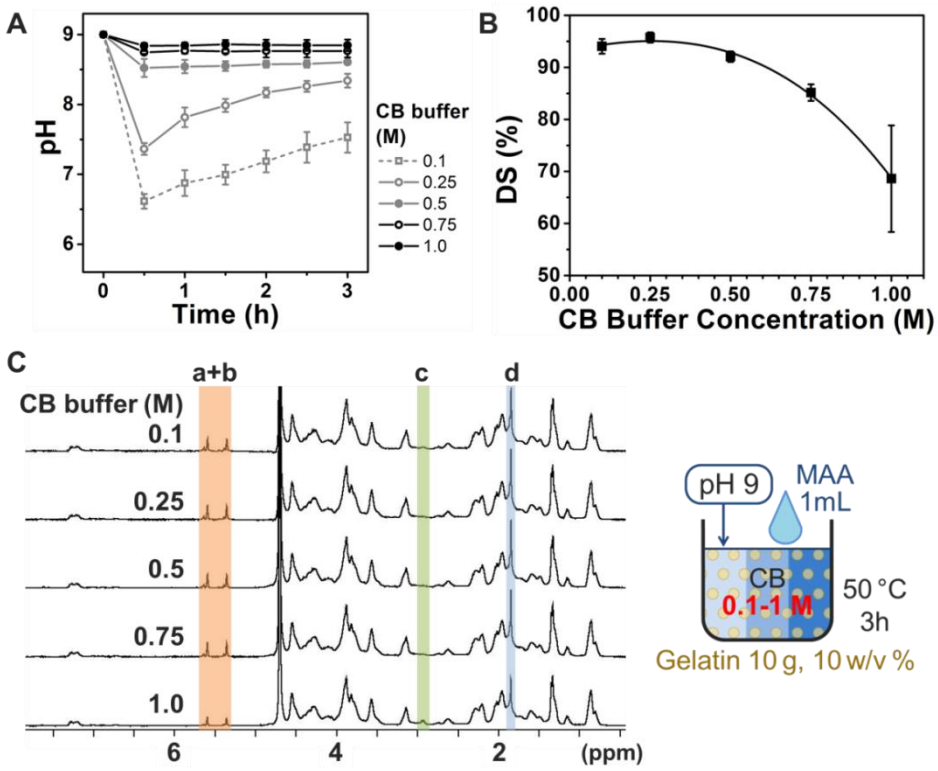

Figure 3.6 Effect of different CB molarities on DS of GelMA synthesis. Error bars indicate the relative standard deviations of three or more different samples ($n \geq 3$). Redrawn from reference [20]. **(A)** pH transition kinetics during the reaction. **(B)** DS versus CB molarity, obtained from TNBS assay. **(C)** ^{1}H NMR verification. Schematic illustration denotes parameters used in this series of experiment.

The peaks of methylene lysine protons (2H) around 2.8 ppm (peak c) did not appear in the spectra with a high DS, indicating the complete conjugation of lysine with MAA. Further, the acrylic protons (2H) of the methacrylamide grafts around 5.5 ppm (peak a + b) and those of the methyl protons (3H) of methacrylamide around 1.9 ppm (peak d) were higher in the higher DS samples. Nearly complete substitution (DS = 95.75 ± 0.98%) was achieved at a CB buffer concentration of 0.25 M, which is the highest DS among the experimental groups. The polynomial fitting curves of the data points suggest a local maximum value at 0.257 M, which implies that 0.25 M CB buffer is close to the optimal buffer concentration. This concentration was therefore selected for further investigation.

Effect of initial pH adjustment

We then investigated the optimal pH for the initial pH adjustment step in order to further optimize the synthesis conditions. In the preceding set of experiments that identified the dependence on CB buffer concentration, the pH of the gelatin solution was adjusted to 9 prior to MAA addition. In this next set, different initial pH adjustments were conducted, including pH 8, 9, 10, and 11, in order to determine the optimal initial pH adjustment condition based on determining which one yielded the highest DS. The pH transitions in **Figure 3.7A** show that 0.25 M CB buffer stabilized the pH around pH 8–10 as the reaction progressed. The corresponding DS results in **Figure 3.7B** show that the initial pH adjustment step to pH 9 led to a higher DS than the reactions conducted with other pH adjustment steps above or below this optimal value (pH 8, 10 and 11). This finding indicates that reactions at a lower pH (pH 8) may be hindered by greater protonation of the free amino groups, whereas those at a higher pH (pH 10 and 11) may be hampered by excess MAA hydrolysis catalyzed by a strong base (hydroxide ion). The polynomial fitting curve reached a local maximum value at pH 8.8, which implies that initial adjustment to pH 9 is optimal among the test cases. As shown in **Figure 3.7C**, the TNBS results agree well with the ^{1}H NMR results. Taken together, these findings support that initial pH adjustment to 9 with 0.25 M CB buffer creates the optimal conditions for balancing the deprotonation of amino groups with MAA hydrolysis.

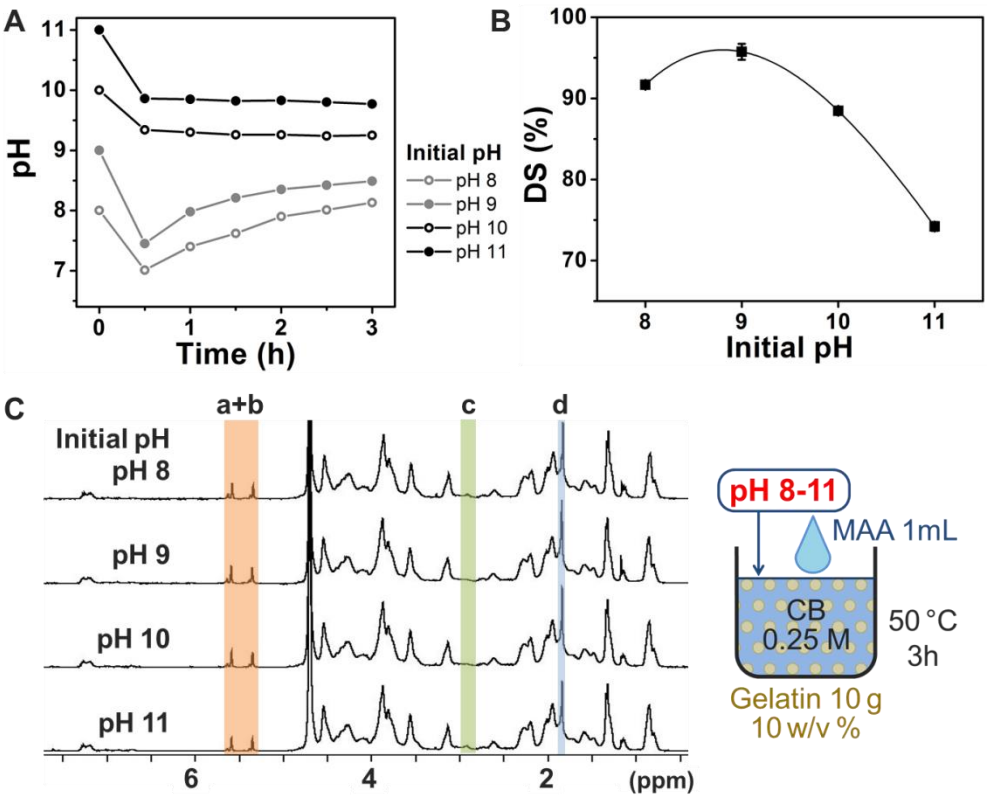

Figure 3.7 Effect of different initial pH adjustments on DS of GelMA synthesis. Error bars indicate the relative standard deviations of three independent measurements (n = 3). Adopted from reference [20]. **(A)** pH transition kinetics during the reaction. **(B)** DS versus initial pH. **(C)** ^{1}H NMR verification.

Effect of methacrylic anhydride/gelatin feed ratio

The dependence of GelMA DS on the MAA concentration was next investigated in order to identify the range or DS controllability and to compare the results with those obtained by other synthesis methods with regards to the MAA supply. The feed ratio was varied from 0.012 to 0.2 ml of MAA per gram of gelatin, which corresponds to 0.265–4.4 molar ratios of the MAA over the amino group. As shown in Fig. 4A, when a larger MAA amount was used, a lower pH was observed during synthesis, as the by-product of methacrylic acid is proportional to the amount of MAA consumed. **Figure 3.8B** summarizes the DS results based on different feed ratios compared with literature values. Our present findings agree well with our previous identification of a streamlined approach (0.1 M CB with pH adjustment), with the additional advantage that no pH

adjustment is required in our improved reaction scheme. As a result, the optimized scheme enables simple, facile one-pot GelMA synthesis under conditions of a 0.25 M CB buffer concentration and initial pH adjustment to 9 with a similar effect on DS as sequential GelMA synthesis under conditions of multistep pH adjustment and MAA addition every 30 min. Moreover, in the present study, the DS results for the MAA/gelatin feed ratio from 0.012 to 0.05 mL/g increased linearly, showing better controllability of DS, compared to a conventional method where the relationship is less controllable [31,32]. In particular, we observed that methacrylation of lysine groups almost reached saturation around 0.1 mL/g. In Fig. 4C, additional peaks were observed at around 5.6 ppm and 6.1 ppm (peak e) in the ^{1}H NMR spectrum of the 0.2 mL/g (MAA/gelatin) sample. These peaks can be attributed to partial methacrylation of the hydroxyl groups of gelatin, which occurs when a high molar excess of MAA is supplied.

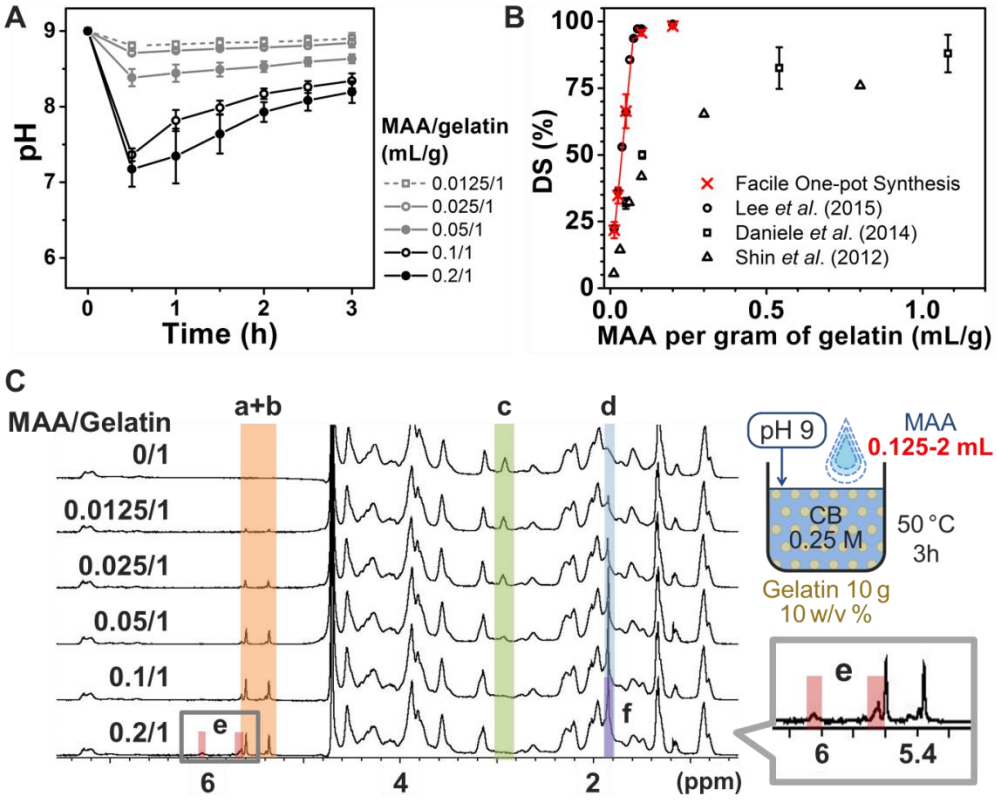

Figure 3.8 Effect of MAA/gelatin ratios on DS of GelMA synthesis. Error bars indicate the relative standard deviations of three independent measurements (n = 3). Adopted from reference [20]. **(A)** pH transition kinetics during the reaction. **(B)** DS versus MAA/gelatin ratio. **(C)** ^{1}H NMR verification.

Effect of gelatin concentration

Based on the aforementioned conditions, we further optimized the gelatin concentration, a parameter which was not discussed in the original paper [12] although 10 w/v% is conventionally used in most GelMA studies. We investigated gelatin concentrations ranging from 1, 2.5, 5, 10, and 20 w/v%, with all samples containing 10 g gelatin. During synthesis, the 1 w/v% gelatin group exhibited highly separated phases of aqueous (gelatin in CB buffer) and organic compounds (MAA). MAA did not disperse evenly, and it appeared to form large oil droplets in the reaction solution. This apparent phase separation could be the result of the low gelatin concentration, and gelatin is known to be a good emulsifier due to its amphiphilic structure [33]. Indeed, it is reported that surface tension decreases with an increase in gelatin concentration [34], and this surfactant behavior could help MAA to become evenly dispersed in the reaction solution. Based on these characteristic properties of MAA in aqueous suspensions, we observed that a lower gelatin concentration with a higher buffer capacity maintained a more constant pH (**Figure 3.9A**), but the aforementioned strong phase separation resulted in a lower DS compared with the other groups with a higher gelatin concentration (**Figure 3.9B**). Hence, higher gelatin concentrations are favorable due to improved dispersibility taking into account its surfactant behavior. This result was supported by ^{1}H NMR analysis, in which small peaks of methylene of the unreacted lysine amino groups still appeared in the 1 w/v% gelatin group, indicating that some of the lysine amino groups did not react with MAA. One possibility is that MAA may be quickly hydrolyzed at the interface between the MAA droplets and water. The DS was almost saturated above 10 w/v% and the highest DS was obtained with the 20 w/v% concentration. In conclusion, a high concentration of gelatin improved the reaction efficacy with MAA due to the improved miscibility of MAA with gelatin. Importantly, this result indicates that MAA's solubility in the gelatin solution is an important parameter in the MAA-gelatin reaction.

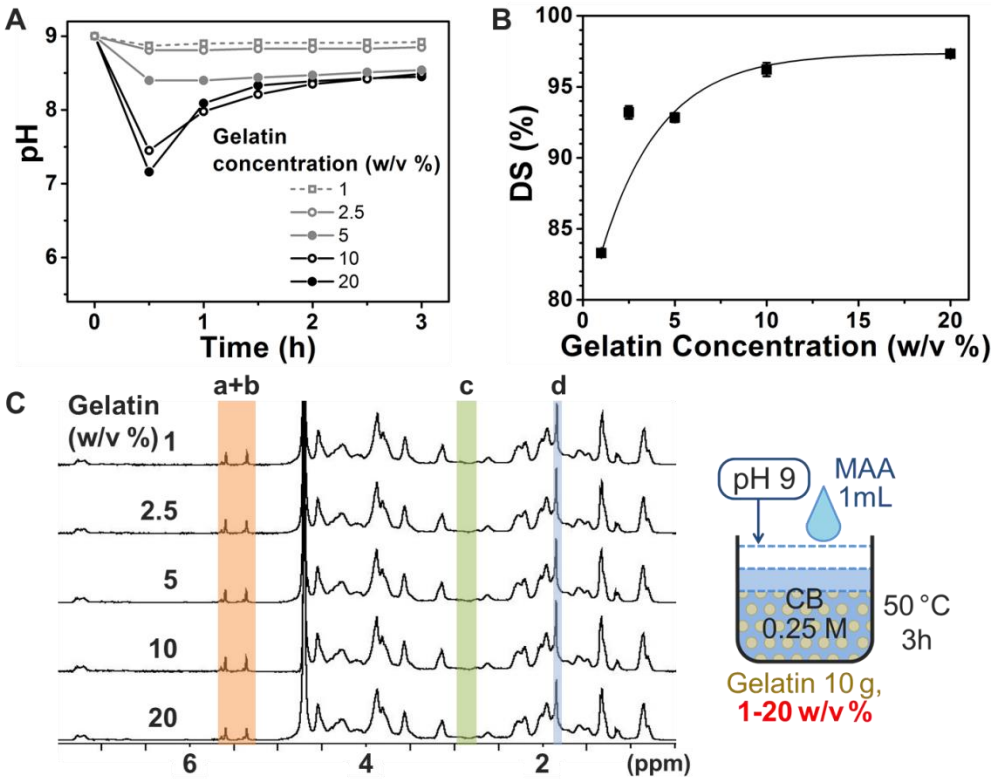

Figure 3.9 Effect of gelatin concentrations on GelMA synthesis. Error bars indicate the relative standard deviations of three independent measurements (n = 3). Adopted from reference [20]. **(A)** pH transition kinetics during the reaction. **(B)** DS versus gelatin concentration. DS was obtained from TNBS assay. Gelatin solutions at 10 w/v% and above led to a high DS. **(C)** ^{1}H NMR verification.

Effect of reaction temperature

Similarly, the effect of reaction temperature on DS was also investigated. In most reports, a single temperature has been used, with the original protocol utilizing a reaction temperature of 50 °C, whereas some studies conducted the GelMA reaction at temperatures between 40 and 60 °C. In our experiments herein, we systematically evaluated the reaction efficacy in lower temperature range to seek possibility in reducing heat supply. Temperatures below 30 °C were excluded because 30 °C is the approximate gelling point of 10% type A gelatin of 250 bloom [35], and stirring could become inefficient below this temperature. Note that the actual gelling temperature in our case may be slightly lower than that reported in the literature because gelatin of a lower bloom

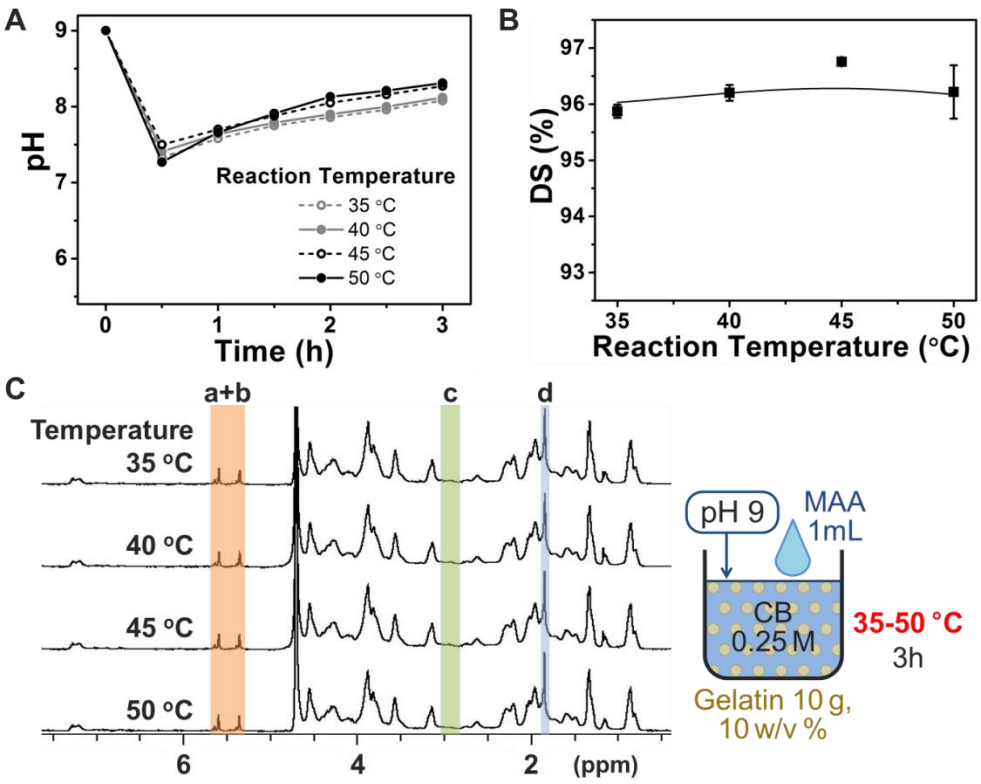

Figure 3.10 Effect of reaction temperature on GelMA synthesis. Error bars indicate the relative standard deviations of three independent measurements (n = 3). Adopted from reference [20]. **(A)** pH transition kinetics during the reaction. **(B)** DS versus reaction temperature. DS was obtained from TNBS assay. All conditions led to a high DS. **(C)** ^{1}H NMR verification.

(175 bloom) was used in our experiments. Besides taking into consideration the gelling point, the temperature could also be expected to influence the reaction kinetics, although the effects on the corresponding DS ratio remained to be investigated. Across the evaluated temperatures, the pH transition was similar in the different experimental groups (**Figure 3.10A**), while higher temperatures yielded modestly faster reaction kinetics with more moderate drops in pH during the initial reaction stage. Nevertheless, the DS results in Fig. 6B showed no significant differences across the test groups, with even the 35 °C sample resulting in 96% DS. Collectively, these results support that the GelMA reaction can be conducted at 35 °C with equivalent results to the conventional 50 °C.

Time dependent monitoring of the synthesis

The final experimental series was focused on identifying the dependence of GelMA synthesis on the reaction time. Van Den Bulcke et al. used a reaction time of 1 h, and

subsequent studies used 1–3 h. To investigate the DS as a function of reaction time, sampling was carried out during the standard reaction (0.25 M CB, 0.1 mL/g of MAA/gelatin, 10 w/v% gelatin at 50 °C reaction temperature with initial pH adjustment at 9) at time points 0, 1, 5, 10, 15, 30, 60, 120, and 180 min after MAA addition. The collected samples were immediately quenched, dialyzed, and lyophilized. **Figure 3.11A** shows the DS versus reaction time results. It can be seen that the DS continued to increase until 30 min, but after 1 h there was no significant difference among the reaction time points. The ^{1}H NMR result in **Figure 3.11B** corroborates the TNBS result, showing a decrease and chemical shift in the methylene peaks of unreacted lysine amino groups (peak c) until and after 30 min, respectively.

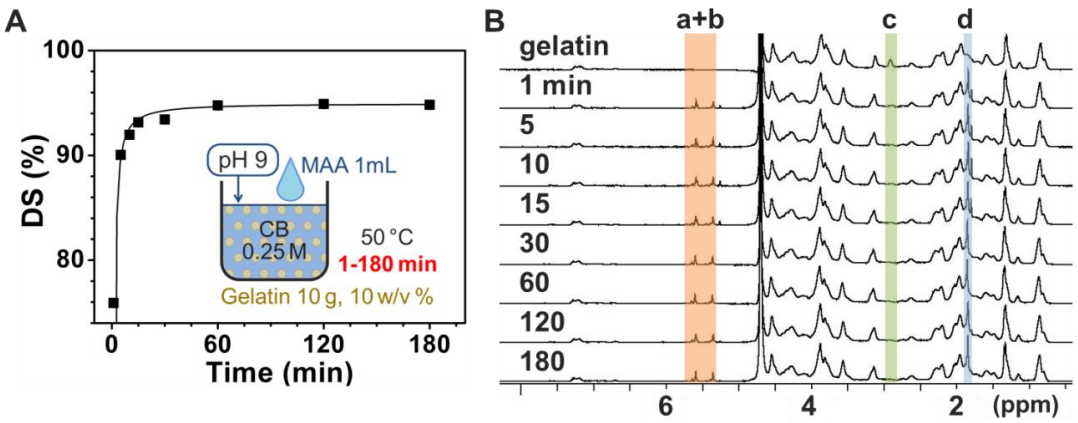

Figure 3.11 Time-dependent DS monitoring of GelMA synthesis, conducted at standard condition. **(A)** DS versus reaction time obtained from TNBS assay. **(B)** ^{1}H NMR verification.

The immediately lyophilized samples without dialysis showed the exact same tendency in ^{1}H NMR peak signatures as shown in **Figure 3.12A**. Peaks at around 2.8 ppm, which correspond to methylene protons (2H) of unreacted lysine groups, disappeared almost completely after 60 min. Additional peaks, appeared at 1.8, 5.3 and 5.6 ppm, are attributed to methacrylic acid (the reaction byproduct) [36]. The spectra between 5.2 and 5.4 ppm are enlarged and shown in **Figure 3.12B**. Peak α at 5.35 ppm corresponds to an acrylic proton in methacrylated grafts of GelMA, and peak β at 5.25 ppm corresponds to an acrylic proton in methacrylic acid. They are integrated and presented in **Figure 3.12C**. All the integrations are normalized to peaks of aromatic groups at around 7.2 ppm.

Methacrylation reached a plateau after 60 min whereas production of methacrylic acid increased slightly. These results support that the GelMA reaction can be completed within 1 h, also suggesting that there is a small amount of unreacted MAA after 1 h, being hydrolyzed further.

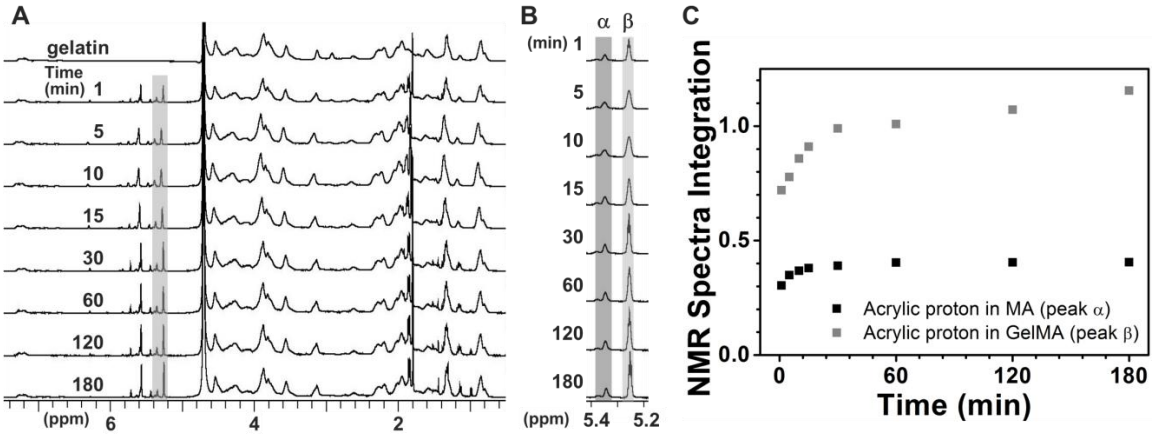

Figure 3.12 (A) NMR spectra of samples, taken during GelMA synthesis, conducted at standard conditions (cf. **Figure 3.11**). **(B)** Enlarged spectra of shadowed part in (A), between 5.2 and 5.4 ppm. Peak α and β corresponds to methacrylated grafts of GelMA and methacrylic acid, respectively. **(C)** Normalized and integrated NMR peaks of α and β.

3.4. Conclusions

In summary, we have proven that efficacy and controllability of GelMA synthesis can be improved by considering pH during the process. First, we employed CB buffer and sequential pH adjustment, resulted in high DS with an appreciably smaller molar excess of MAA. Next, CB buffer molarity and other experimental parameters were comprehensively investigated to realize a facile GelMA synthesis, which is to achieve high DS with minimal MAA consumption without manual pH adjustment. The parameters systematically examined were CB buffer molarities, MAA concentrations, gelatin concentrations, reaction temperatures, initial pH adjustment steps, and reaction time. The results suggested that a simplified synthesis process with a feed ratio of MAA/gelatin at 0.1 mL/g (equivalent to 2.2 molar excess of MAA) in 0.25 M CB buffer (pH 9) produces GelMA with nearly complete substitution within 1 h. This is more efficient than previous studies, which employed 10-47 molar excess of MAA. Regarding

other experimental parameters, most previous studies on GelMA synthesis set the reaction temperature at 50 °C with gelatin concentration at 10 w/v%. Additionally, the results presented herein show the possibility of obtaining GelMA with a high DS at reaction temperature of 35–50 °C or higher gelatin concentration of 10–20 w/v%. Our one-pot GelMA synthesis method yields a GelMA with a controllable DS and is less laborious and more efficient compared to the conventional methods.

References

1 Di Lullo GA, Sweeney SM, Korkko J, Ala-Kokko L, San Antonio JD. Mapping the ligand-binding sites and disease-associated mutations on the most abundant protein in the human, type I collagen. *J Biol Chem* **277**, 4223-4231 (2002).

2 Weng YJ *et al.* Surface engineering of Ti–O films by photochemical immobilization of gelatin. *Materials Science and Engineering: C* **28**, 1495-1500 (2008).

3 Zhu Y, Gao C, He T, Shen J. Endothelium regeneration on luminal surface of polyurethane vascular scaffold modified with diamine and covalently grafted with gelatin. *Biomaterials* **25**, 423-430 (2004).

4 Schiele NR, Chrisey DB, Corr DT. Gelatin-based laser direct-write technique for the precise spatial patterning of cells. *Tissue Eng Part C Methods* **17**, 289-298 (2011).

5 Salamon A *et al.* Gelatin-Based Hydrogels Promote Chondrogenic Differentiation of Human Adipose Tissue-Derived Mesenchymal Stem Cells In Vitro. *Materials* **7**, 1342-1359 (2014).

6 Lynn AK, Yannas IV, Bonfield W. Antigenicity and immunogenicity of collagen. *J Biomed Mater Res B Appl Biomater* **71**, 343-354 (2004).

7 Starin WA. The Antigenic Properties of Gelatin. *J Infect Dis* **23**, 139-158 (1918).

8 Gorgieva S, Kokol V. *Collagen- vs. Gelatine-Based Biomaterials and Their Biocompatibility: Review and Perspectives*. (InTech, 2011).

9 Farris S, Song J, Huang Q. Alternative reaction mechanism for the cross-linking of gelatin with glutaraldehyde. *J Agric Food Chem* **58**, 998-1003 (2010).

10 Sisson K, Zhang C, Farach-Carson MC, Chase DB, Rabolt JF. Evaluation of Cross-Linking Methods for Electrospun Gelatin on Cell Growth and Viability. *Biomacromolecules* **10**, 1675-1680 (2009).

11 Sivakumar M, Radhakrishnan PRG, Kothandaraman H. Grafting of Glycidyl Methacrylate onto Gelatin. *Journal of Applied Polymer Science* **43**, 1789-1794 (1991).

12 Bulcke AIVD *et al.* Structural and Rheological Properties of Methacrylamide Modified Gelatin Hydrogels. *Biomacromolecules* **1**, 31-38 (2000).

13 Yue K *et al.* Synthesis, properties, and biomedical applications of gelatin methacryloyl (GelMA) hydrogels. *Biomaterials* **73**, 254-271 (2015).

14 Pedron S, Becka E, Harley BA. Regulation of glioma cell phenotype in 3D matrices by hyaluronic acid. *Biomaterials* **34**, 7408-7417 (2013).

15 Pedron S, Harley BA. Impact of the biophysical features of a 3D gelatin microenvironment on glioblastoma malignancy. *J Biomed Mater Res A* **101**, 3404-3415 (2013).

16 Coimbra P, Gil MH, Figueiredo M. Tailoring the properties of gelatin films for drug delivery applications: influence of the chemical cross-linking method. *Int J Biol Macromol* **70**, 10-19 (2014).

17 Zhou L *et al.* Biomimetic mineralization of anionic gelatin hydrogels: effect of degree of methacrylation. *RSC Advances* **4**, 21997 (2014).

18 Suo H, Xu K, Zheng X. Using glucosamine to improve the properties of photocrosslinked gelatin scaffolds. *J Biomater Appl* **29**, 977-987 (2015).

19 Jeon O, Wolfson DW, Alsberg E. In-situ formation of growth-factor-loaded coacervate microparticle-embedded hydrogels for directing encapsulated stem cell fate. *Advanced Materials* **27**, 2216-2223 (2015).

20 Shirahama H, Lee BH, Tan LP, Cho NJ. Precise Tuning of Facile One-Pot Gelatin Methacryloyl (GelMA) Synthesis. *Sci Rep* **6**, 31036 (2016).

21 Martineau L, Peng HT, Shek PN. Development of a novel biomaterial: Part II. Evaluation of a photo cross-linking method. (Defence Research and Development Canada, Toronto, 2005).

22 Kim J, Bencherif SA, Li WA, Mooney DJ. Cell-friendly inverse opal-like hydrogels for a spatially separated co-culture system. *Macromol Rapid Commun* **35**, 1578-1586 (2014).

23 Gómez-Guillén MC, Giménez B, López-Caballero ME, Montero MP. Functional and bioactive properties of collagen and gelatin from alternative sources: A review. *Food Hydrocolloids* **25**, 1813-1827 (2011).

24 Hoch E, Schuh C, Hirth T, Tovar GEM, Borchers K. Stiff gelatin hydrogels can be photo-chemically synthesized from low viscous gelatin solutions using molecularly functionalized gelatin with a high degree of methacrylation. *Journal of Materials Science: Materials in Medicine* **23**, 2607-2617 (2012).

25 Sutter M, Siepmann J, Hennink WE, Jiskoot W. Recombinant gelatin hydrogels for the sustained release of proteins. *J Control Release* **119**, 301-312 (2007).

26 Engelhardt S *et al.* Fabrication of 2D protein microstructures and 3D polymer-protein hybrid microstructures by two-photon polymerization. *Biofabrication* **3**, 025003 (2011).

27 Lee BH, Shirahama H, Cho N-J, Tan LP. Efficient and controllable synthesis of highly substituted gelatin methacrylamide for mechanically stiff hydrogels. *RSC Advances* **5**, 106094 (2015).

28 Hoch E, Hirth T, Tovar GEM, Borchers K. Chemical tailoring of gelatin to adjust its chemical and physical properties for functional bioprinting. *Journal of Materials Chemistry B* **1**, 5675 (2013).

29 Bubnis WA, Ofner CM, 3rd. The determination of ϵ-amino groups in soluble and poorly soluble proteinaceous materials by a spectrophotometric method using trinitrobenzenesulfonic acid. *Anal Biochem* **207**, 129-133 (1992).

30 Levett PA *et al.* A biomimetic extracellular matrix for cartilage tissue engineering centered on photocurable gelatin, hyaluronic acid and chondroitin sulfate. *Acta Biomater* **10**, 214-223 (2014).

31 Daniele MA, Adams AA, Naciri J, North SH, Ligler FS. Interpenetrating networks based on gelatin methacrylamide and PEG formed using concurrent thiol click chemistries for hydrogel tissue engineering scaffolds. *Biomaterials* **35**, 1845-1856 (2014).

32 Shin H, Olsen BD, Khademhosseini A. The mechanical properties and cytotoxicity of cell-laden double-network hydrogels based on photocrosslinkable gelatin and gellan gum biomacromolecules. *Biomaterials* **33**, 3143-3152 (2012).

33 O'Sullivan J, Murray B, Flynn C, Norton I. The effect of ultrasound treatment on the structural, physical and emulsifying properties of animal and vegetable proteins. *Food Hydrocolloids* **53**, 141-154 (2016).

34 Sato H, Ueberreiter K. Surface Tension of Aqueous Gelatin Solutions, 1 Concentration Dependence. *Die Makromolekulare Chemie* **180**, 829-835 (1979).

35 Tosh SM, Marangoni AG. Determination of the maximum gelation temperature in gelatin gels. *Applied Physics Letters* **84**, 4242 (2004).

36 Ibarra-Montaño EL, Rodríguez-Laguna N, Sánchez-Hernández A, Rojas-Hernández A. Determination of pK_a Values for Acrylic, Methacrylic and Itaconic Acids by ^{1}H and ^{13}C NMR in Deuterated Water. *Journal of Applied Solution Chemistry and Modeling* **4**, 7-18 (2015).

Chapter 4 Characterization of gelatin methacryloyl hydrogel*

With improved synthesis method, gelatin methacryloyl (GelMA) could be synthesized with a controlled degree of substitution (DS). In this chapter, GelMA aqueous solutions and its hydrogels with different DS were characterized from various perspectives; namely viscosity, stiffness, nanomaterial composite, density, swelling property and degradation property. This fundamental report could be useful for extensive studies utilizing GelMA as a material.

* This chapter was partially published as: (1) Lee BH[†], Shirahama H[†], Tan LP[‡], Cho NJ[‡]. "Efficient and Controllable Synthesis of Highly Substituted Gelatin Methacrylamide for Mechanically Stiff Hydrogels." *RSC Advances* **5**, 106094-106097 (2015). (2) Shirahama H[†], Lee BH[†], Tan LP[‡], Cho NJ[‡]. "Precise Tuning of Facile One-pot Gelatin Methacryloyl (GelMA) Synthesis." *Scientific Reports* **6**, 31036 (2016). ([†] denotes equal first authors; [‡] denotes equal corresponding authors).

4.1. Introduction

Gelatin is a denatured form of collagen, which is the most abundant and ubiquitous protein in the body [1]. It inherits most of the advantages of the parent material, such as biocompatibility, biodegradability, good cell attachment, and versatility of applicable tissues. In addition, gelatin has further benefits of reduced immunogenicity [2,3] and being relatively economical.

A functionalized form of gelatin, gelatin methacryloyl (GelMA), is a popular material that can be crosslinked under ultraviolet (UV) light and photoinitiator. It is utilized for wide bio-applications. This GelMA is obtained from a reaction between free amine groups of gelatin and methacrylic anhydride (MAA) [4]. Since this functionalization does not largely affect important amino acid sequences (e.g. arginine-glycine-aspartic acid (RGD) and matrix metalloproteinase (MMP) cleavage site), GelMA keeps the bioactivities such as cell adhesion and biodegradation [5].

The biodegradation is one of the essential properties of GelMA that widens in vivo applications. So far, various studies were conducted against different experimental parameters such as GelMA concentration [6-9], the degree of substitution (DS) of GelMA [9-12], types of enzymes [13], and enzyme concentration [14,15]. However, these experiments were conducted with different experimental systems and effect of each parameter is not comparable. Therefore, a systematic, comparable degradation study is expected. Also, although extensive measurements have been conducted on mass swelling of GelMA hydrogels, to our best knowledge, dimensional swelling is not well investigated. The degree of dimensional swelling would be important information in designing GelMA hydrogels, especially in delicate structure. Altogether this chapter provides comprehensive information on mechanical properties of GelMA hydrogels. Multiple characterizations were conducted specifically on viscosity, storage modulus, reinforcing with nanomaterials, swelling, and degradation property. The results would be useful guidance in utilizing GelMA hydrogels with various concentration and DS.

4.2. Experimental details

4.2.1. Gelatin methacryloyl synthesis

GelMA samples were prepared as described in the previous chapter, Chapter Three [16,17]. Briefly, type A gelatin (175 bloom) was dissolved at 10 w/v% in different buffers (phosphate-buffered saline [PBS] or carbonate-bicarbonate buffer) at 50 °C. After adjusting pH at 9 with hydrochloric acid, MAA was added at a different amount to vary resulting DS. The reaction proceeded for 3 h under magnetic stirring, and then the pH was readjusted to 7.4 with sodium hydroxide to stop the reaction. After being filtered, dialyzed, and lyophilized, the samples were stored at −20 °C until further use. Heretofore and hereinafter, all the chemicals were purchased from Sigma-Aldrich unless specified.

4.2.2. Rheological measurements

Viscosity measurement

The viscosity of GelMA samples (30 w/v% in distilled water) containing 1 w/v% of 2-hydroxy-4'-(2-hydroxyethoxy)-2-methylpropiophenone (I2959) were measured using steady shear rheometry. Temperature-sweep measurements were performed using an Anton Paar Physica MCR 501 instrument with 25 mm cone-plate geometry with a cone angle of 1 degree at the shear rate of 50 s^{-1}. The temperature was decreased from 40 °C at the rate of 2 °C/min until the collapse of the physically-gelled sample.

Gelling properties measurement

Similarly, the gelling properties of GelMA solutions (30 w/v% in distilled water with 1 w/v% I2959) upon UV curing were performed using sinusoidal shear rheometry. The instrument was equipped with a Peltier temperature-controlled transparent glass plate and connected to a UV curing system (365 nm, 150 mW/cm^2) through an 8 mm light guide and the same cone-plate geometry was used. The testing conditions for all measurements were 2% strain amplitude, and the temperature was maintained at 37 °C throughout the measurements.

Time-sweep measurement was conducted to examine the response of the GelMA samples against UV exposure. The UV irradiation was conducted 30 seconds after running the rheometer under constant oscillation frequency at 1 Hz.

Frequency-sweep measurement was conducted for obtaining storage modulus. UV exposure times were 2 min for GelMA solutions and 8 min for those containing graphene oxide (GO), whose preparation method is described hereinafter, to ensure the complete crosslinking through the turbid solution. The oscillation frequency was between 0.1 and 10 Hz within the linear viscoelastic regime.

4.2.3. Graphene Oxide composite preparation

GelMA samples of 96% DS were mixed with distilled water at 30 w/v%, containing GO at 0 (control), 0.1, 0.25, 0.5, or 1.0 mg/mL. The mixtures were subsequently applied ultrasonication (S 60H, 150 W; Elma Schmidbauer) for 1 h to obtain a suspension with good dispersity.

4.2.4. Bulk hydrogel fabrication and demonstrating their deformations

Bulk samples were fabricated with GelMA solutions (30 w/v% in distilled water with 1 w/v% I2959) with and without GO. A volume of 200 μL of each GelMA solution in silicone tube molds (inner diameter of 6 mm) was photocrosslinked by UV irradiation for 6 min. Deformation of the GelMA hydrogels was demonstrated with a 10 mm parallel-plate, applying a normal force (1.0 N) to each GelMA hydrogel.

4.2.5. Density measurement of gelatin methacryloyl precursor solutions

To obtain the density of the precursor solutions, aforementioned silicon molds were placed on a balance and GelMA solutions (in distilled water with 1 w/v% I2959) with different concentration and DS, preheated at 50 °C, were poured into each mold by 50 μL. The densities were calculated based on the volume (50 μL).

4.2.6. Swelling analysis in mass and size

Fabrication of discoidal samples

Discoidal samples for swelling measurement were fabricated with the same silicone molds. GelMA solutions (in distilled water with 1 w/v% I2959) with different concentration and DS, prepared at 50 °C, were cast in the mold by 50 μL respectively and cured with UV light for 6 min. After the fabrication, the samples were kept in PBS or

water for at least overnight in the fridge. Prior to swelling analysis and degradation study, samples were equilibrated at room temperature.

Mass swelling analysis

First, the weight of each discoidal sample at wet state ($W_{\text{w.spl}}$) was measured. After lyophilizing them, each freeze-dried sample was weighed ($W_{\text{d.spl}}$) to calculate mass swelling ratio as following:

$$\text{Mass Swelling} = \frac{W_{\text{w.spl}} - W_{\text{d.spl}}}{W_{\text{d.spl}}}$$

Dimensional swelling analysis

The discoidal samples were taken pictures by a microscope, or a camera for large samples (diameter over 12 mm). In each picture, three diameters were picked for quantification using ImageJ. In the case of pictures taken by the camera, a cap of 12-well plate was used as a reference size. The diameter of sample (D_{spl}) was normalized by the diameter of mold (D_{mold} = 6 mm) as following:

$$\text{Dimensional Swelling } = \frac{D_{\text{spl}} - D_{\text{mold}}}{D_{\text{mold}}}$$

4.2.7. Accelerated Enzymatic Degradation

The fabricated GelMA discoidal samples being kept in PBS were utilized for degradation study. Type IA collagenase was dissolved in PBS and prewarmed at 37 °C for at least an hour. Each discoidal sample was weighed as initial wet weight ($W_{\text{w.spl}}$). After enzymatic treatment, the samples were immediately lyophilized and eventually weighed as treated dried weight ($W_{\text{d.spl}}$). The initial dried weight was estimated from the ratio of wet weight ($W_{\text{w.ctl}}$) and dried weight ($W_{\text{d.ctl}}$) of untreated, control samples (n ≥ 3). Finally, mass loss was obtained as following;

$$\text{Mass Loss (\%)} = \left\{1 - W_{\text{d.spl}} \Big/ \left(W_{\text{w.spl}} \times \frac{W_{\text{d.ctl}}}{W_{\text{w.ctl}}}\right)\right\} \times 100$$

4.3. Results and discussions

4.3.1. Characterizations on mechanical property of gelatin methacryloyl hydrogels

Viscosity vs temperature

In general, aqueous protein solutions have high viscosity, which limits fabrication of complicated structures. Therefore it often compromised by lowering the protein concentration [18]. Gelatin itself is relatively viscous with low gelling temperature [19]; however, methacrylation can reduce the viscosity [19-21]. This reason can be explained due to the hindrance of helix formation physically and electrostatically (reduced ionic interaction between amino groups and carboxyl groups [22]). As shown in **Figure 4.1**, the viscosity at 40 °C was below 200 mPa·s for high DS solutions (>76%), which can widen its applications.

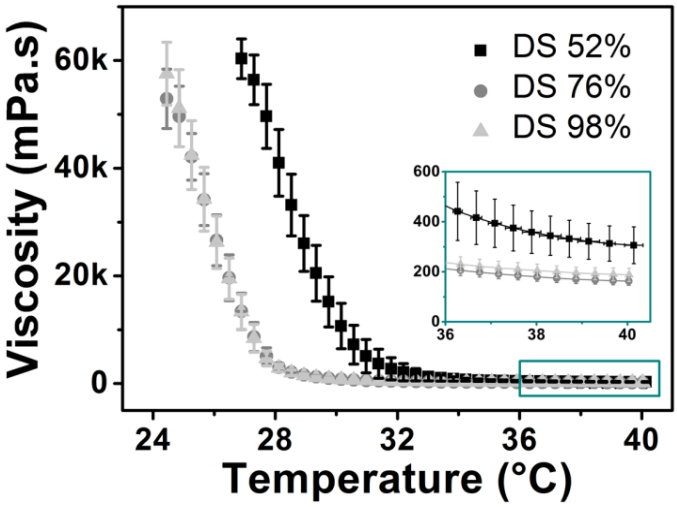

Figure 4.1 Viscosity of GelMA solutions (30 w/v% in distilled water, 1 w/v% I2959) with different DS versus temperature. Error bars indicate the standard deviations of three independent measurements (n = 3).

Response against UV irradiation

To examine the response of GelMA samples against UV exposure, the time-sweep experiment was performed as shown in **Figure 4.2**. The UV irradiation was initiated 30 seconds after the measurement, and the storage modulus was immediately increased. The crosslinking was saturated around 30 seconds, within submillimeter thickness.

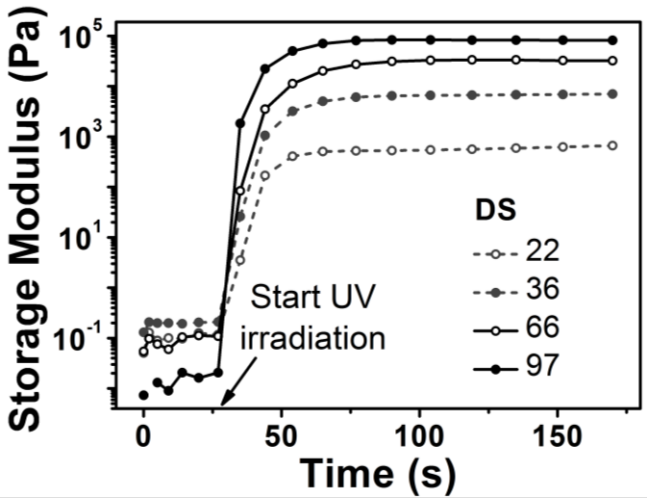

Figure 4.2 Rheological analysis of storage modulus on UV irradiated GelMA solutions (30 w/v% in distilled water, 1 w/v% I2959) with different DS. Error bars indicate the standard deviations of three independent measurements (n = 3).

Bulk hydrogel deformation

Similarly, storage moduli of the GelMA samples (30 w/v% and 1 w/v% I2959) were obtained from in situ curing as shown in **Figure 4.3A.** The storage modulus showed dependency on DS; ranging from 0.38 ± 0.06 kPa (25% DS) to 86.03 ± 0.96 kPa (98% DS). This trend is in agreement with previous reports [4]. To demonstrate GelMA hydrogels with different stiffness values, bulk hydrogels were fabricated and a 1.0 N normal force was applied (**Figure 4.3B**). The DS of 98+% signifies substitution of hydroxyl groups in addition to amino groups (cf. **Figure 3.4**). The hydrogel of the lowest

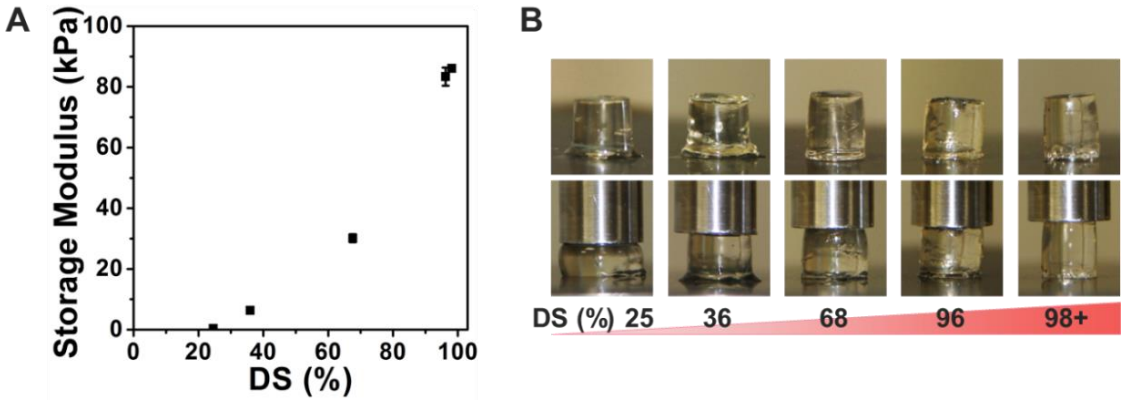

Figure 4.3 (A) Storage moduli of GelMA hydrogels (30 w/v% in distilled water, 1 w/v% I2959) **(B)** Bulk samples for demonstrating deformation, before and after applying normal force.

DS (25%) deformed significantly due to low crosslinking density, while hydrogels of higher DS values showed less deformation. These results support the controllability of GelMA hydrogel stiffness.

Reinforcement with graphene oxide

In order to further explore the possibility of GelMA applications, GelMA composite was studied with GO as a model composite material. GelMA (96% DS) hydrogels were fabricated with different GO concentrations, specifically 0 (control), 0.1, 0.25, 0.5, and 1.0 mg/mL (**Figure 4.4**). Overall, there was a positive correlation between stiffness and GO concentration, which agrees well with previous reports [23] and further supports that even highly substituted GelMA can be reinforced with nanomaterials in composite configurations.

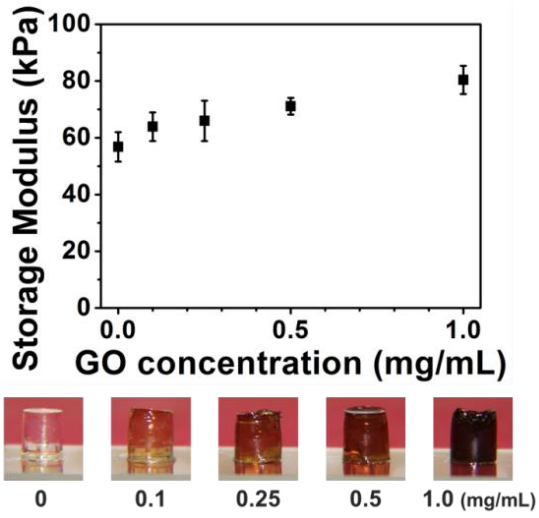

Figure 4.4 (Top) Storage moduli of GelMA-GO composites with different GO concentrations. (**Bottom)** Pictures of corresponding bulk hydrogels.

4.3.2. Characterizations on swelling properties of gelatin methacryloyl hydrogels

Density of precursor solutions

The densities of GelMA precursor solutions at 50 °C were measured. First, the solutions were prepared at different concentrations from 10 to 40 w/v% with different DS. By dissolving the material, the total volume of the solution was increased. Subsequently the

solutions were taken out by 50 μL and poured on a balance to obtain the weight.The results in **Figure 4.5** show no significant difference of the density in terms of DS. There is an overall dependency on the concentration and higher density was seen in higher concentration; however, the density did not change linearly. This is due to increase in volume by dissolving GelMA, which is a partially-hydrophobic macromolecule.

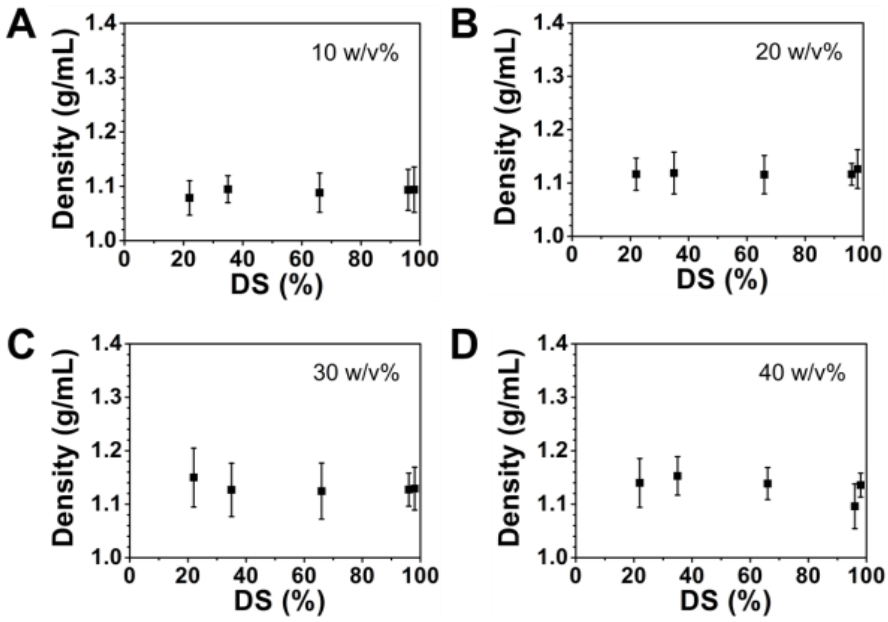

Figure 4.5 Density of GelMA precursor solutions at 50 °C, containing 1 w/v% I2959. GelMA solutions were prepared at different DS (22, 35, 66, 96, and 98%) with different concentration: **(A)** 10, **(B)** 20, **(C)** 30, and **(D)** 40 w/v%. Error bars indicate the standard deviations of more than three independent measurements (n > 3).

Mass swelling

Crosslinked GelMA hydrogels have the ability to confine water molecules within the polymer network. However, the degree of water uptake differs by mass concentration and the DS, which can affect system design. Also, it can be altered further by storage solution (e.g. water or PBS).

Mass swelling of GelMA hydrogel has been extensively investigated in different studies with PBS as a storage solution [12,19,20,24-26]. In general, a consistent tendency is that lower GelMA concentration and lower DS can recruit more water molecules, which could be due to looser crosslinking density and higher ionic interaction between water

molecules. The measurement results in **Figure 4.6A** are well consistent with previous reports. The sample with 22% DS with 10 w/v% were not able to measure the mass and size since it lacked mechanical integrity. When the hydrogels are kept in water, the degree of swelling is further enhanced (**Figure 4.6B**). Analogous behaviors can be found in other hydrogels based on poly(hydroxyethyl methacrylate) [27], poly(ethylene oxide) [28], poly(ethylene glycol) [29], silk fibroin [30], chemically crosslinked gelatin [31] and so on. Hydrogels in the saline buffer undergo dehydration, which is known as "salting-out" or biphasic effect and to be explained further together with dimensional swelling results.

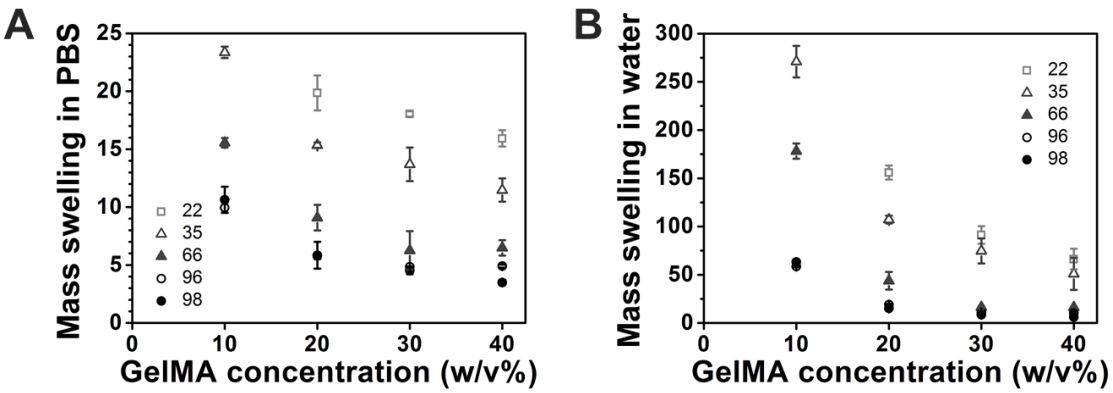

Figure 4.6 Mass swelling ratio of GelMA hydrogels (30 w/v% in distilled water, 1% I2959) kept in different solvents. **(A)** Mass swelling of GelMA hydrogels in water. **(B)** Mass swelling of GelMA hydrogels in PBS. Error bars indicate the standard deviations of more than three independent samples (n > 3).

Dimensional swelling

Similar to the mass swelling, DS, mass concentration, and storage solution influence the hydrogel size as well. The degree of dimensional swelling could be critical for designing the hydrogel, especially for building a delicate configuration. However, to our best knowledge, the dimensional swelling of GelMA hydrogels has not been well investigated.

Figure 4.7A shows the dimensional swelling ratio of the GelMA hydrogels (1 w/v% I2959) with different DS and concentration, kept in PBS. The sizes are standardized by the diameter of the mold (6 mm); showing swelling (> 0) or shrinkage (< 0). The measurement results showed shrinkage of hydrogels with high DS. It can be explained as due to reduced presence of amino groups by functionalization, which limits retention of

water molecules. Hydrogels at high DS tend to release water molecules easily by the presence of salts. At low DS (22-35%), the dimensional swelling is larger with high GelMA concentration. This could be because of higher mechanical stiffness that enables water confinement better. In the case of hydrogels in water in **Figure 4.7B**, there is nothing to hinder the uptake of water molecules. Therefore hydrogels with lower concentration and DS could hold more water in looser and ionic networks.

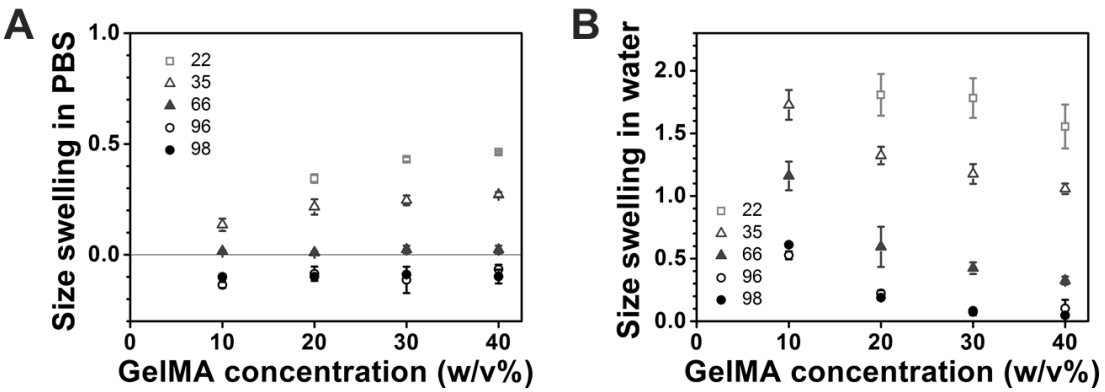

Figure 4.7 Swelled size of GelMA hydrogels with different DS (30 w/v% in distilled water, 1 w/v% I2959). Error bars indicate the standard deviations of more than three independent samples (n > 3).

4.3.3. Enzymatic degradation studies

Subsequently, enzymatic degradation property of GelMA was systematically investigated. First, the discoidal GelMA samples (96% DS, 30 w/v%) were immersed in different concentration (0.1, 0.5 and 1.0 mg/mL; corresponds to 12.5, 62.5 and 125 CDU/mL respectively) of type IA collagenase solution and incubated at 37 °C. They were degraded in time-dependent and concentration-dependent manner. At high collagenase concentrations, the degradation speed increases which makes the two groups (62.5 and 125 CDU) close to each other as reported elsewhere [15].

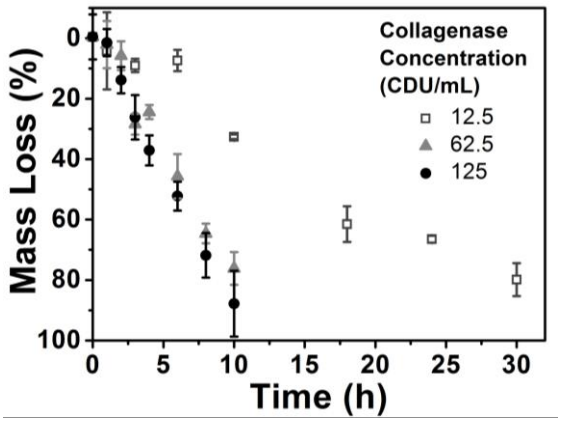

Figure 4.8 Mass loss of GelMA hydrogels (96%DS, 30 w/v% in distilled water) in different collagenase concentration. Error bars indicate the standard deviations of three independent samples (n = 3).

The dependency on GelMA concentration (96% DS) was examined similarly in 12.5 CDU collagenase concentration (**Figure 4.9**). Half time of 10 w/v% samples was around 1 h while those of 20 is 6-7h and 30 and 40 w/v% is more than 8 h, respectively.

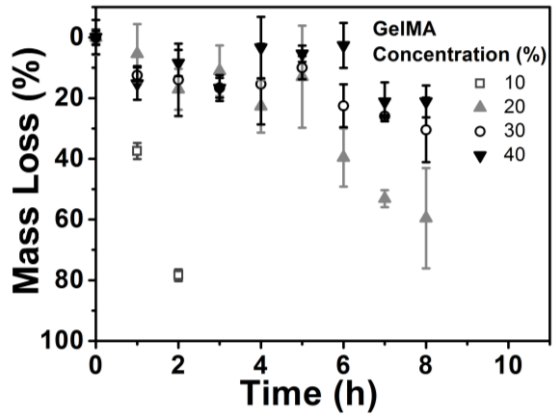

Figure 4.9 Mass loss of GelMA hydrogels (96% DS, dissolved in distilled water, 1w/v% I2959) with a different GelMA concentration in collagenase solution at 12.5 CDU/mL. Error bars indicate the standard deviations of three independent samples (n = 3).

Lastly, the dependency on DS of GelMA degradation was studied. The GelMA hydrogels were prepared with different DS (22, 35, 66, 96, and 98%) prepared at 30 w/v% concentration and incubated in collagenase solution (12.5 and 125 CDU/mL). At high collagenase concentration, the hydrogels of low DS (22 and 35%) were degraded quickly within 1 h. Especially, 22% DS samples were completely dissolved within 2 h in collagenase solution at 12.5 CDU/mL. This is faster than 10 w/v% GelMA sample (96%

DS). This result shows degradation speed is highly tailorable by altering mass concentration and DS.

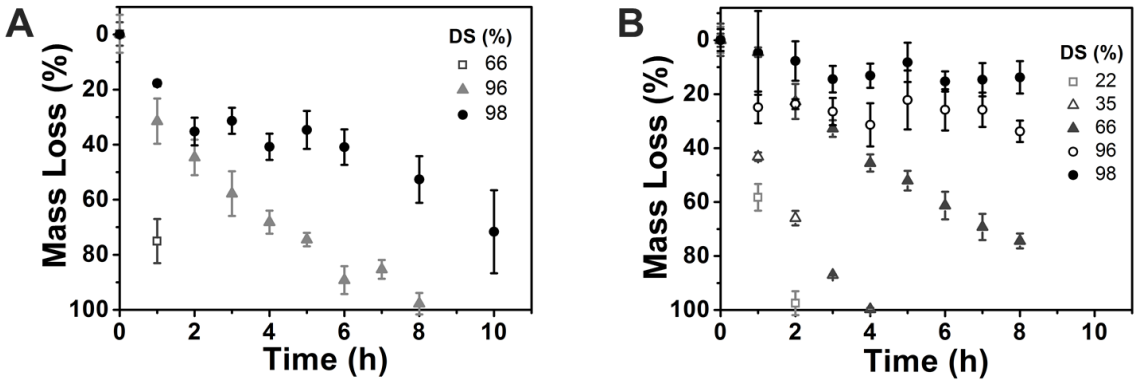

Figure 4.10 Mass loss of Gelatin hydrogel (30 w/v% in distilled water, 1 w/v% I2959) with different DS in collagenase solution at **(A)** 125 CDU and **(B)** 12.5 CDU/mL. Error bars indicate the standard deviations of three independent samples (n = 3).

4.4. Conclusions

In this chapter, mechanical properties of GelMA aqueous solution and hydrogels were investigated from the perspective of viscosity, storage modulus, density, swelling properties, and degradation. As for viscosity, GelMA aqueous solution with high DS samples exhibited lower viscosity, which could be due to reduced ionic interaction between molecules. The solutions between parallel plates at submicron thickness could crosslink within 30 seconds in the presence of UV light and photoinitiator. The mechanical stiffness of the GelMA hydrogels could be tailored by mass concentration and DS, and even further reinforced by the amount of composite additive. The swelling in size also depended on GelMA concentration and DS, showing lower DS and higher concentration can attract more water molecules that resulted in higher degree of swelling. Finally, degradation speed dependency on DS, GelMA concentration and enzyme concentration was investigated systematically to enable comparison between the parameters. The overall information could be useful for designing GelMA hydrogels suitable for their applications.

References

1 Di Lullo GA, Sweeney SM, Korkko J, Ala-Kokko L, San Antonio JD. Mapping the ligand-binding sites and disease-associated mutations on the most abundant protein in the human, type I collagen. *J Biol Chem* **277**, 4223-4231 (2002).

2 Lynn AK, Yannas IV, Bonfield W. Antigenicity and immunogenicity of collagen. *J Biomed Mater Res B Appl Biomater* **71**, 343-354 (2004).

3 Starin WA. The Antigenic Properties of Gelatin. *J Infect Dis* **23**, 139-158 (1918).

4 Nichol JW *et al.* Cell-laden microengineered gelatin methacrylate hydrogels. *Biomaterials* **31**, 5536-5544 (2010).

5 Eng G *et al.* Assembly of complex cell microenvironments using geometrically docked hydrogel shapes. *Proc Natl Acad Sci U S A* **110**, 4551-4556 (2013).

6 Hsieh HY *et al.* Gradient static-strain stimulation in a microfluidic chip for 3D cellular alignment. *Lab Chip* **14**, 482-493 (2014).

7 Hasan A, Paul A, Memic A, Khademhosseini A. A multilayered microfluidic blood vessel-like structure. *Biomed Microdevices* **17**, 88 (2015).

8 Gauvin R *et al.* Microfabrication of complex porous tissue engineering scaffolds using 3D projection stereolithography. *Biomaterials* **33**, 3824-3834 (2012).

9 Boere KW *et al.* Covalent attachment of a three-dimensionally printed thermoplast to a gelatin hydrogel for mechanically enhanced cartilage constructs. *Acta Biomater* **10**, 2602-2611 (2014).

10 Schuurman W *et al.* Gelatin-Methacrylamide Hydrogels as Potential Biomaterials for Fabrication of Tissue-Engineered Cartilage Constructs. *Macromol Biosci* **13**, 551-561 (2013).

11 Hoch E, Hirth T, Tovar GEM, Borchers K. Chemical tailoring of gelatin to adjust its chemical and physical properties for functional bioprinting. *Journal of Materials Chemistry B* **1**, 5675 (2013).

12 Billiet T, Gevaert E, De Schryver T, Cornelissen M, Dubruel P. The 3D printing of gelatin methacrylamide cell-laden tissue-engineered constructs with high cell viability. *Biomaterials* **35**, 49-62 (2014).

13 Levato R *et al.* Biofabrication of tissue constructs by 3D bioprinting of cell-laden microcarriers. *Biofabrication* **6**, 035020 (2014).

14 Bulcke AIVD *et al.* Structural and Rheological Properties of Methacrylamide Modified Gelatin Hydrogels. *Biomacromolecules* **1**, 31-38 (2000).

15 Yue K *et al.* Synthesis, properties, and biomedical applications of gelatin methacryloyl (GelMA) hydrogels. *Biomaterials* **73**, 254-271 (2015).

16 Van Vlierberghe S, Dubruel P, Lippens E, Cornelissen M, Schacht E. Correlation between cryogenic parameters and physico-chemical properties of porous gelatin cryogels. *J Biomater Sci Polym Ed* **20**, 1417-1438 (2009).

17 Nafea EH, Poole-Warren LA, Martens PJ. in *World Congress on Medical Physics and Biomedical Engineering.* (ed Long M) 91-94 (Springer Berlin Heidelberg).

18 Van Hoorick J *et al.* Indirect additive manufacturing as an elegant tool for the production of self-supporting low density gelatin scaffolds. *J Mater Sci Mater Med* **26**, 247 (2015).

19 Nguyen AH, McKinney J, Miller T, Bongiorno T, McDevitt TC. Gelatin methacrylate microspheres for controlled growth factor release. *Acta Biomater* **13**, 101-110 (2015).

20 Sutter M, Siepmann J, Hennink WE, Jiskoot W. Recombinant gelatin hydrogels for the sustained release of proteins. *J Control Release* **119**, 301-312 (2007).

21 Pedron S, Harley BA. Impact of the biophysical features of a 3D gelatin microenvironment on glioblastoma malignancy. *J Biomed Mater Res A* **101**, 3404-3415 (2013).

22 Coimbra P, Gil MH, Figueiredo M. Tailoring the properties of gelatin films for drug delivery applications: influence of the chemical cross-linking method. *Int J Biol Macromol* **70**, 10-19 (2014).

23 Muthusubramanian N. *Stimuli Responsive Polymer Actuated Microstructures using SI-ATRP* Master of Science in Engineering thesis, Johns Hopkins University, (2013).

24 Benton JA, DeForest CA, Vivekanandan V, Anseth KS. Photocrosslinking of Gelatin Macromers to Synthesize Porous Hydrogels That Promote Valvular Interstitial Cell Function. *Tissue Engineering Part A* **15**, 3221-3230 (2009).

25 Ovsianikov A *et al.* Laser fabrication of three-dimensional CAD scaffolds from photosensitive gelatin for applications in tissue engineering. *Biomacromolecules* **12**, 851-858 (2011).

26 Lee BH, Shirahama H, Cho N-J, Tan LP. Efficient and controllable synthesis of highly substituted gelatin methacrylamide for mechanically stiff hydrogels. *RSC Advances* **5**, 106094 (2015).

27 Shirahama H, Lee BH, Tan LP, Cho NJ. Precise Tuning of Facile One-Pot Gelatin Methacryloyl (GelMA) Synthesis. *Sci Rep* **6**, 31036 (2016).

28 Swinerd VM, Collins AM, Skaer NJV, Gheysens T, Mann S. Silk inverse opals from template-directed beta-sheet transformation of regenerated silk fibroin. *Soft Matter* **3**, 1377-1380 (2007).

29 Hoch E, Schuh C, Hirth T, Tovar GEM, Borchers K. Stiff gelatin hydrogels can be photo-chemically synthesized from low viscous gelatin solutions using molecularly functionalized gelatin with a high degree of methacrylation. *Journal of Materials Science: Materials in Medicine* **23**, 2607-2617 (2012).

30 Lee BH, Lum N, Seow LY, Lim PQ, Tan LP. Synthesis and Characterization of Types A and B Gelatin Methacryloyl for Bioink Applications. *Materials* **9**, 797 (2016).

31 Persikov AV, Ramshaw JAM, Kirkpatrick A, Brodsky B. Electrostatic interactions involving lysine make major contributions to collagen triple-helix stability. *Biochemistry-Us* **44**, 1414-1422 (2005).

32 Cha C *et al.* Controlling mechanical properties of cell-laden hydrogels by covalent incorporation of graphene oxide. *Small* **10**, 514-523 (2014).

33 Zhao X *et al.* Photocrosslinkable Gelatin Hydrogel for Epidermal Tissue Engineering. *Adv Healthc Mater* (2015).

34 Daniele MA, Adams AA, Naciri J, North SH, Ligler FS. Interpenetrating networks based on gelatin methacrylamide and PEG formed using concurrent thiol click chemistries for hydrogel tissue engineering scaffolds. *Biomaterials* **35**, 1845-1856 (2014).

35 Hutcheon GA, Messiou C, Wyre RM, Davies MC, Downes S. Water absorption and surface properties of novel poly(ethylmethacrylate) polymer systems for use in bone and cartilage repair. *Biomaterials* **22**, 667-676 (2001).

36 Huddleston JG *et al.* Comparative behavior of poly(ethylene glycol) hydrogels and poly(ethylene glycol) aqueous biphasic systems. *Ind Eng Chem Res* **42**, 6088-6095 (2003).

37 Wang DK, Hill DJT, Rasoul FA, Whittaker AK. Synthesis of a new hyperbranched, vinyl macromonomer through the use of click chemistry: Synthesis and characterization of copolymer hydrogels with PEG diacrylate. *Journal of Polymer Science Part A: Polymer Chemistry* **50**, 1143-1157 (2012).

38 Yan LP *et al.* Tumor Growth Suppression Induced by Biomimetic Silk Fibroin Hydrogels. *Sci Rep* **6**, 31037 (2016).

39 Gupta S. *Influence of divalent ions on gelatin hydrogel and its physicochemical characterization* Master of Technology thesis, National Institute of Technology, (2015).

Chapter 5 Development of gelatin methacryloyl inverted colloidal crystal scaffolds and its application for liver tissue engineering

Inverted colloidal crystal (ICC) system possesses hexagonally-interconnected uniform pores, which is favorable for cells to grow and function. On the other hand, gelatin is obtained from collagen, which is the most abundant extracellular matrix in the liver. Herein, we developed gelatin methacryloyl (GelMA) ICC scaffolds that mimic the liver regarding structure and material. Liver cells seeded on the scaffolds showed higher hepatic functions compared to those on a flat substrate. The results demonstrate the potential of GelMA ICC to be an artificial liver platform.

* This chapter was submitted substantially as: Lee BH[†], Shirahama H[†], Kim M[†], Lee JH[†], Cho NJ[‡], Tan LP[‡]. "Colloidal Templating of Highly Ordered Gelatin Methacryloyl-Based Hydrogel Platforms for Liver Tissue Engineering." *NPG Asia Materials*

5.1. Introduction

The liver is an assiduous organ, bearing various essential functions for sustaining life such as protein synthesis, glucose homeostasis, and drug metabolism [1]. Unfortunately, this metabolic activity makes the liver as the main organ to suffer from drug toxicity [2]. This hepatotoxicity occurs at the late stage of drug development or post-marketing since preclinical animal testing is not always effective due to species-specific metabolism [3]. Reconstruction of the human liver ex vivo could be a potent tool for drug screening purpose. Culturing the primary hepatocyte could be a possible solution; however, it loses its function rapidly on a conventional two-dimensional (2D) substrate [4]. In the body, cells reside in a three-dimensional (3D) extracellular matrix (ECM) environment; studies on tissue engineering are revealing that cells in 3D systems can respond closer to in vivo in terms of cell morphology and functions [5-7]. Therefore different approaches were taken for maintaining hepatic function with 3D in vitro systems.

An inverted colloidal crystal (ICC) scaffold is one of the promising 3D systems that possesses uniform pores, which are hexagonally arranged and interconnected [8]. The size of the pores is controllable, and the structure has good diffusivity to transport nutrients and the oxygen. The configuration is generally made of a base material and sacrificial colloidal crystal. Regarding liver tissue engineering, early ICC systems exhibited hepatosphere formation with long-term viability [8], maintenance of albumin production [9], and in vivo-like response against nanoparticle [10]. However, these scaffolds were made from polyacrylamide, lacking cell-ECM interaction. Recently our group developed collagen-coated polyethylene glycol diacrylate (PEGDA) ICC scaffolds [11,12]. Hepatocytes in these scaffolds attached well to the cavity walls, having both cell-cell and cell-ECM interaction eminently. The presence of ECM proteins led to higher albumin production compared to bare PEGDA ICC, in which cells exhibited aggregated shape. Also, the albumin level depended on the amount of collagen coating. However, this ICC system requires an additional fabrication step, being possible to have an uneven coating and batch-to-batch difference, not to mention its non-biodegradability. Protein-based ICC could be an ideal platform to provide innate bioactivity in a more reproducible manner as well as to be useful for in vivo applications.

Some ICC systems of native natural polymers such as alginate [13-15], chitin [16,17], chitosan [18-20], inclusive of their composites have been reported. As these native materials have high viscosity, the base material solutions were prepared at below 5%, leading repetition of the process or low mechanical strength. Also, most systems employed chemical crosslinkers (calcium chloride [13-15], genipin [16,17,19-21], etc.) for crosslinking, which require longer processing time (1 h ~ days) and could result in inhomogeneous crosslinking over the samples. Recently, Kim et al. developed a porous platform based on functionalized protein, gelatin methacryloyl (GelMA) [22]. This UV crosslinking system with this photocrosslinkable material allowed shortening the curing time within 20 min. With reduced viscosity by the methacryloyl functionalization, the GelMA material solution could be prepared at 20 wt%. Mouse mesenchymal stem cells seeded in the platform were highly viable. However, the system does not have structural uniformity, as the alginate sacrificial beads were utilized without crystal formation. In addition, detailed cell function studies in the system have not been investigated.

The microscopic units where liver cells reside in the body are lobules which are roughly hexagonal in shape, and collagens are the main structural proteins of the hepatic extracellular matrix. Gelatin is a partially hydrolyzed form of collagen, and the functionalized gelatin, GelMA, maintains important bioactivity of gelatin such as cell attachment and enzyme degradation [23]. Thereby we demonstrate highly-ordered, ECM-based ICC scaffolds, which mimic the liver environment from structure and material points of view. We hypothesized that this GelMA ICC could furnish hepatocytes with a better microenvironment compared with 2D systems. Systematic examinations were conducted in terms of structural stability, uniform pore interconnectivity, and tailorable degradation properties. Finally, the efficacy of the GelMA ICC platform for liver tissue engineering was examined with model liver cells.

5.2. Experimental methods

5.2.1. Fabrication of gelatin methacryloyl inverted colloidal crystal scaffolds

GelMA samples with different DS were synthesized according to the literature [24]. Briefly, type A gelatin (175 bloom) was dissolved at 10 w/v% at 60°C in two buffer systems (phosphate buffered saline [PBS] and 0.1M carbonate-bicarbonate [CB] buffer).

GelMA samples were prepared by reaction of gelatin with methacrylic anhydride (MAA, 94%) at a feed ratio of MAA (1 mL) to gelatin (10 g) at 50 °C for 3 h in three different conditions (PBS, CB, and CB with pH maintenance at 9.0) in a time-lapse loading manner. After 3 h of reaction, the solutions were readjusted to pH of 7.4, filtered, dialyzed using PALL Minimate TFF Capsule with 10 kDa MWCO at 40 °C for 1 day, lyophilized, and stored at -20 °C until further use. The DS of GelMA was quantitatively measured by 2,4,6-trinitrobenzene sulfonic acid (TNBS) and were verified by ^{1}H NMR (Avance I 400 MHz, Bruker) in deuterium oxide.

Polystyrene (PS) beads with a diameter of 138 ± 2.0 μm (Duke Scientific Corporation) were self-assembled in 70% ethanol solution in polypropylene molds of 6 mm-diameter by shaking for two overnights and annealed at 134 °C for 6 h to obtain lattices. GelMA samples with different DS were dissolved at 5, 10, 20, 30, and 40 w/v% in distilled water at 50 °C. The solutions of GelMA containing 1% 2-hydroxy-4'-(2-hydroxyethoxy)-2-methylpropiophenone (I2959) were soaked into the lattices by centrifugation at 15,000 rpm at 40 °C for 10 min. The GelMA infiltrated lattices were cured by ultraviolet light (UV; 365 nm at 100 mW/cm^2) for 10 min and then lattices were removed in tetrahydrofuran. The GelMA ICC scaffolds were sterilized by 70% ethanol solution and washed three times with PBS, finally being stored in distilled water or PBS at 4 °C until further use. The fabricated scaffolds with different concentrations and different DS were evaluated in terms of structural integrity by whether they can be easily handled with tweezers. Heretofore and hereinafter, all the chemicals were purchased from Sigma-Aldrich unless specified.

5.2.2. Morphological Observations

To investigate the microscopic morphology, a scanning electron microscope (SEM) was utilized. ICC scaffolds and cell-seeded samples fixed with 4% paraformaldehyde (PFA) were treated by sequential ethanol dehydration at 25, 50, 75, 95 and 100% for 15 min each. The scaffolds were stored at -80 °C, followed by lyophilization for 48 h. The SEM samples were coated by Pt with a thickness of 10 nm using a sputter coater (JFC-1600, JEOL), and the images were taken with FESEM (JSM-7600F, JEOL) at an acceleration voltage of 5 kV.

5.2.3. Rheological measurements

Mechanical properties of aqueous GelMA solutions (30 w/v%) containing I2959 (1 w/v%) were characterized with sinusoidal shear rheometry. Frequency-sweep measurements were conducted using a rheometer (Anton Paar Physica MCR 501), equipped with a temperature-controllable glass plate, UV curing system (365nm, 100 mW/cm^2), and a 25 mm cone-plate geometry with an angle of 1 degree. The measurement conditions were 2% strain amplitude at an oscillation frequency of 0.1–10 Hz. Similarly, the storage modulus of each GelMA ICC scaffold was measured with 10 mm diameter of parallel-plate geometry at 0.1 % strain and 0.1 Hz. The temperature was maintained at 37 ºC throughout the measurements.

5.2.4. Accelerated enzyme degradation study

ICC scaffolds made of GelMA (30 w/v%) with different DS were tested for enzymatic degradation in 1 mg/mL of collagenase (125 CDU/mg solid) in Hank's Balanced Salt Solution (HBSS), containing 3 mM $CaCl_2$. Surface morphology of GelMA ICC scaffolds was observed through an optical microscope during the degradation, and mass loss of GelMA ICC scaffolds was also measured.

5.2.5. Cell culture

Human hepatocellular carcinoma cells (Huh7.5, Apath) were maintained in Dulbecco's Modified Eagle's Medium (Hyclone) with 10% fetal bovine serum (Hyclone) and 1% penicillin/streptomycin (Life Technologies) in a humidified atmosphere at 37 °C with 5% CO_2. The medium was changed every 3 days. Prior to cell seeding, GelMA ICC scaffolds were placed in 24-well plates, consequently washed with PBS and kept in 2 mL of media for 30 min. After media aspiration, 1×10^6 cells in 25 µL of medium were carefully pipetted on top of the each GelMA ICC scaffold. After 4 h, the scaffolds were transferred into a new 24-well with 1 mL of media. As a control, the same number of cells was seeded on 2D GelMA substrates with around 2 mm thickness in 6-well plates. For both conditions, media were changed every day.

5.2.6. Live/Dead assay and confocal microscopy

The cell viability in 3D GelMA ICC scaffolds and on 2D GelMA substrates was characterized using LIVE/DEAD® Cell Viability/Cytotoxicity kit (Life Technologies). Briefly, 4 μM Calcein-AM and 8 μM ethidium homodimer-1 (EthD-1) in media were added to the samples, followed by 1 h of incubation at 37 °C. The cytoplasm of live cells and nucleus of dead cells were stained by Calcein-AM (green) and EthD-1 (red), respectively, by confocal microscope (TCS SP8, Leica) under a laser excitation of 488 nm. A number of live and dead cells were counted using ImageJ.

5.2.7. Immunostaining

Cell-seeded samples were collected at different time points (day 1, 3, 6, and 9) for immunocytochemistry. The samples were washed twice with PBS, fixed with 4% PFA for 5 min, permeabilized with 0.1% Triton X-100 for 30 min, washed twice with PBS, and incubated in a 3% bovine serum albumin blocking buffer for 1 h. Albumin and cytochrome P450 (CYP) 3A4 were separately bound with specific primary antibodies (sc-53850 and sc-271605, respectively, Santa Cruz Biotechnology) overnight at 4 °C. After being washed three times with PBS, they were incubated with a secondary antibody, conjugated with Alexa Flour® 555 (Life Technologies). Simultaneously, filamentous actins (f-actin) were stained with Alexa Flour® 488 labelled phalloidin (Life Technologies) for 2 h at room temperature. Next, the samples were washed twice with PBS, and then nuclei were stained with 10 μg/mL 4,6-Diamidino-2-Phenylindole, Dihydrochloride (DAPI; Life Technologies) for 10 min. Images of stained cells were captured and reconstructed with confocal microscopes (LSM710 with a ZEN program, Carl Zeiss, or TCS SP8, Leica).

5.2.8. Western blot assay

Intracellular protein amount at different time points (day 1, 3, 6, and 9) were qualitatively measured by Western blot assay. First, total proteins were extracted with the Protein Extraction kit (Life Technologies), and the amount was determined using BCA protein assay kit (Thermo Fisher Scientific). The protein samples were boiled with 4x laemmli sample buffer (Bio-Rad) for 5 min, and 20 μL of each boiled sample was loaded into

wells of a 10% polyacrylamide gel. Subsequently, electrophoresis was performed using the Mini-PROTEAN® 3 Cell (Bio-Rad). Proteins separated on the gels were transferred onto nitrocellulose membrane (Bio-Rad) and the transferred membranes were stained with Ponceau S staining solution in order to ascertain the loading process. The stained membranes were washed with a blocking buffer (10 mM Tris-HCl, 150 mM NaCl, 0.1% Tween 20, and 3% nonfat dry milk), and separately incubated for 2 h at room temperature in the blocking buffer with 1:1000 diluted primary antibody (albumin: sc-271605, E-cadherin: sc-21791, and beta-actin: sc-47778, Santa Cruz Biotechnology). After being washed with the blocking buffer three times for 15 min, the membrane was probed with 1:2000 diluted secondary antibody (#1706516, Bio-rad) for 2 h. The membrane was then washed three times for 15 min and developed with Immun-Star™ AP Chemiluminescence Kits (Bio-Rad). Chemiluminescent signal was detected with a luminescent image analyzer (LAS-4000, GE Healthcare Life Sciences).

5.2.9. Gene expression analysis

The expression levels of regulative and functional genes of cells were quantified at different time points (day 1, 3, 6, and 9). First, total RNA was isolated with TRIzol reagent (Life Technologies) and reverse transcribed with primers in **Table 5.1** and iScript Reverse Transcription Supermix (Bio-Rad). The synthesized complementary DNAs were amplified based on real-time quantitative PCR (RT-qPCR) with the SYBR select Master Mix for CFX (Life Technology) in the CFX connect Real-Time PCR system (95 °C for 20 s, followed by 40 cycles of 10 s at 95 °C, and 40 s at 60 °C). All reactions were run in three times, and $2^{-\Delta\Delta CT}$ method was used for analyzing the data. The value of each gene was normalized against the housekeeping gene, glyceraldehyde 3-phosphate dehydrogenase (GAPDH).

Table 5.1 List of the primer sequences used in amplification.

Target genes	Forward (5'-3')	Reverse (5'-3')
AAT	GATGCTGCCCAGAAGACAGA	GGAGTTCCTGGAAGCCTTCA
Albumin	CTGCACAGAATCCTTGGTGA	CTCCTTATCGTCAGCCTTGC
CYP3A4	ACCGTGACCCAAAGTACTGG	TTCAGGGGGATCTGTGTTTC
CYP3A7	AAGTGGACCCAGAAACTGCA	GGCTCCACTTACGGTCTCAT
G6Pase	TTCCTGTTCAGCTTCGCCAT	TCAAAGACGTGCAGGAGGAC
HNF4α	TCGTTGAGTGGGCCAAGTAC	TGTCATCGATCTGCAGCTCC
HNF6	TTGAGCCATTGAGCGGACAT	GGCAGGTTCAAACGTTAGGC
E-cadherin	AGGCCAAGCAGCAGTACATT	AAATGTGTCTGGCTCCTGGG
N-cadherin	CCTTTCAAACACAGCCACGG	TGTTTGGGTCGGTCTGGATG
Claudin-1	TGGAAGACGATGAGGTGCAG	GCTGGAAGGTGCAGGTTTTG
ZO-1	AAACAGCCAGCCGTTAGTCA	CTTCATACATGGGGACGCGA

5.3. Results and discussions

5.3.1. Fabrication and morphological observations

Fabrication of gelatin methacryloyl inverted colloidal crystal

The degree of substitution (DS) of GelMA is an important parameter to control its crosslink density and mechanical properties as well as degradation speed. GelMA samples with various DS were synthesized for fabrication of ICC scaffolds as seen in **Figure 5.1** [24]. GelMA samples with different DS of 52, 76, and 98% were prepared at the same feed ratio of MAA (1 mL) to gelatin (10 g) in three different systems (PBS, CB, and CB with pH 9 adjustment), respectively. Bulk stiffness of the GelMA hydrogels (30 w/v% in distilled water with 1 w/v% I2959) were 22, 61, and 99 kPa respectively.

To fabricate GelMA ICC scaffolds, first colloidal crystals were prepared by self-assembling of PS beads with a diameter of 138.1 ± 2.2 μm (**Figure 5.1C**). The dried beads were subsequently annealed to obtain template lattices. Next, aqueous GelMA solutions (5, 10, 20, 30, and 40 w/v%) were infiltered to the lattices by centrifuging at 40 ºC. As GelMA has low viscosity, due to reduced ionic intermolecular interaction, all the solutions could penetrate the interstice. For more concrete example, GelMA solutions of 30 w/v% have such low viscosity values (52% DS at 394 ± 97 mPa.s, 76% DS at 191 ± 19 mPa·s, and 98% DS at 215 ± 27 mPa·s under 37 °C at 50 s^{-1}) as shown in **Figure 4.1**.

After UV crosslinking of GelMA infiltered lattices, the templates were removed by tetrahydrofuran to obtain GelMA ICC scaffolds.

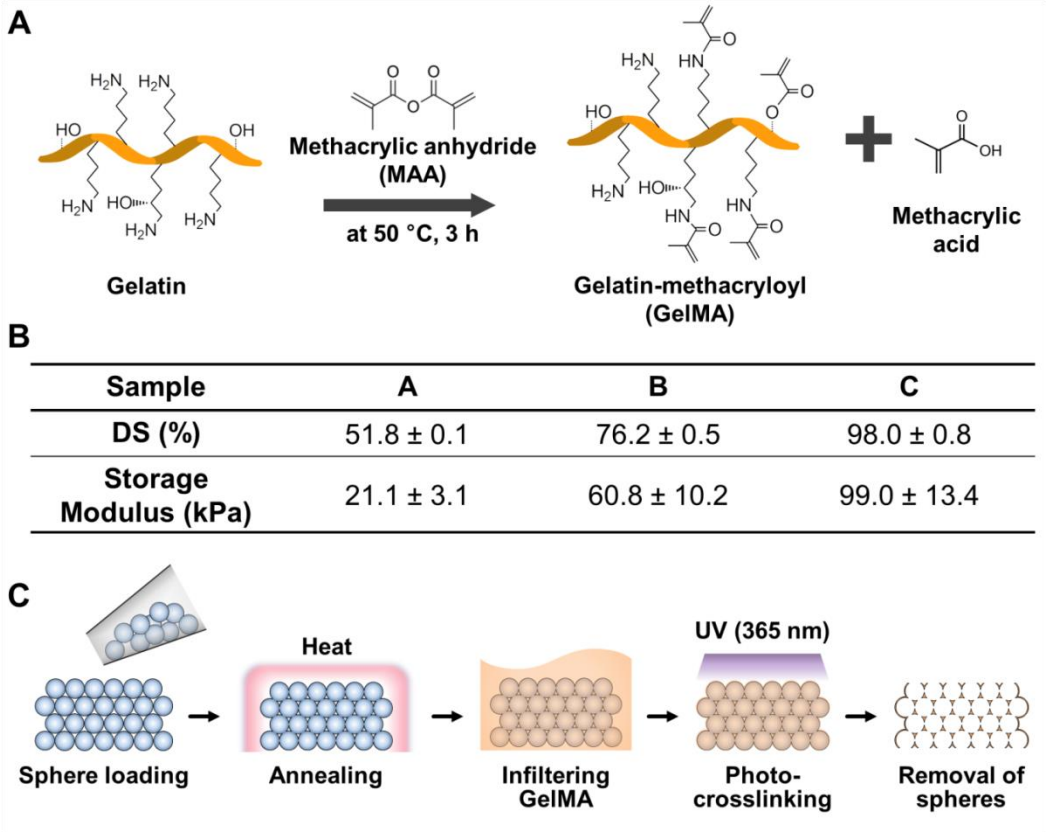

Sample	A	B	C
DS (%)	51.8 ± 0.1	76.2 ± 0.5	98.0 ± 0.8
Storage Modulus (kPa)	21.1 ± 3.1	60.8 ± 10.2	99.0 ± 13.4

Figure 5.1 GelMA ICC scaffold preparation. **(A)** Gelatin methacryloyl (GelMA) synthesis scheme. GelMA synthesis was conducted at a feed ratio of MAA/gelatin (0.1 mL/1 g) in different buffer systems (PBS, 0.1 M CB, and 0.1 M CB with pH 9 adjustment). **(B)** Storage moduli of GelMA hydrogels (30 w/v% in distilled water with 1 w/v% I2959) as a function of degrees of substitution (DS) of 52%, 76%, and 98%. **(C)** Schematic illustration of the fabrication process of GelMA ICC scaffolds by ICC templating.

Morphological observations and dimensional measurements of the scaffolds

In terms of structural integrity, GelMA ICC scaffolds made of 5 and 10 w/v% GelMA solutions appeared to be collapsed and were difficult to handle with tweezers as presented in the optical images in **Figure 5.2**. GelMA ICC with the highest DS (98%) provided the best structural integrity at above 20 w/v% concentrations, whereas those with 52 and 76% DS exhibited good structural integrity at above 30 w/v%. The scaffolds at 30 w/v% were measured mechanical stiffness, whose storage moduli exhibited a range

of 1-4 kPa as shown in **Figure 5.3**. Among them, 96% DS scaffold was applied to cell culture as described later, maintaining mechanical integrity throughout 9 days of culture period with around a million of cells. These results show overcoming the shortage of highly porous protein-based hydrogels, often lacking structural integrity because of low protein concentration and inefficient crosslinking methods.

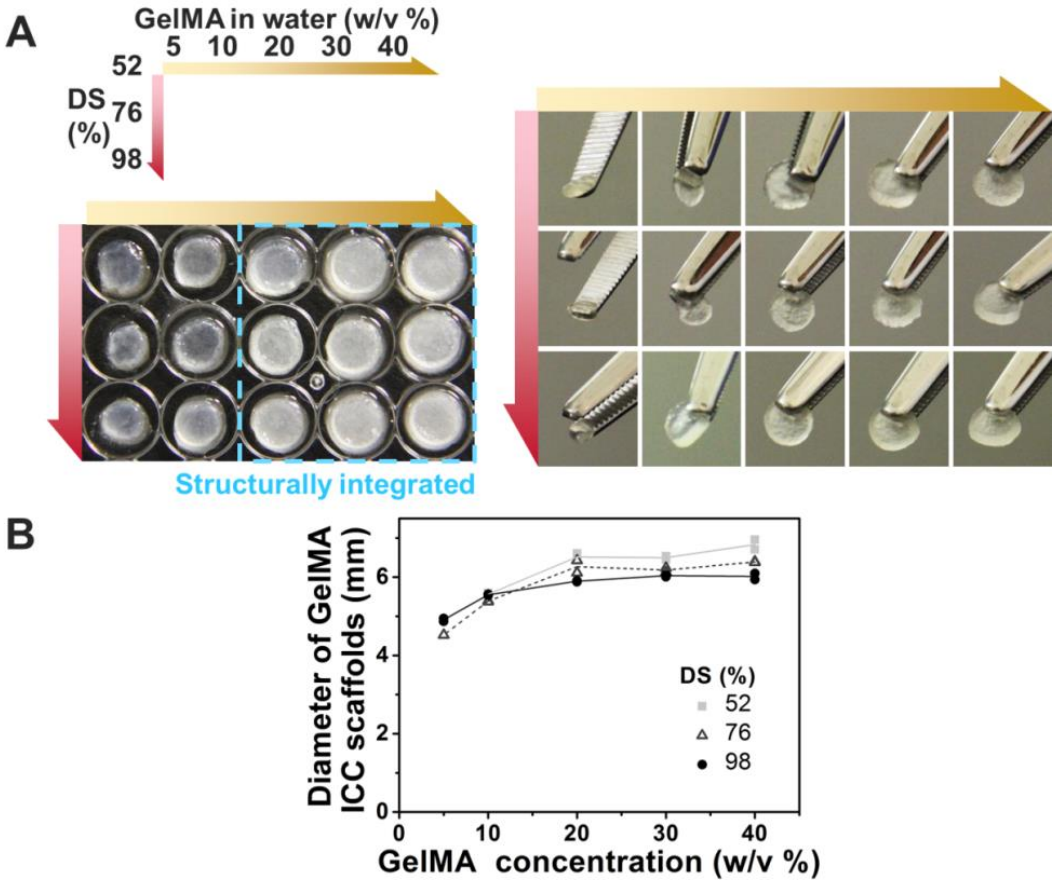

Figure 5.2 Demonstration of structural integrity of GelMA ICC scaffolds. **(A)** Optical images of GelMA ICC scaffolds with different GelMA concentrations (5, 10, 20, 30, and 40 w/v%) and different DS (52, 76 and 98%). **(B)** Diameter of GelMA ICC scaffolds versus different concentrations of GelMA (n=2; each sample was measured three times in different angles).

Regarding the size, as shown in **Figure 5.2B**, scaffolds made of lower DS were more swollen as they have higher interaction with water [25]. However, at lower gelatin concentration, they were easily collapsed due to less sufficient mechanical support. As for material concentration dependency, there is a moderate correlation with the size.

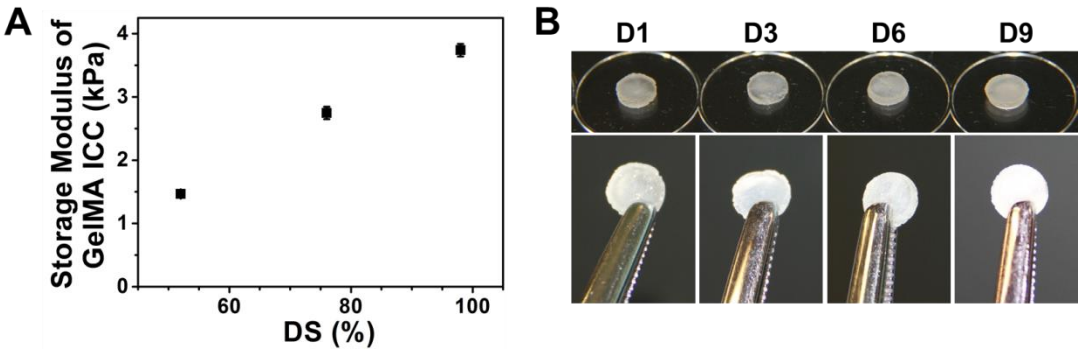

Figure 5.3 (A) Storage moduli of GelMA ICC scaffolds with different DS at 30 w/v%. **(B)** Optical images of cell-seeded GelMA (DS 98%) ICC scaffolds at day 1, 3, 6 and 9. Cell-seeded GelMA ICC scaffolds showed sufficient structural integrity over the culture for easily handling with a tweezer. Cells were fixed by 4% PFA for 5 min for CYP3A4 immunohistochemical staining purpose.

Similar to the human body with around 30% organic mass and 70% water, GelMA scaffolds of 30 w/v% with three different DS (52, 76, and 98%), resulting in relatively good structural stability, were used in the further investigations. SEM images and microscope images of GelMA ICC scaffolds in **Figure 5.4A** showed that GelMA ICC scaffolds featured a hexagonal honey comb-like microstructure with uniform cavities of about 139 μm and with connection window channels of about 30 μm regardless of DS (52, 76, and 98%). GelMA ICC scaffolds displayed six uniform connection window channels in each cavity as presented in the 3D confocal images. In the ICC system, the sizes of cavity and connection channel between the cavities are controlled by the size of the self-assembled PS beads and the annealing temperature, respectively, influencing the size of the cell constructs and cell-cell interaction between pores. We used around 140 μm diameter PS beads in order not to go beyond the maximum permeability of the oxygen and nutrients in cell constructs (150–200 μm) [26]. Some of the ICC systems were fabricated without annealing the sacrificial beads, leading irregular configurations. Uniformity is important not only for reproducibility but also for good internal diffusivity, resulting in better cellular activity [27]. In our system, we utilized tightly annealed colloidal crystals as sacrificial templates, which consequently produced the highly organized structure with homogeneous microporosity and interconnectivity.

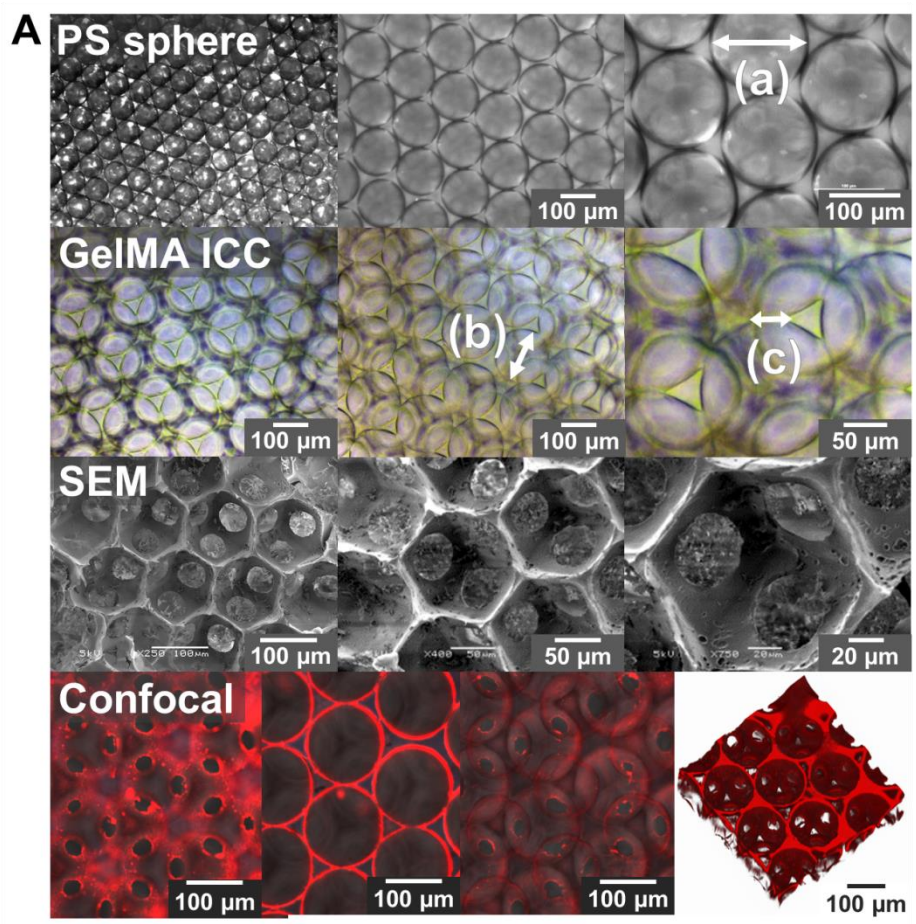

B

	(a) Colloidal Spheres (μm)	(b) Cavity (μm)	(c) Connection Channel (μm)
DS 52%	138.1 ± 2.2	139.9 ± 3.2	27.9 ± 7.6
DS 76%		139.1 ± 5.0	30.4 ± 6.2
DS 98%		139.1 ± 5.6	34.8 ± 6.0

Figure 5.4 Micro-scale features of ICC scaffolds made from GelMA (30 w/v%). **(A)** Optical microscopic images of assembled colloidal crystals made of PS beads, optical microscopic images of GelMA ICC scaffolds, scanning electron microscopic (SEM) images of GelMA ICC scaffolds, and confocal images of fibronectin-coated GelMA ICC scaffolds via immunohistochemical staining (fibronectin in red). **(B)** Dimensions of GelMA ICC scaffolds with different DS (52, 76, and 98%) (a) diameter of colloidal beads (provided by manufacturer). (b) Diameters of cavity (n=; mean ± SD). (c) Diameters of connection channels (n> 140; mean ± SD).

5.3.2. Accelerated degradation in enzyme

Tailorable biodegradability is an essential requirement of scaffolds for tissue engineering especially for in vivo applications. Here, we conducted the accelerated degradation tests of GelMA ICC scaffolds using collagenase at 1 mg/mL (125 U/mL). As presented in **Figure 5.5**, the degradation of GelMA ICC scaffolds by the enzyme was apparent, and its speed was highly dependent on the DS of GelMA, which relates to the crosslink density of GelMA. The lower the DS of GelMA ICC scaffolds, the faster degradation was observed. GelMA ICC scaffolds with 52% DS lost a half of their masses within 2 h. Half-lives of GelMA ICC scaffolds of 76 and 98% DS were around 3 to 5 h, respectively. Also, the morphological features of GelMA ICC scaffolds during the degradation were monitored by a microscope as seen in **Figure 5.5A**. The time profile of their morphology changes was in good accordance with that of their mass loss. The cavity rings of the first layers of GelMA ICC scaffolds with 52 and 76% DS disintegrated after 1 and 2 h, respectively, whereas those of GelMA ICC with 98% DS started to lose their integrity between 4 and 6 h. Obviously, GelMA ICC scaffolds could maintain the collagenase cleavage site (-R-Pro-X-Gly-Pro-R-, X: a neutral amino acid) even after the chemical modification process since methacryloyl groups mainly react with amino groups of gelatin [23]. These results demonstrated that GelMA ICC scaffolds even with relatively high concentration (30 w/v%) possess relatively fast enzymatic degradation property and their degradation was controlled by the designed DS of GelMA.

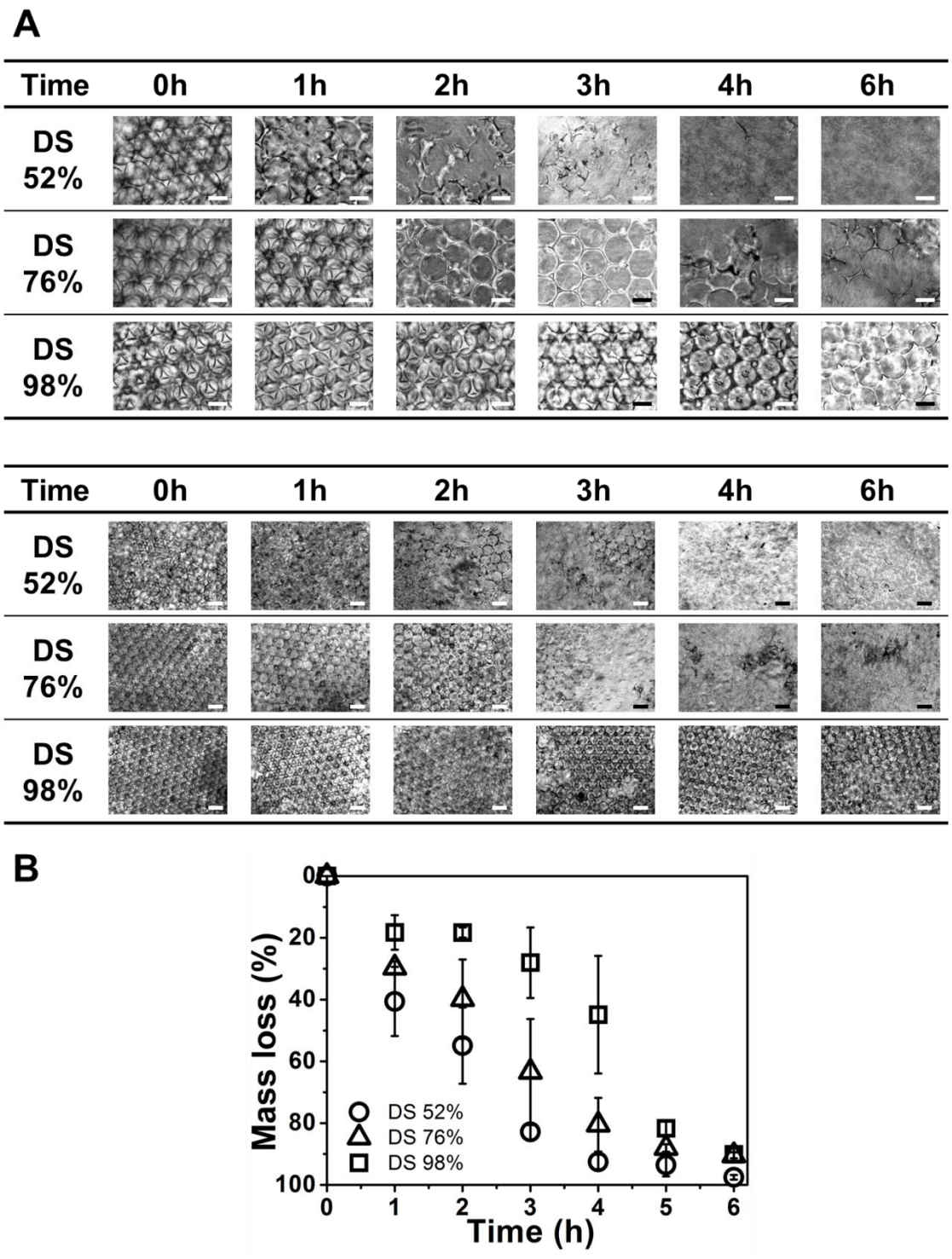

Figure 5.5 Accelerated enzymatic degradation study of GelMA ICC scaffolds. **(A)** Micro-scale surface morphology observation of GelMA ICC scaffolds with different DS (scale bar = 100 μm) during enzymatic degradation. **(B)** Mass loss of GelMA ICC scaffolds with different DS at 1 mg/mL collagenase Type 1A solution (125 U/mL) (n=3; mean ± SD). GelMA ICC scaffolds experienced enzymatic degradation and GelMA ICC with a lower DS degraded in a faster mode.

5.3.3. Viability of Huh7.5 cells

To understand the effect of the protein-based microarchitecture of 3D GelMA ICC scaffolds on cells, we used a liver cell line as surrogate model cells. Huh7.5 cells were chosen as they still retain several hepatic functions such as liver specific gene expression, hepatic enzyme activity as well as permissibility to HCV infection [28]. The microscopic units where liver cells reside are lobules which are roughly hexagonal in shape, and collagens are the main structural proteins of the ECM. As the environment GelMA ICC provides is similar to the liver, we expect the hepatocytes to maintain their function well. The cell line, Huh7.5 cells, retains several hepatic functions such as liver-specific gene expression, hepatic enzyme activity as well as permissibility to HCV infection. We assessed their organization, cell viability, growth, and functions in 2D and 3D GelMA (30 w/v%, 98% DS) systems.

After seeding Huh7.5 cells into cavities of GelMA ICC scaffolds, they were rapidly infiltered inside and attached to the cavity walls. Cell areas in the cavity areas grew larger and larger over the 9 days of culture period as seen in the live/dead micrographs in **Figure 5.6**. The images show that Huh7.5 cells were highly viable (above 80%) both in 3D ICC scaffolds and on 2D substrate. In ICC scaffolds, Huh7.5 cells stretched along the cavity walls, appearing to form thicker cell sheets over time. The result of the thickness measurement of 3D cell layers shows more than twice of increase from around 22 μm on day 1 to 50 μm on day 9 ($p < 0.0001$, one-way ANOVA). Three-dimensional confocal images (blue: nucleus; green: actin; red: CYP3A4 in **Figure 5.7A, B**) and SEM images (**Figure 5.7C**) provide the clear morphological difference between the cells grown in scaffolds and on substrates. Huh7.5 cells in ICC scaffolds initially attached sheet-like to the cavity walls and then were gradually packed into constructs. At day 9, most of the cavities were filled with cells, growing into multi-cell clusters in a 3D manner. This trend was prominent in the first layer and second layer (**Figure 5.8**). On the other hand, cells on 2D substrates initially formed island-like clusters made up of several cells at day 1, and then they were merged to form a large cell sheet with only a few cell layers.

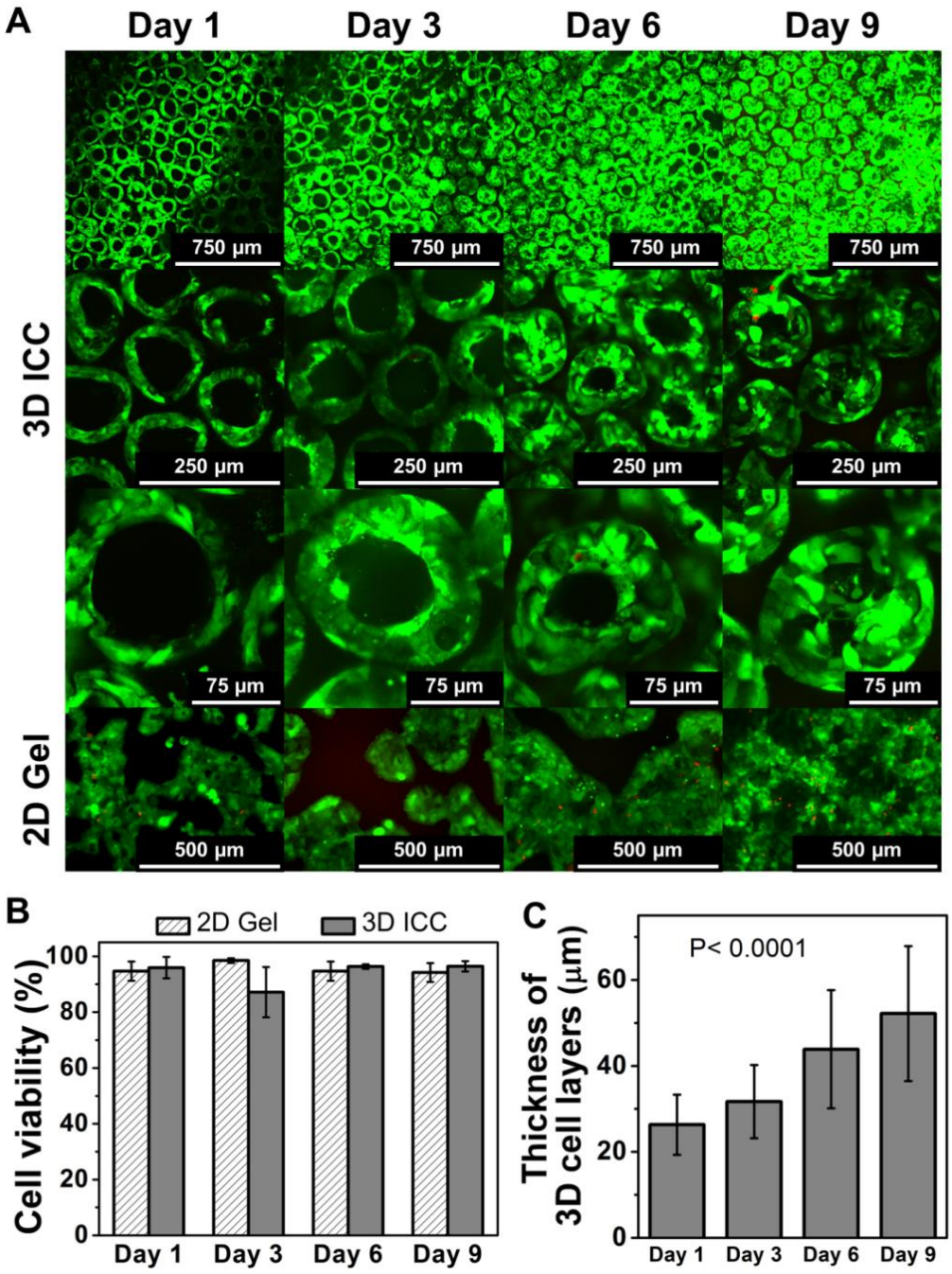

Figure 5.6 Evaluation of Huh7.5 cells viability and growing pattern in 3D GelMA ICC scaffolds and on 2D GelMA substrates. **(A)** Live/dead staining images. Green and red indicate live and dead cells respectively. **(B)** Cell viability values, quantified from live/dead staining images by ImageJ. (For each group, 3 pictures were analyzed averaging > 250 cells per picture, mean ± SD). **(C)** The cell multilayer thickness in cavities of GelMA ICC scaffolds was quantified by analyzing the confocal images with ImageJ. (n=22, mean ± SD, P < 0.0001, one-way ANOVA).

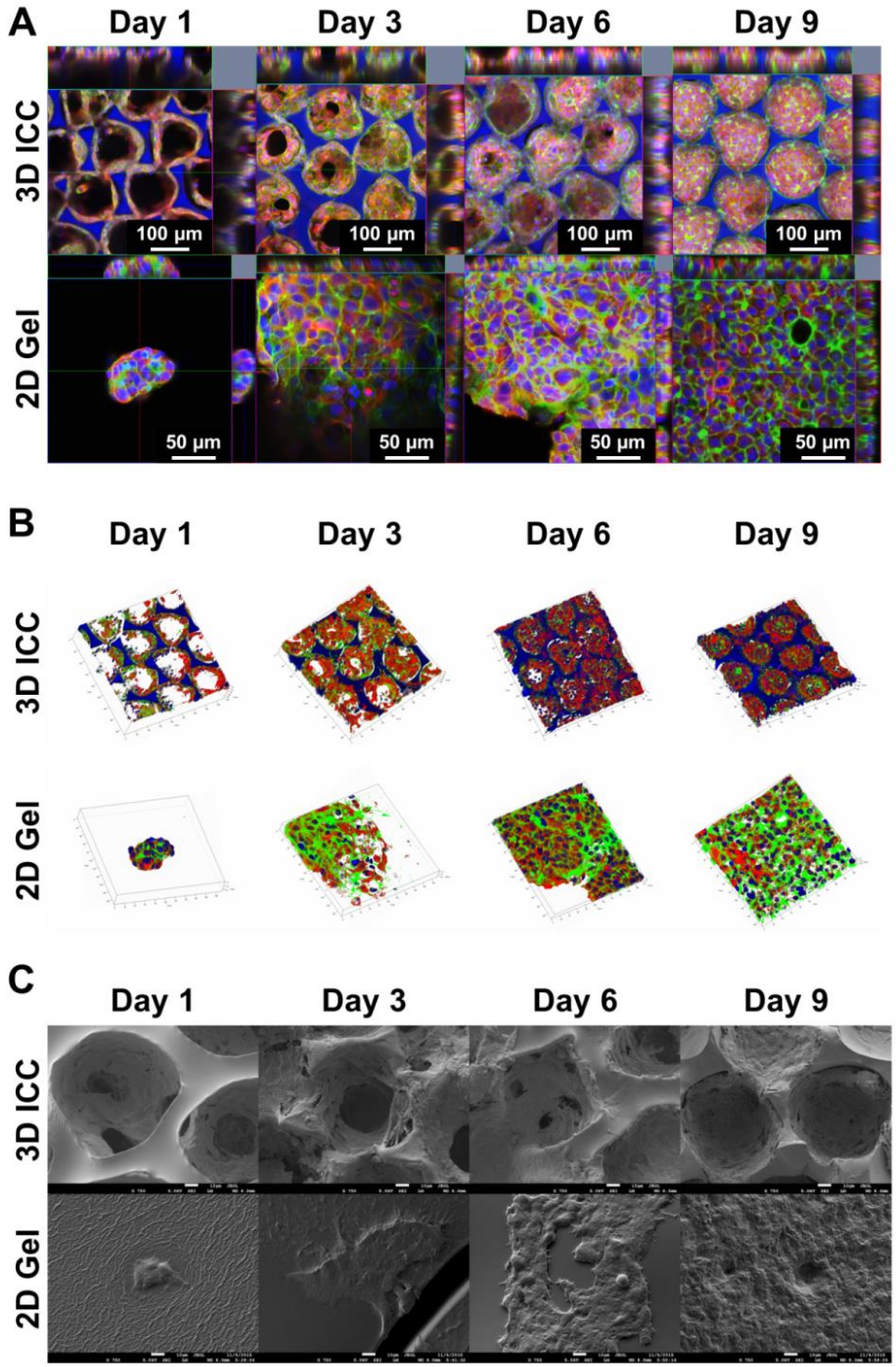

Figure 5.7 Characterization of Huh7.5 morphologies in 3D GelMA ICC scaffolds and on 2D GelMA substrates during the culture. Huh7.5 cells in 3D GelMA scaffolds formed hepatic multilayer constructs in a 3D manner whereas Huh7.5 cells on 2D GelMA scaffolds grew into 2D cell sheets. **(A)** Orthogonal projection images. The immunofluorescent images were taken via confocal microscopy (red: CYP3A4, green: f-actin, blue: nuclei). **(B)** 3D reconstruction images taken via confocal microscopy. (red: CYP3A4, green: f-actin, blue: nuclei). **(C)** Microscopic images via SEM.

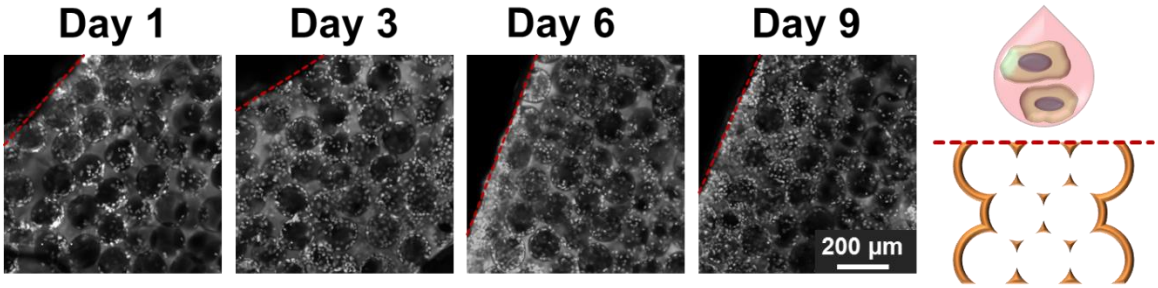

Figure 5.8 Cell distribution in different layers (depths) of cross-sectional GelMA ICC from the top (the first layer, marked with red dash line) to bottom. The nucleus of Huh7.5 cells was stained with DAPI for imaging via fluorescence microscopy. The images are displayed in black and white for visual clarification.

5.3.4. Cell-based functional assay of Huh7.5 cells

Immunostaining on liver functionality

In order to understand the influence of the scaffolds on cell function, Huh7.5 cells on 2D GelMA substrates and in 3D GelMA ICC scaffolds were assessed by immunohistochemical staining and Western blot assay as presented in **Figure 5.9**. The target proteins of immunohistochemical staining were albumin and CYP3A4, which are an essential secretory protein and a drug metabolic enzyme, respectively. The images displayed the morphological changes of Huh7.5 cells in 2D and 3D, revealing intracellular activities on albumin and CYP3A4. Overall, Huh7.5 cells in ICC scaffolds appeared to produce a higher concentration of albumin and a more obvious CYP activity over time in culture, especially near the center of the cell constructs. Contrastingly, those activities on 2D substrate were much less and showed a peak at early days, when the cells formed island-like clusters. After the clusters were merged to be sheet-like, the intensity decreased. These results imply correlation of morphology and cell functions, which was further investigated by Western blot assay.

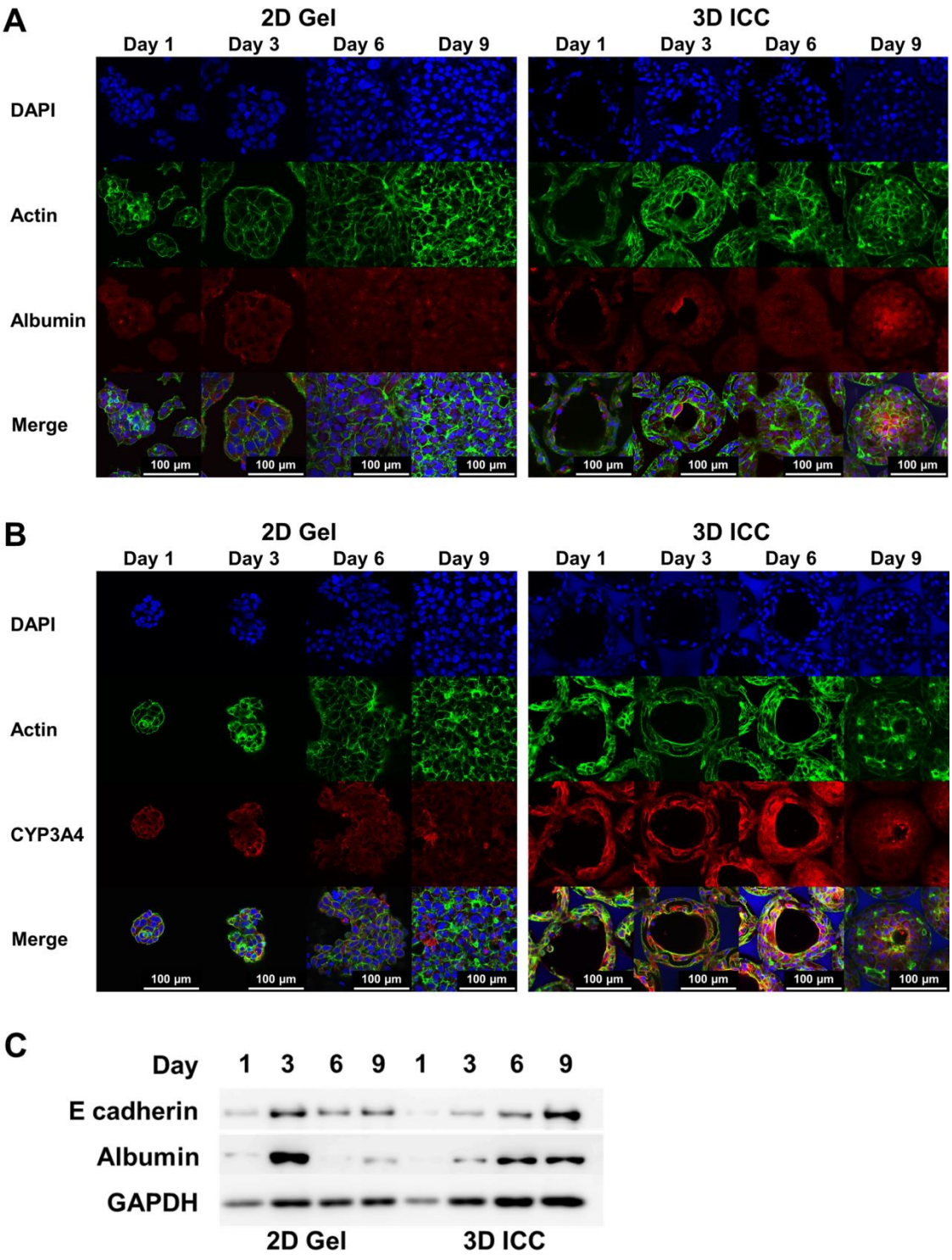

Figure 5.9 Evaluation of liver-specific functions of Huh7.5 cell constructs in 3D GelMA ICC scaffolds and on 2D GelMA substrates. **(A, B)** Confocal microscopy via immunohistochemistry (red: (A) CYP3A4 or (B) albumin, green: f-actin, blue: nuclei). **(C)** Western blot results of E-cadherin, albumin, and GAPDH.

Western blot assay was conducted on albumin and E-cadherin, a transmembrane component of adherens junction. In the liver, E-cadherin is present in the periportal zone [29], where has higher albumin expression [30]. In vitro, it is reported that hepatospheres, which is a well-studied configuration for its enhanced cell-cell interaction and hepatic function maintenance [31], has high expression of E-cadherin compared to cell suspensions [32]. The result of Western blot analysis shows a close correlation between albumin and E-cadherin. In 2D system, the expression levels of both molecules were maximized at day 3 when they formed clusters. Meanwhile, in ICC system, where cell construct grew gradually, both amount increased as time proceeds. This result suggests that curvatures of GelMA ICC system could provide high and lasting intercellular interaction, resulting in higher albumin production.

Gene expression analysis on liver functionality

For investigating a wider range of cell functions, hepatocyte-specific gene expressions of Huh7.5 cells on 2D GelMA substrates and in 3D GelMA ICC scaffolds was quantified by RT-qPCR. Hepatocyte nuclear factors (HNFs), regulating the expression of liver secretory proteins [33], and liver-specific molecules including albumin, CYPs, alpha 1-antitrypsin (AAT), and glucose 6-phosphatase (G6Pase) were chosen as hepatic markers as seen in **Figure 5.10A-G**. Among these molecules, the drastic difference between 2D and 3D was observed in CYPs; gene expression of CYP3A4 and CYP3A7 considerably increased in 3D systems while those of 2D system decreased by more than half after 9 days of culture. Although the contrast is lesser, HNFs and other secretory molecules were significantly upregulated in GelMA ICC system compared with those of 2D substrate, remaining moderate increase.

The mRNA levels on cell junctions were also quantified. **Figure 5.10H,I** shows the result of transmembrane components of adherens junction, E-cadherin, and N-cadherin. As for E-cadherin, the expression of the 3D system at day 9 was significantly higher than that of 2D. This result is consistent with Western blot, supporting better hepatic behavior in ICC system. Contrastingly, N-cadherin did not show a large difference between 2D and 3D. Also in both systems, the difference between day 1 and day 9 remained insignificant ($p > 0.05$). As N-cadherin is related to cellular motility and increases during

liver fibrosis [34], this result shows favorable, non-mesenchymal characteristics. Another cell junction, tight junction, was also assessed through relevant molecules, Claudin-1 and

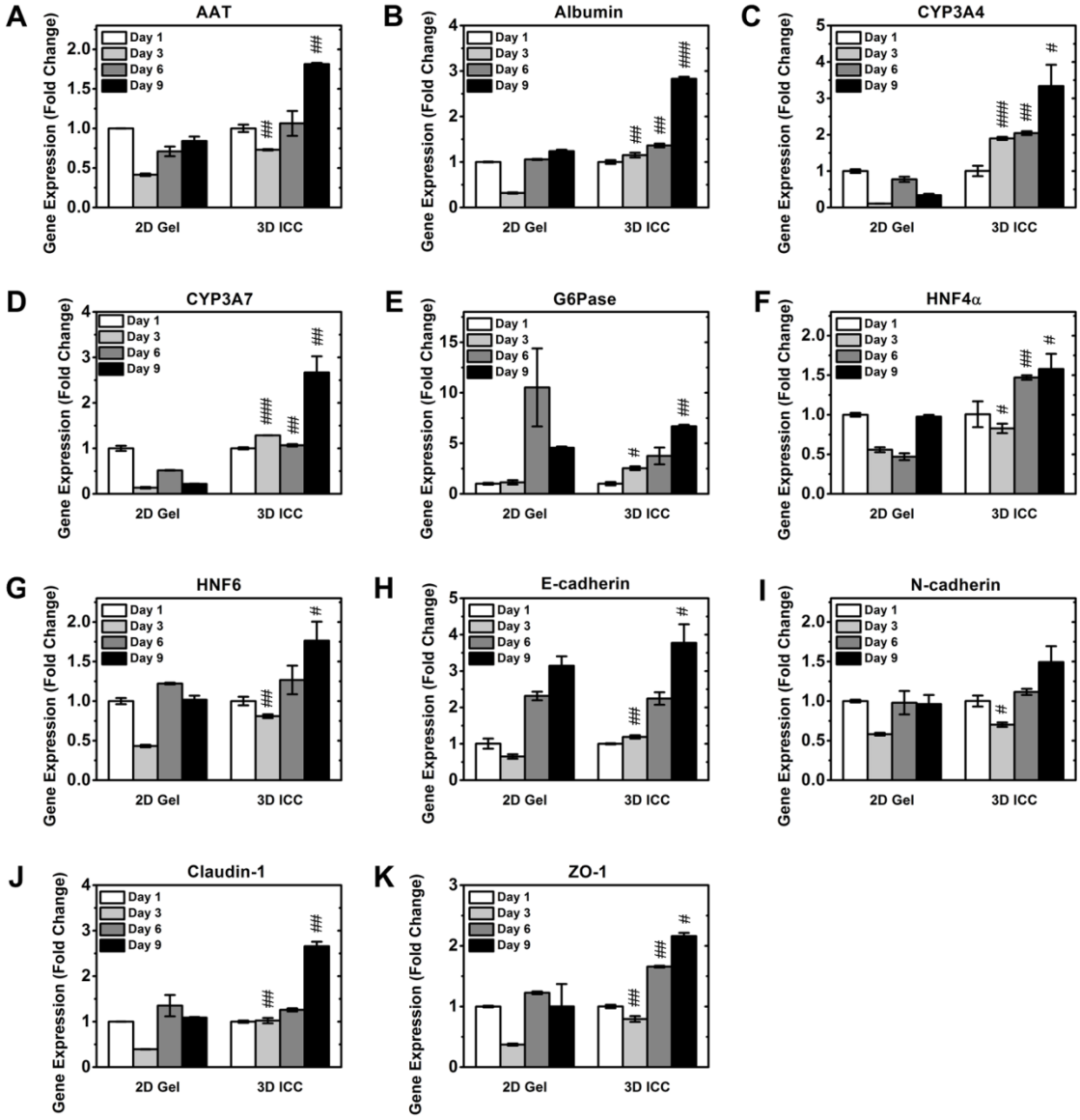

Figure 5.10 Effect of hepatic cell culture in 3D GelMA ICC scaffolds and on 2D GelMA substrates on liver-specific gene expression. Huh7.5 cells were cultured in both systems, and RNA was extracted for the quantitative real-time PCR analysis of **(A)** AAT, **(B)** albumin, **(C)** CYP3A4, **(D)** CYP3A7, **(E)** G6Pase, **(F)** HNF4a, **(G)** HNF6, **(H)** E-cadherin, **(I)** N-cadherin, **(J)** Claudin-1, **(K)** ZO-1. The mRNA expression levels were normalized to GAPDH of the corresponding day and Day 1 of the respective target gene. (n=3, mean ± SD; #: $P < 0.05$; ##: $P < 0.01$; ###: $P < 0.001$, compared to 2D of corresponding day.)

zonula occludens (ZO)-1 as shown in **Figure 5.10J,K**. In the liver, tight junctions exist between cells and play important role in regulating paracellular diffusion and maintaining cellular polarity [35,36]. In 3D ICC system, both Claudin-1 and ZO-1 were increased over culture after day 3. On the other hand, those in 2D system peaked on day 6 and did not show time-dependent behavior. This result signifies enhanced intercellular communication and polarity maintenance. To sum up, these results on gene expression shows upregulated hepatic functions in 3D GelMA ICC system compared to 2D GelMA substrate.

5.4. Conclusions

In conclusion, we successfully constructed protein-based ICC scaffolds with a highly organized interconnected porous structure, tunable degradation properties, and an easy-to-handle feature. This system negates the need of additional ECM coating, which is cumbersome and may not assure reproducibility. The pores of GelMA ICC scaffolds were highly interconnected and regular, enabling excellent cell infiltration and subsequent cell-cell interaction between pores. The scaffolds were susceptible to collagenase degradation, which could be tailorable by differing DS of GelMA. Hepatocytes, when loaded into 3D GelMA ICC scaffolds, displayed high viability and enhanced cell-cell and cell-ECM interactions during the 9-day culture period. The mRNA levels of multiple hepatocyte-specific genes were significantly upregulated due to improved cell-cell and cell-ECM interactions from 3D GelMA ICC geometry in comparison with GelMA 2D system. These GelMA ICC scaffolds could be not only an effective artificial liver platform for drug screening but also versatile platforms for diverse tissue engineering purpose as well as in vivo applications.

References

1 McCuskey R. in *Zakim and Boyer's Hepatology (Sixth Edition)* (eds Boyer TD, Manns MP, Sanyal AJ) 3-19 (W.B. Saunders, 2012).

2 Piccini JP *et al.* Current challenges in the evaluation of cardiac safety during drug development: translational medicine meets the Critical Path Initiative. *Am Heart J* **158**, 317-326 (2009).

3 Martignoni M, Groothuis GM, de Kanter R. Species differences between mouse, rat, dog, monkey and human CYP-mediated drug metabolism, inhibition and induction. *Expert Opin Drug Metab Toxicol* **2**, 875-894 (2006).

4 Gómez-Lechón MJ *et al.* Long-term expression of differentiated functions in hepatocytes cultured in three-dimensional collagen matrix. *J Cell Physiol* **177**, 553-562 (1998).

5 Cukierman E, Pankov R, Stevens DR, Yamada KM. Taking cell-matrix adhesions to the third dimension. *Science* **294**, 1708-1712 (2001).

6 Dutta RC, Dutta AK. Cell-interactive 3D-scaffold; advances and applications. *Biotechnol Adv* **27**, 334-339 (2009).

7 Schmeichel KL, Bissell MJ. Modeling tissue-specific signaling and organ function in three dimensions. *J Cell Sci* **116**, 2377-2388 (2003).

8 Kotov NA *et al.* Inverted Colloidal Crystals as Three-Dimensional Cell Scaffolds. *Langmuir* **20**, 7887-7892 (2004).

9 Lee J, Cuddihy MJ, Cater GM, Kotov NA. Engineering liver tissue spheroids with inverted colloidal crystal scaffolds. *Biomaterials* **30**, 4687-4694 (2009).

10 Lee J, Lilly GD, Doty RC, Podsiadlo P, Kotov NA. In vitro toxicity testing of nanoparticles in 3D cell culture. *Small* **5**, 1213-1221 (2009).

11 Kim MH *et al.* Phenotypic regulation of liver cells in a biofunctionalized three-dimensional hydrogel platform. *Integrative Biology* **8**, 156-166 (2015).

12 Kim MH *et al.* Biofunctionalized Hydrogel Microscaffolds Promote 3D Hepatic Sheet Morphology. *Macromol Biosci* **16**, 314-321 (2016).

13 Zhang Y, Xia Y. Formation of Embryoid Bodies with Controlled Sizes and Maintained Pluripotency in Three-Dimensional Inverse Opal Scaffolds. *Adv Funct Mater* **22**, 121-129 (2012).

14 Kuo Y-C, Chung C-Y. TATVHL peptide-grafted alginate/poly(γ-glutamic acid) scaffolds with inverted colloidal crystal topology for neuronal differentiation of iPS cells. *Biomaterials* **33**, 8955-8966 (2012).

15 Kuo Y-C, Chen C-W. Inverted colloidal crystal scaffolds with induced pluripotent stem cells for nerve tissue engineering. *Colloids and Surfaces B: Biointerfaces* **102**, 789-794 (2013).

16 Kuo Y-C, Tsai Y-T. Inverted colloidal crystal scaffolds for uniform cartilage regeneration. *Biomacromolecules* **11**, 731–739 (2010).

17 Kuo Y-C, Tsai Y-T. Heparin-conjugated scaffolds with pore structure of inverted colloidal crystals for cartilage regeneration. *Colloids Surf B Biointerfaces* **82**, 616-623 (2011).

18 Choi S-W, Xie J, Xia Y. Chitosan-Based Inverse Opals: Three-Dimensional Scaffolds with Uniform Pore Structures for Cell Culture. *Advanced Materials* **21**, 2997-3001 (2009).

19 Yang J-T, Kuo Y-C, Chiu K-H. Peptide-modified inverted colloidal crystal scaffolds with bone marrow stromal cells in the treatment for spinal cord injury. *Colloids Surf B Biointerfaces* **84**, 198-205 (2011).

20 Kuo Y-C, Chiu K-H. Inverted colloidal crystal scaffolds with laminin-derived peptides for neuronal differentiation of bone marrow stromal cells. *Biomaterials* **32**, 819-831 (2011).

21 Kuo Y-C, Lin C-C. Accelerated nerve regeneration using induced pluripotent stem cells in chitin–chitosan–gelatin scaffolds with inverted colloidal crystal geometry. *Colloids and Surfaces B: Biointerfaces* **103**, 595-600 (2013).

22 Kim J, Bencherif SA, Li WA, Mooney DJ. Cell-friendly inverse opal-like hydrogels for a spatially separated co-culture system. *Macromol Rapid Commun* **35**, 1578-1586 (2014).

23 Yue K *et al.* Synthesis, properties, and biomedical applications of gelatin methacryloyl (GelMA) hydrogels. *Biomaterials* **73**, 254-271 (2015).

24 Lee BH, Shirahama H, Cho N-J, Tan LP. Efficient and controllable synthesis of highly substituted gelatin methacrylamide for mechanically stiff hydrogels. *RSC Advances* **5**, 106094 (2015).

25 Shin H, Olsen BD, Khademhosseini A. The mechanical properties and cytotoxicity of cell-laden double-network hydrogels based on photocrosslinkable gelatin and gellan gum biomacromolecules. *Biomaterials* **33**, 3143-3152 (2012).

26 Curcio E *et al.* Mass transfer and metabolic reactions in hepatocyte spheroids cultured in rotating wall gas-permeable membrane system. *Biomaterials* **28**, 5487-5497 (2007).

27 Choi S-W, Zhang Y, Xia Y. Three-Dimensional Scaffolds for Tissue Engineering: The Importance of Uniformity in Pore Size and Structure. *Langmuir* **26**, 19001-19006 (2010).

28 Blight KJ, McKeating JA, Rice CM. Highly Permissive Cell Lines for Subgenomic and Genomic Hepatitis C Virus RNA Replication. *J Virol* **76**, 13001-13014 (2002).

29 Koide N *et al.* Continued high albumin production by multicellular spheroids of adult rat hepatocytes formed in the presence of liver-derived proteoglycans. *Biochem Biophys Res Commun* **161**, 385-391 (1989).

30 Hempel M *et al.* Pathological implications of cadherin zonation in mouse liver. *Cell Mol Life Sci* **72**, 2599-2612 (2015).

31 Racine L *et al.* Distribution of albumin, α_1-inhibitor 3 and their respective mRNAs in periportal and perivenous rat hepatocytes isolated by the digitonin-collagenase technique. *Biochem J* **305 (Pt 1)**, 263-268 (1995).

32 Lin RZ, Chang HY. Recent advances in three-dimensional multicellular spheroid culture for biomedical research. *Biotechnol J* **3**, 1172-1184 (2008).

33 Lin RZ, Chou LF, Chien CC, Chang HY. Dynamic analysis of hepatoma spheroid formation: roles of E-cadherin and β1-integrin. *Cell Tissue Res* **324**, 411-422 (2006).

34 Odom DT *et al.* Control of pancreas and liver gene expression by HNF transcription factors. *Science* **303**, 1378-1381 (2004).

35 Lee JM, Dedhar S, Kalluri R, Thompson EW. The epithelial-mesenchymal transition: new insights in signaling, development, and disease. *The Journal of cell biology* **172**, 973-981 (2006).

36 Vinken M *et al.* Involvement of cell junctions in hepatocyte culture functionality. *Crit Rev Toxicol* **36**, 299-318 (2006).

37 Kojima T *et al.* Regulation of the blood-biliary barrier: interaction between gap and tight junctions in hepatocytes. *Med Electron Microsc* **36**, 157-164 (2003).

Chapter 6 Conclusions and proposed future works

Through three previous chapters, improvement of gelatin methacryloyl synthesis and development of the liver-mimicking platform for high throughput drug screening were described. The current chapter offers overall conclusion and future works for the two topics.

6.1. Conclusion

The overall goal of this dissertation was to create artificial liver platforms that can be useful for drug development. Gelatin methacryloyl is one of the ideal materials as it is based on natural, extracellular matrix (ECM) and has favorable advantages to engineer liver-emulating microenvironment.

The first part of this dissertation work focused on this GelMA, and solved one of the problems in synthesizing the material. GelMA is obtained from the reaction between gelatin and methacrylic anhydride (MAA). Previous studies utilized high molar excess of MAA (10-47) to obtain GelMA with high degree of substitution (DS), which is not efficient. To address this problem, we focused on controlling pH of the reaction solution. Control of pH could lead to control of charging of functional groups of gelatin, which potentially governs efficacy of the reaction. First, we adopted carbonate-bicarbonate (CB) buffer and sequential pH adjustment; this resulted in high DS with an appreciably smaller molar excess of MAA (2.2). Next, CB buffer molarity and other experimental parameters were comprehensively investigated to realize a facile GelMA synthesis, which is to achieve high DS with minimal MAA consumption without manual pH adjustment. The parameters systematically examined are CB buffer molarities, MAA concentrations, gelatin concentrations, reaction temperatures, initial pH adjustment steps, and reaction time. The results showed that a simplified synthesis process with a feed ratio of MAA/gelatin at 0.1 mL/g (equivalent to 2.2 molar excess of MAA) in 0.25 M CB buffer (pH 9) could produce GelMA with nearly complete substitution within 1 h without multiple pH adjustment. This one-pot GelMA synthesis method offers a GelMA with a controllable DS in less laborious and more efficient way compared to the conventional methods.

Next, with this material, protein-based structure was constructed. The liver has hexagonally-arranged, porous structure with interconnections. We have achieved this complex by employing colloidal templating method. The resulted GelMA ICC scaffolds possessed a highly organized interconnected porous structure and sufficient mechanical integrity. The scaffolds were susceptible to collagenase degradation, which could be tailored by differing DS of GelMA. Hepatocytes, when loaded into GelMA ICC scaffolds, showed high viability and enhanced cell-cell and cell-ECM interactions during the 9-day

culture period. The mRNA levels of hepatocyte-specific genes were significantly upregulated in comparison with GelMA plain system without geometry. These GelMA ICC scaffolds demonstrated their potential as effective artificial liver platforms for drug screening, and also could be versatile platforms for diverse tissue engineering purpose as well as in vivo applications.

6.2. Proposed future works

This dissertation describes two major contents: improvement of gelatin methacryloyl (GelMA) synthesis and development of an artificial liver platform for drug screening purpose, employing GelMA and colloidal templating. In this section, based on the findings and previous studies, future directions of two topics are discussed; one is GelMA synthesis, and the other is liver tissue engineering (LTE).

6.2.1. Gelatin methacryloyl synthesis

Synthesis with different bloom of gelatin

The result of gelatin concentration study showed that miscibility of the solution is important (**Figure 3.9**). There are different parameters that involve the miscibility, such as stirring speed of the reaction solution, gelatin concentration, and the strength of the gelatin. The gelatin strength, being relative to molecular weight, is defined by a unit called bloom. In this dissertation, type A gelatin of 175 bloom was utilized for whole experiments. Although basic principle could be applicable for gelatin with different blooms (and types [1]), localized optimization might be necessary for different kinds of gelatin.

In tissue engineering, type A gelatin of 300 bloom is often used. Even higher bloom could be chosen to increase the mechanical stiffness [2]. When the bloom is higher, the solution would be more viscous with the higher gelling temperature [3]. Despite our finding of no temperature dependency within 35-50 °C for 3 h of reaction, gelatin with higher bloom might show temperature dependency caused by limited methacrylic anhydride (MAA) dispersity in more viscous reaction solutions. The maximum temperature to reduce the viscosity would be 80 °C, above which hydrolysis of collagen would be initiated and gelatin molecular weight could be changed [4].

Use of surfactant for improving time efficiency

Gelatin in an aqueous solution and MAA is a two-phase reaction, occurring at the interface of water and oil. In our system, even the reaction solution was continuously stirred during MAA addition, droplets of MAA were large enough to be visible. And from time-dependent study (cf. **Figure 3.11**), it was shown that the reaction takes around 1 h. In order to promote the reaction in a time efficient manner, emulsifying the solution by adding a surfactant into the solution might be effective.

The ideal surfactant for this purpose possesses following characteristics: less toxicity, being not reactive against MAA and/or gelatin, being free from altering pH of the reaction solution, less bubble foaming, and being less interactive with gelatin. Surfactants are the combination of hydrophilic groups and hydrophilic groups, and can be classified based on their hydrophilic groups: anionic, cationic, amphoteric, and nonionic surfactant. Interactions between those surfactants and gelatin have been studied as summarized in **Table 6.1**. Anionic and cationic surfactants have a higher physical interaction that may hinder the reaction between gelatin and MAA. Also, they have a high degree of foam formation. In the case of an amphoteric surfactant, most of them possess amino groups that can react with MAA. For facilitating GelMA synthesis, the use of nonionic surfactants would be a suitable choice.

Table 6.1 Interaction between gelatin and different types of surfactant

Types	Example of surfactant	Characteristics
Anionic surfactant	Sodium dodecyl sulfate (SDS)	Strongly interacts with gelatin [5] High foam formation [6]
Cationic surfactant	Cetyl trimethyl ammonium bromide (CTAB)	Can strongly interact with gelatin above IEP [7] Foam formation [6]
Amphoteric surfactant	Phospholipids	Mostly contains amino groups
Nonionic surfactant	Tween 20, Triton X-100	Weak interaction with gelatin [5]

The representative nonionic surfactants are shown in **Figure 6.1**, namely Triton X-100, Tween® 20, and Tween® 80. As hydroxyl groups could react with MAA (although they are not reactive as much as amino groups; cf. **Figure 3.8**), Triton X-100 with fewer hydroxyl groups would be favorable among them. To minimize the reaction between

MAA and the surfactant, the amount to add should be small. The specific concentration that the surfactant should not exceed would be its critical micelle concentration so that they could be surely removed by following dialysis process.

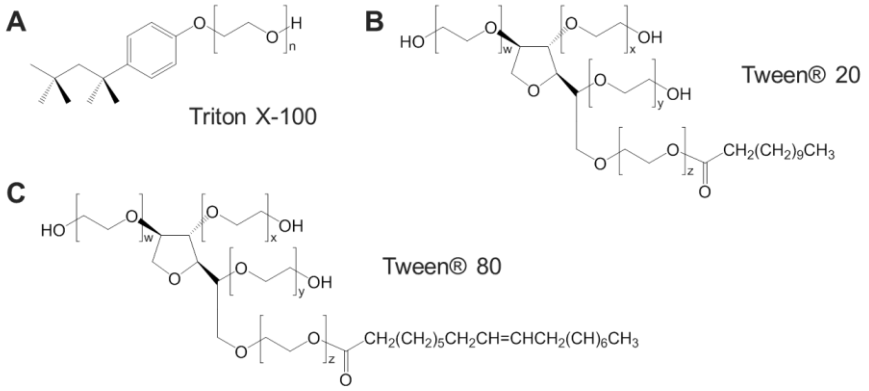

Figure 6.1 Representative nonionic surfactants: **(A)** Triton X-100, **(B)** Tween® 20, and **(C)** Tween® 80.

Enhancement of crosslinking density

The degree of substitution (DS) of GelMA is an important parameter that can influence mechanical stiffness, swelling, and degradation speed of its hydrogels (cf. Chapter Four). Also when GelMA is utilized for material encapsulation (e.g. growth factor [8,9], drugs [10], plasmid DNA [11]), DS can control the speed of the material release [9]. By the reaction between gelatin and MAA, amino groups and hydroxyl groups of the gelatin can be methacrylated (cf. **Figure 3.8**) that involve polymer network formation. To further increase the crosslinking density, carboxyl groups could also be methacrylated.

Previously, Ofner et al. introduced conjugation of carboxyl groups of type B gelatin to ethylenediamine in the presence of 1-Ethyl-3-(3-dimethylaminopropyl)carbodiimide (EDC) for grafting amino groups (**Figure 6.2A**) [12]. Type B gelatin possesses 0.33 mmol/g of primary amino group from lysine and hydroxylysine [13], while aspartic acid and glutamic acid provide 1.26 mmol/g of carboxyl group [12]. By converting carboxyl groups to amino groups, they achieved 2.3 times greater crosslinking by chemical crosslinking with glutaraldehyde that binds two amino groups. Instead of converting functional groups, Shreiber et al. proposed two steps of collagen methacrylation [14], which is to functionalize amino groups and subsequent carboxyl groups with methacrylic acid and amino methacrylate, respectively, both via EDC chemistry as seen in **Figure**

6.2B. However, both methods undergo EDC crosslinking with raw gelatin/collagen, which could lead inter- and intramolecular crosslinking. This may decrease controllability on physical properties of hydrogels and could result in high viscosity.

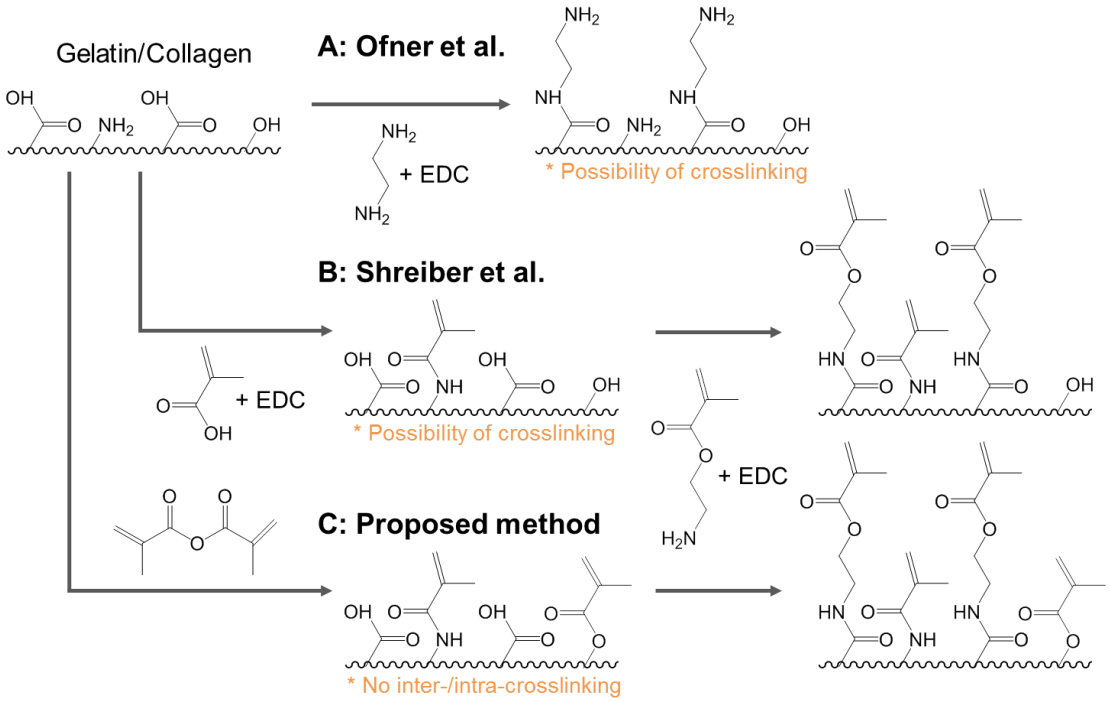

Figure 6.2 Different functionalization methods for increasing crosslinking density of gelatin/collagen hydrogels. **(A)** Ofner et al. demonstrated grafting ethylenediamine to carboxyl groups to increase amino groups for chemical crosslinking with glutaraldehyde [12]. **(B)** Shreiber et al. proposed two-steps of crosslinking methacrylic acid and subsequent amino methacrylate, both via EDC crosslinking [14]. **(C)** Proposed method to first functionalize with MAA and then crosslink with amino methacrylate to avoid inter-/intramolecular crosslinking via EDC chemistry.

The auto-crosslinking could be avoided by additional methacrylation of GelMA of high DS, which is obtained from the reaction with MAA. As shown in **Figure 6.2C**, carboxyl groups of the GelMA could be methacrylated with amino methacrylate or methacrylamide via EDC chemistry. As amino groups are functionalized in advance, carboxyl groups would react with amino groups of only additives but not gelatin molecules. Resulting highly-substituted GelMA, with metacrylated amino groups, hydroxyl groups, and carboxyl groups, could exhibit high crosslinking density; providing a wider range of material properties. In the application of material encapsulation, it would offer longer time range of material release.

6.2.2. Liver tissue engineering

Protein coating

As described in subsection "2.1.3 Extracellular matrices in the liver," the liver comprises from various extracellular matrices (ECMs) not only collagen (the parent material of gelatin) but also fibronectin, laminin and so on. Our recent finding shows that fibronectin plays an important, distinctive role in regulating hepatocyte functions in ICC system [15]. Indeed, the effectiveness of such ECM coatings is widely studied and accepted in different systems as well [16,17]. Although fabrication of fibronectin/laminin-based ICC may not be highly attractive in economical aspect, surface conjugation of both proteins to GelMA would be feasible via EDC chemistry [18,19]. The degree of protein conjugation could be changed by a concentration of the protein solution to soak the scaffolds in [20]. The combination of these proteins and gelatin as a base material could bring the environment even closer to in vivo, expected to enhance hepatic functions further.

Primary cell culture

In this dissertation, a model cell line was utilized to evaluate hepatic phenotype maintenance of the platform. However, it is always ideal to use primary hepatocytes for hepatotoxicity check. Although so far no study was conducted on ICC system with primary hepatocytes, the lobule-like three-dimensional platform with good diffusivity would provide an ideal environment for the cells to reside. Primary cells could be obtained commercially or extracted from the liver tissue via collagenase digestion and centrifugal separation [21]. To maintain the hepatocyte phenotype, dimethyl sulfoxide [22] and/or growth factors [23] could be added to culture media.

Co-culture with non-parenchymal cells

In the liver, hepatocytes occupy 78% of the volume [24], nevertheless number-wise, they account for only for 60%; other non-parenchymal (NP) cells are sinusoidal endothelial cells, Kupffer cells and stellate cells, whose relative number is 19, 15, and 6% respectively [25]. They have distinct roles and involve in the process of hepatic events such as regeneration, inflammatory response, and hepatotoxicity [26,27]. In previous studies, co-culture with such non-parenchymal cells lead longer lifetime and better

function maintenance of the hepatocytes by heterocellular interactions and secretion of cytokines (cf. hepatocyte growth factor) [28-30]. Some previous studies reported that albumin production of rat primary hepatocytes was maintained at the highest with rat embryonic fibroblast, 3T3 cells, among several types of co-cultured cells [31,32]. However, the use of NP cells, which are engaged in the liver biological process, could be more reliable for predicting in vivo reaction against drugs. NP cells are obtainable as cell lines or could be isolated separately from the liver tissue as well as hepatocytes [21].

With ICC system, there could be different ways to employ co-culture. One method is to seed the cells in two-dimensional (2D) well and utilize their secreted cytokines (**Figure 6.3A**). ICC system could be co-cultured via permeable support. Another method is to conduct cell encapsulation of NP cells in GelMA ICC and seed hepatocytes inside (**Figure 6.3B**). Previously, a similar study was conducted with human breast cancer cells and mesenchymal stem cells by utilizing alginate spheres that can be dissolved in less-toxic ethylenediaminetetraacetic acid (EDTA) [33]. GelMA ICC could be fabricated in a like manner with NP cells. This encapsulated ICC system would provide cytokines and controlled heterocellular contact of NP cells to hepatocytes. By including endothelial cells, the structure can mimic vascularization of the liver. The other way is direct co-culture of hepatocytes and NP cells as shown in **Figure 6.3C**. In this case, initial optimization of the ratio between hepatocytes and NP cells may be needed, but the best condition is expected to be the same ratio as in the body (Hepatocytes: NP cells at 60:40) from a previous study in the 2D system [34]. The variables are not only cell ratio but also the seeding days; NP cells could be seeded prior to/after hepatocyte seeding.

By comparing the results of these different co-culture systems, the effects of cytokines from feeder cells controlled heterocellular interaction, and direct hereto-cellular interaction would be elucidated.

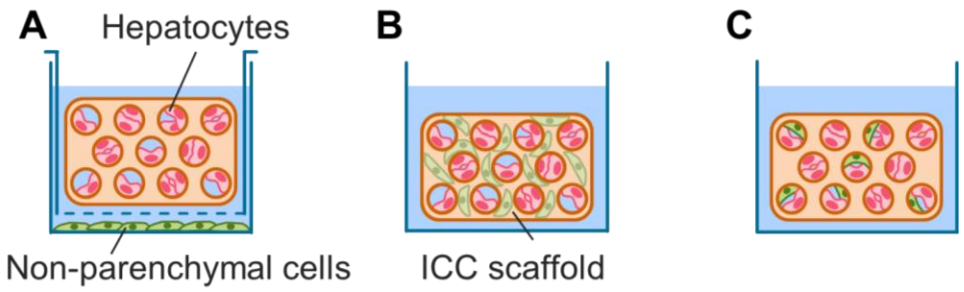

Figure 6.3 Co-culture designs of hepatocytes and non-parenchymal cells in ICC system. **(A)** Seeding NP cells in 2D well for uptake of their cytokines via permeable membrane support. **(B)** Confining NP cells within ICC scaffold for both their cytokines and controlled heterocellular contact. **(C)** Seeding NP cells together with hepatocytes for direct heterocellular communication.

Implementing the external systems

The liver is a highly vascularized organ. External systems with the flow can mimic in vivo environment and also actively supply oxygens/nutrients to the cells, resulting in better maintenance of hepatocyte's viability and functions [35,36]. The systems include microfluidic systems and bioreactors (shaker, stirred tank, perfusion and so on) [37]. ICC scaffold could be implemented in such fluidic environment, simply by installing the scaffold into the system. In designing the system, swelling in size of the GelMA hydrogels needs to be considered, which was investigated in Chapter Four of this dissertation.

6.3. Summary

In this chapter, future outlooks of the GelMA synthesis and GelMA ICC for LTE were discussed. As for GelMA synthesis, three directions were discussed; one is further optimization with gelatin of different blooms, another is the use of surfactant for facilitating the synthesis, and the other is the additional methacrylation via EDC crosslinking for obtaining GelMA hydrogels with higher crosslinking density. Regarding GelMA ICC, four orientations were described; which is (1) protein coating, (2) primary cell culture, (3) co-culture with non-parenchymal cells, and (4) implementing the external system. Adding these external conditions would make GelMA ICC environment even closer to in vivo, improving the system toward semi-genuine liver platforms for drug development and screening purpose.

References

1 Lee BH, Lum N, Seow LY, Lim PQ, Tan LP. Synthesis and Characterization of Types A and B Gelatin Methacryloyl for Bioink Applications. *Materials* **9**, 797 (2016).

2 Bigi A. Relationship between triple-helix content and mechanical properties of gelatin films. *Biomaterials* **25**, 5675-5680 (2004).

3 Leuenberger BH. Investigation of Viscosity and Gelation Properties of Different Mammalian and Fish Gelatins. *Food Hydrocolloids* **5**, 353-361 (1991).

4 Lowe B. *Experimental cookery from the chemical and physical standpoint*. 2nd edn, (J. Wiley & Sons, 1937).

5 Saxena A, Antony T, Bohidar HB. Dynamic light scattering study of gelatin-surfactant interactions. *J Phys Chem B* **102**, 5063-5068 (1998).

6 Wustneck R, Muller HJ. Characterization of Gelatin-Surfactant Interaction by Thickness Measurements of Foam Films. *Colloid Polym Sci* **264**, 97-102 (1986).

7 Greener J, Contestable BA, Bale MD. Interaction of Anionic Surfactants with Gelatin - Viscosity Effects. *Macromolecules* **20**, 2490-2498 (1987).

8 Jeon O, Wolfson DW, Alsberg E. In-situ formation of growth-factor-loaded coacervate microparticle-embedded hydrogels for directing encapsulated stem cell fate. *Advanced Materials* **27**, 2216-2223 (2015).

9 Nguyen AH, McKinney J, Miller T, Bongiorno T, McDevitt TC. Gelatin methacrylate microspheres for controlled growth factor release. *Acta Biomater* **13**, 101-110 (2015).

10 Ahadian S *et al.* Facile and rapid generation of 3D chemical gradients within hydrogels for high-throughput drug screening applications. *Biosensors and Bioelectronics* **59**, 166-173 (2014).

11 Paul A *et al.* Injectable graphene oxide/hydrogel-based angiogenic gene delivery system for vasculogenesis and cardiac repair. *ACS Nano* **8**, 8050-8062 (2014).

12 Ofner CM, 3rd, Bubnis WA. Chemical and swelling evaluations of amino group crosslinking in gelatin and modified gelatin matrices. *Pharm Res* **13**, 1821-1827 (1996).

13 Bubnis WA, Ofner CM, 3rd. The determination of ϵ-amino groups in soluble and poorly soluble proteinaceous materials by a spectrophotometric method using trinitrobenzenesulfonic acid. *Anal Biochem* **207**, 129-133 (1992).

14 Shreiber D, Gaudet I. Process for the synthesis of methacrylate-derivatized type-1 collagen and derivatives thereof. United States patent (2012).

15 Wang Y *et al.* ECM proteins in a microporous scaffold influence hepatocyte morphology, function, and gene expression. *Sci Rep* **6**, 37427 (2016).

16 Bissell DM, Arenson DM, Maher JJ, Roll FJ. Support of cultured hepatocytes by a laminin-rich gel. Evidence for a functionally significant subendothelial matrix in normal rat liver. *J Clin Invest* **79**, 801-812 (1987).

17 Koide N *et al.* Continued high albumin production by multicellular spheroids of adult rat hepatocytes formed in the presence of liver-derived proteoglycans. *Biochem Biophys Res Commun* **161**, 385-391 (1989).

18 Hosseinkhani H *et al.* Engineering Three-Dimensional Collagen-IKVAV Matrix to Mimic Neural Microenvironment. *Acs Chem Neurosci* **4**, 1229-1235 (2013).

19 Bush KA, Pins GD. Carbodiimide Conjugation of Fibronectin on Collagen Basal Lamina Analogs Enhances Cellular Binding Domains and Epithelialization. *Tissue Engineering Part A* **16**, 829-838 (2010).

20 Kim MH *et al.* Biofunctionalized Hydrogel Microscaffolds Promote 3D Hepatic Sheet Morphology. *Macromol Biosci* **16**, 314-321 (2016).

21 Bale SS, Geerts S, Jindal R, Yarmush ML. Isolation and co-culture of rat parenchymal and non-parenchymal liver cells to evaluate cellular interactions and response. *Sci Rep* **6** (2016).

22 Isom HC, Secott T, Georgoff I, Woodworth C, Mummaw J. Maintenance of differentiated rat hepatocytes in primary culture. *Proc Natl Acad Sci U S A* **82**, 3252-3256 (1985).

23 Kost DP, Michalopoulos GK. Effect of 2% dimethyl sulfoxide on the mitogenic properties of epidermal growth factor and hepatocyte growth factor in primary hepatocyte culture. *J Cell Physiol* **147**, 274-280 (1991).

24 Dancygier H. *Clinical Hepatology: Principles and Practice of Hepatobiliary Diseases*. Vol. 1 (Springer, 2010).

25 Blouin A, Bolender RP, Weibel ER. Distribution of Organelles and Membranes between Hepatocytes and Non-Hepatocytes in Rat-Liver Parenchyma - Stereological Study. *J Cell Biol* **72**, 441-455 (1977).

26 Taub R. Liver regeneration: from myth to mechanism. *Nat Rev Mol Cell Biol* **5**, 836-847 (2004).

27 Laskin DL, Gardner CR. in *Drug-Induced Liver Disease* Vol. 9 (eds Kaplowitz N, DeLeve L, D.) (Marcel Dekker, Inc., 2002).

28 Yamamoto N, Imazato K, Masumoto A. Stimulation of Growth of Primary Cultured Adult Rat Hepatocytes without Growth Factors by Coculture with Nonparenchymal Liver Cells. *Exp Cell Res* **172**, 228-242 (1987).

29 Mitaka T, Sato F, Mizuguchi T, Yokono T, Mochizuki Y. Reconstruction of hepatic organoid by rat small hepatocytes and hepatic nonparenchymal cells. *Hepatology* **29**, 111-125 (1999).

30 Shulman M, Nahmias Y. in *Epithelial Cell Culture Protocols: Second Edition* (eds Randell HS, Fulcher LM) 287-302 (Humana Press, 2013).

31 Bhatia SN, Balis UJ, Yarmush ML, Toner M. Effect of cell–cell interactions in preservation of cellular phenotype: cocultivation of hepatocytes and nonparenchymal cells. *Faseb J* **13**, 1883-1900 (1999).

32 Cho CH, Berthiaume F, Tilles AW, Yarmush ML. A new technique for primary hepatocyte expansion in vitro. *Biotechnol Bioeng* **101**, 345-356 (2008).

33 Kim J, Bencherif SA, Li WA, Mooney DJ. Cell-friendly inverse opal-like hydrogels for a spatially separated co-culture system. *Macromol Rapid Commun* **35**, 1578-1586 (2014).

34 Zinchenko YS, Culberson CR, Coger RN. Contribution of non-parenchymal cells to the performance of micropatterned hepatocytes. *Tissue Eng* **12**, 2241-2251 (2006).

35 Coward SM, Selden C, Mantalaris A, Hodgson HJF. Proliferation rates of HepG2 cells encapsulated in alginate are increased in a microgravity environment compared with static cultures. *Artif Organs* **29**, 152-158 (2005).

36 Fiegel HC *et al.* Influence of flow conditions and matrix coatings on growth and differentiation of three-dimensionally cultured rat hepatocytes. *Tissue Eng* **10**, 165-174 (2004).

37 Martin I, Wendt D, Heberer M. The role of bioreactors in tissue engineering. *Trends Biotechnol* **22**, 80-86 (2004).

Appendix

List of publication

Works related to Liver Tissue Engineering and Gelatin Methacryloyl

1 Lee BH*, **Shirahama H*,** Kim MH*, H*, Glenn JS, Cho NJ**, Tan LP**. Colloidal Templating of Highly Ordered Gelatin Methacryloyl-Based Hydrogel Platforms for Three-Dimensional Tissue Analogues. *NPG Asia Materials* 2017.

2 Wang Y*, Kim MH*, **Shirahama H**, Lee JH, Ng SS, Glenn JS, Cho NJ. ECM Proteins in a Microporous Scaffold Influence Hepatocyte Morphology, Function, and Gene Expression. *Scientific Reports* 2016.

3 Wang Y*, Lee JH*, **Shirahama H**, Seo JE, Glenn JS, Cho NJ. Extracellular matrix functionalization and Huh-7.5 cell co-culture promote the hepatic differentiation of human adipose-derived mesenchymal stem cells in a 3D ICC hydrogel scaffold. *ACS Biomaterials Science & Engineering* 2016.

4 **Shirahama H*,** Lee BH*, Tan LP**, Cho NJ**. Precise Tuning of Facile One-pot Gelatin Methacryloyl (GelMA) Synthesis. *Scientific Reports* 2016; 6, 31036.

5 **Shirahama H,** Kumar SK, Jeon WY, Kim MH, Lee JH, Ng SS, Tabaei SR, Cho NJ. Fabrication of Inverted Colloidal Crystal Poly(ethylene glycol) Scaffold: A Three-Dimensional Cell Culture Platform for Liver Tissue Engineering. *Journal of Visualized Experiments* 2016; 114, e54331.

6 Kim MH, Kumar SK, **Shirahama H,** Seo J, Lee JH, Cho NJ. Phenotypic Regulation of Liver Cells in a Biofunctionalized Three-Dimensional Hydrogel Platform. *Integrative Biology* 2016; 8(2), 156-166.

7 Lee BH*, **Shirahama H*,** Tan LP**, Cho NJ**. Efficient and Controllable Synthesis of Highly Substituted Gelatin Methacrylamide for Mechanically Stiff Hydrogels. *RSC Advances* 2015; 5(128), 106094-106097.

8 Kim MH, Kumar SK, **Shirahama H,** Seo J, Lee JH, Zhdanov VP, Cho NJ. Biofunctionalized Hydrogel Microscaffolds Promote Three-Dimensional Hepatic Sheet Morphology. *Macromolecular Bioscience* 2016; 16(3), 314-321.

(* denotes equal first authors; ** denotes equal corresponding authors)

Other contributions

1 Mundargi RC, Potroz MG, Park SH, Park JH, **Shirahama H,** Lee JH, Seo J, Cho NJ. Lycopodium Spores: A Naturally Manufactured, Superrobust Biomaterial for Drug Delivery. *Advanced Functional Materials* 2016; 26(4), 487-497.

2 Mundargi RC, Potroz M, Park SH, **Shirahama H,** Lee JH, Seo JE, Cho NJ. Natural Sunflower Pollen as a Drug Delivery Vehicle. *Small* 2016; 12, 1167-1173.